

AN ABSTRACT OF THE THESIS OF

Tom Yao for the degree of Doctor of Philosophy

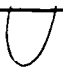
in Oceanography presented on February 28, 1978

Title: Some Effects of Topography and Vertical Shear on

Low-Frequency Ocean Fluctuations

Redacted for privacy

Abstract approved: _____

 (John S. Allen)

The role of coastal boundaries and bottom features in the ocean response to fluctuating winds is investigated with a simple model of a channel with depth variation along its length. The response is composed of linearized, barotropic topographic Rossby waves.

Normal modes, which are expected to dominate the observed response, are calculated for the case of exponential depth separating two regions of uniform depth. If the ratio of the width of the sloping region to the channel width, $d/L \geq 1$, the modes resemble those found in a closed rectangular basin with sloping bottom. As d/L decreases, this resemblance ceases and currents extend far beyond the sloping region. In the limit of a step discontinuity, the eigenfrequencies for those modes with a single maximum in stream function amplitude across the slope, approach a single value $(h_0 - h_1) / (h_0 + h_1)$ where h_0 and h_1 are depths on either side of the step. The eigenfrequencies approach zero for

those modes with a higher number of maxima in stream function amplitude across the slope.

For sufficiently low frequency, wave energy generated over a topographic feature, may radiate by Rossby waves. The asymptotic limit of topographic scale exceeding channel width is studied. Waves which are generated through a local resonance, radiate energy to the west if the atmospheric disturbance is eastward moving.

An initial value problem for the perturbation by a bottom feature to a two-layer flow on a beta plane is discussed. The development in space and in time of the linearized baroclinically unstable disturbance is investigated. When the conditions for temporal instability are met, the transient grows in amplitude as it propagates. With layer depths taken to be equal, the transient behavior is governed by two parameters, $\beta^*L_D^2/U$ and a ratio of cross-stream wave scale to L_D , where β^* is the beta parameter, L_D is the internal radius of deformation and U is a characteristic velocity.

If the currents in the two layers are in the same direction and sufficiently strong, the growing part of the disturbance is advected completely downstream. A steady solution is established in the region between the bottom feature and the tail of the transient. This solution may be a stationary wave if both currents are eastward. In other cases it is a net deflection of streamlines across the topography.

Some Effects of Topography and Vertical Shear
on Low-Frequency Ocean Fluctuations

by

Tom Yao

A THESIS

submitted to

Oregon State University

in partial fulfillment of
the requirements for the
degree of

Doctor of Philosophy

June 1978

APPROVED:

Redacted for privacy

Associate Professor of Oceanography in charge of major

Redacted for privacy

Acting Dean of Oceanography

Redacted for privacy

Dean of Graduate School

Date thesis is presented February 28, 1978

Typed by Errol Beecher for Tom Yao

ACKNOWLEDGEMENTS

John Allen freely provided encouragement, guidance and stimulating questioning throughout the course of this study. I thank him for his vital contribution. Douglas Caldwell served as thesis advisor at an earlier stage of my studies. The experience gained at that time has been valuable and his help is appreciated. I thank committee members Gunnar Bodvarsson, Julius Dasch and Peter Niiler for their comments and questions.

I am grateful to the International Decade of Ocean Exploration, National Science Foundation, for their support of this work.

TABLE OF CONTENTS

1. Introduction.....	1
1.1 The barotropic model.....	1
1.2 The instability problem.....	4
2. Formulation for barotropic model.....	8
3. Trapped modes, exponential depth.....	12
4. Short wavelength limit, free waves.....	24
5. Short wavelength limit, forced waves.....	31
5.1 Trapped waves.....	34
5.2 Propagatory waves.....	40
6. Summary of barotropic model.....	46
7. Formulation of instability problem.....	47
8. A criterion for the transformed solution.....	53
9. Transient solution on f plane.....	55
10. The steady state on f plane.....	72
11. The beta effect.....	77
11.1 General considerations.....	77
11.2 Low wavenumber neutral modes.....	79
11.3 High wavenumber neutral modes.....	89
12. Summary of instability problem.....	92
Appendix.....	93
Bibliography.....	100

LIST OF ILLUSTRATIONS

<u>Figure</u>		<u>Page</u>
1	Drake Passage bathymetry.....	2
2a	Amplitude and phase of stream function for normal mode $\omega = 0.0652$	15
2b	Amplitude and phase of stream function for normal mode $\omega = 0.0433$	16
2c	Amplitude and phase of stream function for normal mode $\omega = 0.0372$	17
3	Phase of stream function with beta.....	19
4	Frequencies of lowest normal modes.....	20
5	Amplitude and phase of stream function for lowest normal mode with $d/L = 0.1$	22
6	Variation of $k_{\alpha 1}(X)$ and $k_{\alpha 2}(X)$	30
7	Non-resonant response, frequency range II.....	33
8	Resonant response, frequency range IV.....	44
9	Stream function amplitude of Rossby wave.....	45
10	The two-layer model.....	48
11a	The root $m_1(s)$	58
11b	The root $m_2(s)$	59
11c	The root $m_3(s)$	60
11d	The root $m_4(s)$	61
12	Branch points of $m_j(s)$	64
13a	Growth rates for f plane.....	66
13b	Asymptotic phase speed and ratio of lower to upper layer stream function $\ell^2 = 0.25$	68

LIST OF ILLUSTRATIONS (Continued)

<u>Figure</u>		<u>Page</u>
14	Neutral dispersion, f plane.....	70
15	Flow on f plane.....	74
16	Growth rates for $\beta = 0.5$	78
17	Neutral dispersion relation $\beta = 0.5, \ell^2 = 0.25..$	81
18a	The root $m_1(s)$	82
18b	The root $m_2(s)$	83
18c	The root $m_3(s)$	84
18d	The root $m_4(s)$	85
18e	The root $m_5(s)$	86
18f	The root $m_6(s)$	87
19	Neutral dispersion relation $\beta = 0.5, \ell^2 = 1.....$	91
20	The contour for the Laplace transform inversion	94
21	Contour for $0 < x/t < 0.14$	96
22	Contour for $0.14 < x/t < 1.46$	97
23	Contour for $x/t > 1.46$	99

SOME EFFECTS OF TOPOGRAPHY AND VERTICAL SHEAR ON LOW-FREQUENCY OCEAN FLUCTUATIONS

1. Introduction

1.1 The barotropic model

A possible source for eddy motion in the open ocean is forcing by fluctuating winds. We explore this possibility by investigating the response to atmospheric forcing of a homogeneous ocean with an idealized coastline and bottom configuration. We consider a zonal channel on a beta plane with bottom topography varying in the along-channel direction. It is an attempt to represent some of the topographic features of the Drake Passage region, where an extensive set of experiments is presently being conducted.

Figure 1 shows the bathymetry of Drake Passage. It is assumed that the continental boundaries and the prominent North and South Scotia Arc systems are necessary components of the model since the dominant atmospheric scales are comparable with or exceed the Passage width. The bottom topography is rugged and complex. We shall confine ourselves to topography with scale comparable to the Passage width. In particular, there is a decrease in depth from the Pacific basin into Drake Passage. Neglect of smaller scale topography may be a serious omission, since topography at the internal radius of deformation may force baroclinic wave motions (see Rhines, 1977).

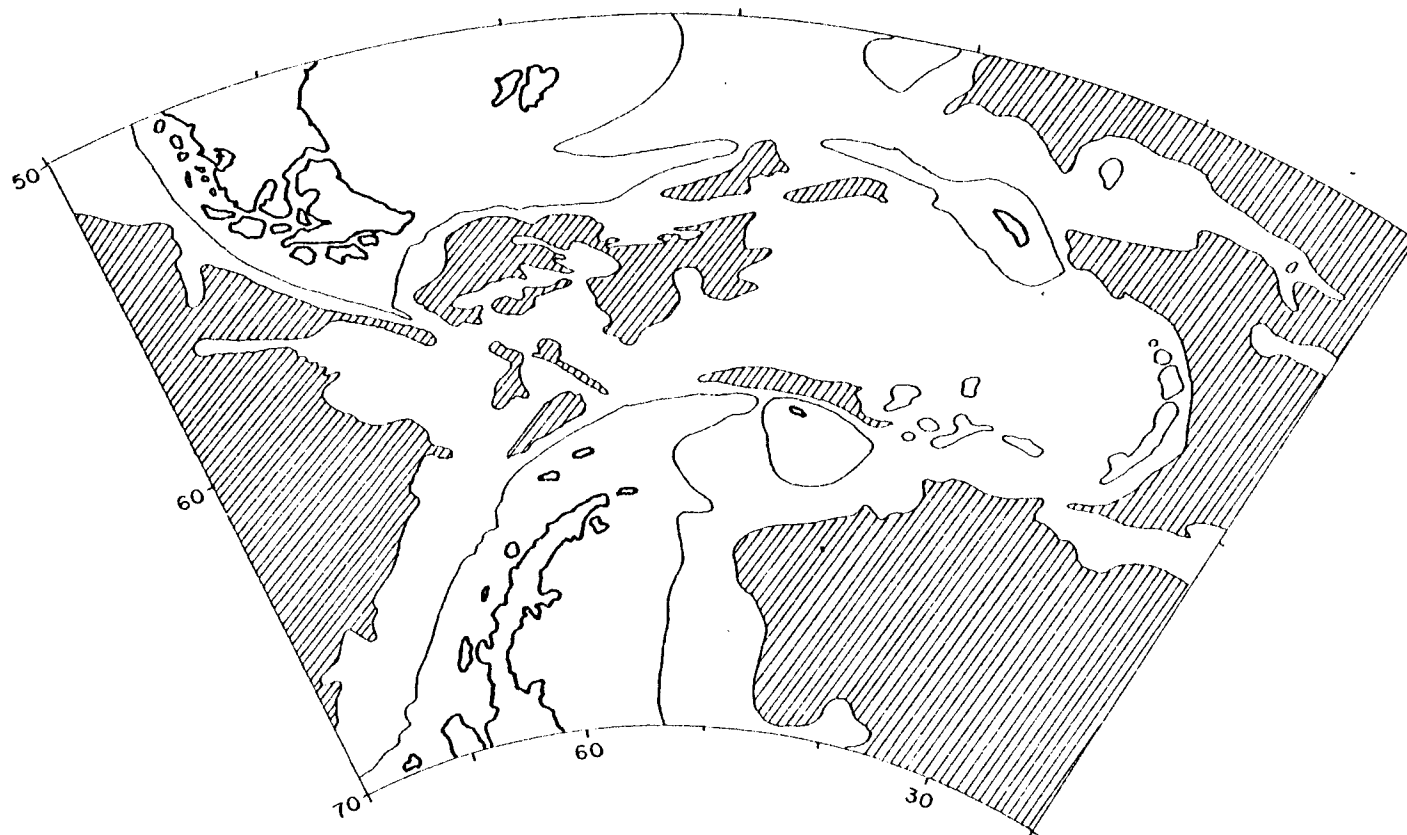


Figure 1. Bathymetry of the Drake Passage region (after Heezen, Tharp and Bentley, 1972). Depth contours of 2000 and 4000 m are drawn. Hatched areas indicate depths exceeding 4000 m.

Rhines (1969), Buchwald and Adams (1968) and Longuet-Higgins (1968a,b) have shown that an escarpment may guide wave energy. We anticipate that for an escarpment across a channel, reflections could result in a modal structure at certain frequencies. We shall calculate eigenfrequencies and the corresponding spatial structures. Waves trapped by topography have been found previously by Platzman (1975) in a numerical study of planetary-gravity normal modes of the Atlantic and Indian Oceans.

The problem is formulated in Section 2. Variable depth appears in variable coefficients in an elliptic equation which, in general, is not separable in the horizontal space coordinates. In Section 3 we choose a particular depth profile in which two uniform depth regions are joined by a region in which the depth varies exponentially. Formal series solutions can be written for each region and the solution is fully determined by matching at the boundaries between the regions. We examine the limit in which the width of the sloping region is decreased and a step discontinuity is approached.

Variable depth supports waves at higher frequency than exist in the surrounding uniform depth region thus resulting in trapped modes. At low enough frequency, however, wave energy which is generated over topography may radiate in the form of Rossby waves. We investigate this process under the approximation that the variable depth region merges slowly (topographic scale greatly exceeding wave scale) and smoothly into the uniform depth regions. Free

waves, described in Section 4, of a given frequency undergo a change in wave number as they propagate over the slowly varying topography. If, at some point, the local wavenumber of a free wave coincides with the wavenumber of the atmospheric forcing there is a form of resonant excitation. This is described in Section 5. The results are summarized in Section 6.

1.2 The instability problem

The remaining sections deal with a separate but related problem. Stratification and a mean current sheared in the vertical are added but the possibility of topographic oscillations is excluded.

Recent studies of the slow (small Rossby number) steady flow of a rotating stratified fluid on a beta plane have demonstrated how slight bottom topography may generate features such as eddies and meandering wakes (McCartney (1975, 1976) for example). These studies are of considerable interest in the interpretation of ocean circulation in the vicinity of seamounts and ridges. The steady solutions are not unique unless it is specified that no stationary wave is found in an "upstream" direction which is determined by group velocity (Lighthill, 1967). It has been recognized that the incoming flow in such models may be baroclinically unstable. If this is the case, random disturbances may grow in amplitude, but the steady solution is still of importance since it is forced by flow over topography. For a free wave in an

unstable system, the derivative of frequency by wavenumber may be complex and cannot be interpreted as a group velocity. Thus, the problem of determining the physically relevant steady solution is revived. Our purpose here is to show how this problem is resolved with an initial value approach.

Hogg (1976) has found that for a baroclinic flow in which the vertical shear varies continuously with depth, there are steady solutions with complex wavenumber. Hogg suggested these may represent stationary waves with growth downstream of topographic features. This remains a suggestion since details of the generation mechanism were not given. We shall discuss a simpler system than the one considered by Hogg (1976), that of a two-layer flow, with no horizontal shear, confined to a zonal channel on a beta plane.

We impose a north-south step at an initial instant and study the linearized disturbance. In the cases we consider, the flow is unstable in the temporal sense, and the transient contains growing waves. The growing wave packet may propagate upstream (the flow in upper and lower layers is taken to be in the same direction) in which case a steady state is not reached. If the upper and lower layer flow are sufficiently strong, the transient is advected completely downstream allowing a steady state to be established in the region between the step and the tail of the transient. We describe in detail the conditions which govern the behavior of the transient.

The initial value problem for a baroclinically unstable flow has been considered by Pedlosky (1976), Gadgil (1976) and Thacker (1976). Pedlosky (1976) was concerned primarily with finite amplitude effects but included a linearized initial value problem. With oscillatory forcing, at the frequency of a marginally unstable wave, a steady-state disturbance with spatial growth was generated. The system considered by Gadgil (1976) contained continuous stratification with density fluctuations caused by horizontal advection rather than by vertical velocity fluctuations. The instability in this system is at high wavenumber. The results of the present study are in agreement with the general features of Gadgil (1976). The problem and the techniques we employ are up to a point, equivalent to those of Thacker¹ (1976). We use a different asymptotic approximation (suggested but not carried out by Thacker) which has allowed us to extend his results somewhat. Furthermore, motivated by Hogg's (1976) work we discuss the steady solution which Thacker (1976) did not consider. It should be noted that when Thacker (1976) refers to a wave with spatial growth he is referring to an unstable transient which propagates away

¹ I became aware of Thacker (1976) only after the present study was essentially completed and a draft of the work was written. The earlier stages of this work are therefore redundant but are retained for continuity. It is of interest to compare the different fields in which spatial instability has been studied. Thacker (1976) cites work from plasma physics whereas Hogg (1976) cites work from homogeneous shear flow.

from the source region so that after a long enough time, the transient in the vicinity of the source is decaying. Our use of the term spatial growth is in reference to a steady wave (or perhaps one with purely oscillatory time dependence if there is an oscillating source) which amplifies away from the region of the source.

The approach presented here follows closely along lines developed by Gaster (1965, 1968) who studied instability in homogeneous shear flow. Gaster (1965) considered spatially growing waves excited by oscillatory forcing in an attempt to improve agreement between theory and laboratory experiments. Aspects of the unstable transient were discussed by Gaster (1968).

2. Formulation for barotropic model

Consider an infinite channel of width L , aligned in the zonal direction. Choose a coordinate system with the x axis eastward, the y axis poleward and the channel walls at $y = 0, L$. Assume the depth, h , varies only along the channel, i.e., $h = h(x)$ and that $dh/dx \rightarrow 0$ as $|x| \rightarrow \infty$. Forcing is by a surface wind stress, $\tau(t)$, which for simplicity is chosen to be zonal, uniform in space and oscillatory in time. It is indicated in Section 5 how the addition of a travelling disturbance with non-zero curl would modify the result. The linearized, inviscid vertically integrated shallow water wave equations are

$$u_t - fv = -g\eta_x + \tau/\rho h \quad (2.1)$$

$$v_t + fu = -g\eta_y \quad (2.2)$$

$$\eta_t + (hu)_x + (hv)_y = 0. \quad (2.3)$$

Here u and v are depth averaged velocity components in the x and y directions, η the elevation of the free surface above the equilibrium level, ρ the water density, g the acceleration of gravity and f the Coriolis parameter. Boundary conditions at the channel walls are that there be no normal flow. If $f^2 L^2 (gh)^{-1} \ll 1$ then fluctuations of the free surface, η_t in (2.3) may be neglected. Although this condition is not well satisfied for $L = 600$ km which is about the width of the deep part of Drake Passage, free

surface divergence is neglected. The effect of making this approximation is not completely clear and Longuet-Higgins (1968a) has found a case in which the inclusion of free surface divergence introduces a qualitative difference. A stream function, $\psi(x,y,t)$, can be defined as

$$hu = -\psi_y \quad hv = \psi_x \quad (2.4)$$

A potential vorticity equation is formed from (2.1) and (2.2) and the substitution of (2.4). With time dependence $e^{-i\omega f_0 t}$, where f_0 is a mean value of the Coriolis parameter, this equation is

$$\nabla^2 \psi - \frac{1}{h} \frac{dh}{dx} \psi_x + i \frac{\beta}{\omega} \psi_x + \frac{i}{\omega h} \frac{dh}{dx} \psi_y = 0 \quad (2.5)$$

The beta plane approximation has been made so that where f appears in (2.5) as a factor it is replaced by the constant f_0 and the y derivative of f is replaced by the constant $f_0 \beta$.

The wind stress does not appear explicitly in (2.5) since it was chosen to be uniform in space. In order to see how the wave motion is forced we rewrite the x -momentum balance (2.1) as

$$hu_t - hfv = -g(h\eta)_x + g \frac{dh}{dx} \eta + \frac{\tau}{\rho} \quad (2.6)$$

The term $g(dh/dx)\eta$ represents a topographic stress resulting from correlations between slope and bottom pressure. We integrate (2.6) from $x = -\gamma L$ to γL

$$\int_{-\gamma L}^{\gamma L} (hu_t - \frac{\tau}{\rho}) dx = \int_{-\gamma L}^{\gamma L} (hfv + g \frac{dh}{dx} \eta) dx - gh\eta \Big|_{-\gamma L}^{\gamma L} \quad (2.7)$$

and take the limit as $\gamma \rightarrow \infty$. For an isolated topographic feature the integrated topographic stress is finite. With free surface divergence neglected the zonally integrated meridional transport across a line of latitude is bounded. The zonal pressure difference is also bounded. The two terms on the left of (2.7) both $\rightarrow \infty$ as $\gamma \rightarrow \infty$ and must balance. This balance is represented in a stream function, $\phi(y)e^{-i\omega f_0 t}$ for the zonally averaged zonal flow

$$i\omega f_0 \frac{d\phi}{dy} = \frac{\tau_0}{\rho} \quad (2.8)$$

where $\tau = \tau_0 e^{-i\omega f_0 t}$. The total stream function is written as

$$\psi(x, y, t) = [\phi(y) + \phi(x, y)] e^{-i\omega f_0 t} \quad (2.9)$$

where $\phi(x, y)$ is the perturbation caused by topography. Since the zonal transport is independent of x (with free surface divergence neglected) the transport is contained entirely in $\phi(y)$ and appropriate boundary conditions for ϕ at the channel walls are $\phi = 0$ at $y = 0, L$. The foregoing steps are self-consistent but admittedly unrealistic. The basic question of how transport through Drake Passage is expected to vary with fluctuating wind is not resolved.

We substitute (2.9) in (2.5) to obtain

$$\nabla^2 \phi - \frac{1}{h} \frac{dh}{dx} \phi_x + i \frac{\beta}{\omega} \phi_x + \frac{i}{\omega h} \frac{dh}{dx} \phi_y = - \frac{i}{\omega h} \frac{dh}{dx} \phi_y \quad (2.10)$$

Boundary conditions as $|x| \rightarrow \infty$ are that ϕ remain bounded or if the solution is wavelike, that group velocity be outgoing. The second term in (2.10) is relatively unimportant and its neglect is equivalent to assuming quasi-geostrophy.

3. Trapped modes, exponential depth

In this section a numerical method is used to study the character of trapped wave solutions. The topography consists of two regions of uniform depth separated by a sloping region in which the depth is exponential;

$$h(x) = \begin{cases} h_0 & x < 0 \\ h_0 e^{-bx} & 0 < x < d \\ h_1 & x > d \end{cases} \quad (3.1)$$

where $h_1 = h_0 e^{-bd}$. The usefulness of the exponential depth dependence is that the coefficients in (2.10) are constant.

In the uniform depth regions (2.10) becomes

$$\nabla^2 \phi + i \frac{\beta}{\omega} \phi_x = 0 \quad (3.2)$$

Solutions satisfying the boundary conditions can be written as series in the cross-channel eigenfunctions

$$\phi(x,y) = \begin{cases} \sum_n A_n e^{-i\beta x/2\omega + \kappa_n x} \sin(n\pi y/L) & x < 0 \\ \sum_n D_n e^{-i\beta x/2\omega - \kappa_n x} \sin(n\pi y/L) & x > d \end{cases} \quad (3.3)$$

where $\kappa_n = (n^2\pi^2/L^2 - \beta^2/4\omega^2)^{1/2}$

These correspond to propagating Rossby waves if $\beta^2/4\omega^2 > n^2\pi^2/L^2$. The highest frequency for which a Rossby wave exists is $\omega = \beta L/2\pi$ which is the $n = 1$ cross-channel eigenfunction. This is equiva-

lent to a period of about 2 months for $L = 600$ km. In this section only frequencies greater than this cutoff are discussed, so that waves are trapped.

Over the sloping region (2.10) is

$$\nabla^2 \phi + (b + i\frac{\beta}{\omega}) \phi_x - i\frac{b}{\omega} \phi_y = i\frac{b}{\omega} \phi_y \quad (3.4)$$

We again expand in series in the cross-channel eigenfunctions

$$\begin{aligned} \phi(x,y) &= e^{iby/2\omega} \sum_n \phi_n(x) \sin(n\pi y/L) \\ i\frac{b}{\omega} \phi_y &= e^{iby/2\omega} \sum_n \phi_n \sin(n\pi y/L) \end{aligned} \quad (3.5)$$

and obtain

$$\frac{d^2}{dx^2} \phi_n + (b + i\frac{\beta}{\omega}) \frac{d}{dx} \phi_n + \left(\frac{b^2}{4\omega^2} - \frac{n^2\pi^2}{L^2} \right) \phi_n = \phi_n \quad (3.6)$$

This has a particular solution

$$\phi_n = \frac{\phi_n}{\frac{b^2}{4\omega^2} - \frac{n^2\pi^2}{L^2}} \quad (3.7)$$

and free solution

$$\phi_n(x) = B_n e^{ik_{n1}x} + C_n e^{ik_{n2}x} \quad (3.8)$$

where

$$\left. \begin{matrix} k_{n1} \\ k_{n2} \end{matrix} \right\} = -\frac{\beta}{2\omega} + \frac{ib}{2} \pm \left[-\frac{1}{4}(b + i\frac{\beta}{\omega})^2 + \frac{b^2}{4\omega^2} - \frac{n^2\pi^2}{L^2} \right]^{1/2} \quad (3.9)$$

Across $x = 0$ and $x = d$, ϕ and ϕ_x must be continuous.

Observe that (3.5) may be rewritten as

$$\phi(x,y) = \sum_m \sum_n a_{mn} \phi_n(x) \sin(m\pi y/L) \quad (3.10)$$

$$i\frac{b}{\omega} \phi_y(y) = \sum_m \sum_n a_{mn} \phi_n \sin(m\pi y/L)$$

where

$$a_{mn} = \frac{2}{L} \int_0^L e^{iby/2\omega} \sin(n\pi y/L) \sin(m\pi y/L) dy$$

The Fourier coefficients in (3.10) and (3.3) are equated in the matching conditions resulting in four systems of equations for the coefficients A_n , B_n , C_n and D_n . The series are truncated to give a matrix eigenvalue problem although frequency does not appear in the matrix in the same form as in conventional problems. Eigenfrequencies are found by setting $\phi_n = 0$, varying ω and locating the zeros of the determinant. The lowest modes are well approximated by a relatively small truncation point (eight Fourier terms were used). This procedure of a series expansion and matching along boundaries has been used in a number of wave problems with simple geometry and more details may be found in Webb (1976), Mooers (1976), Mofjeld and Rattray (1971) and Taylor (1922).

The gravest modes (those with largest spatial scale and highest frequency) for zero beta, $d = L$ and $h_1 = 0.6 h_0$ are shown in Figure 2. The amplitude and phase of the complex stream

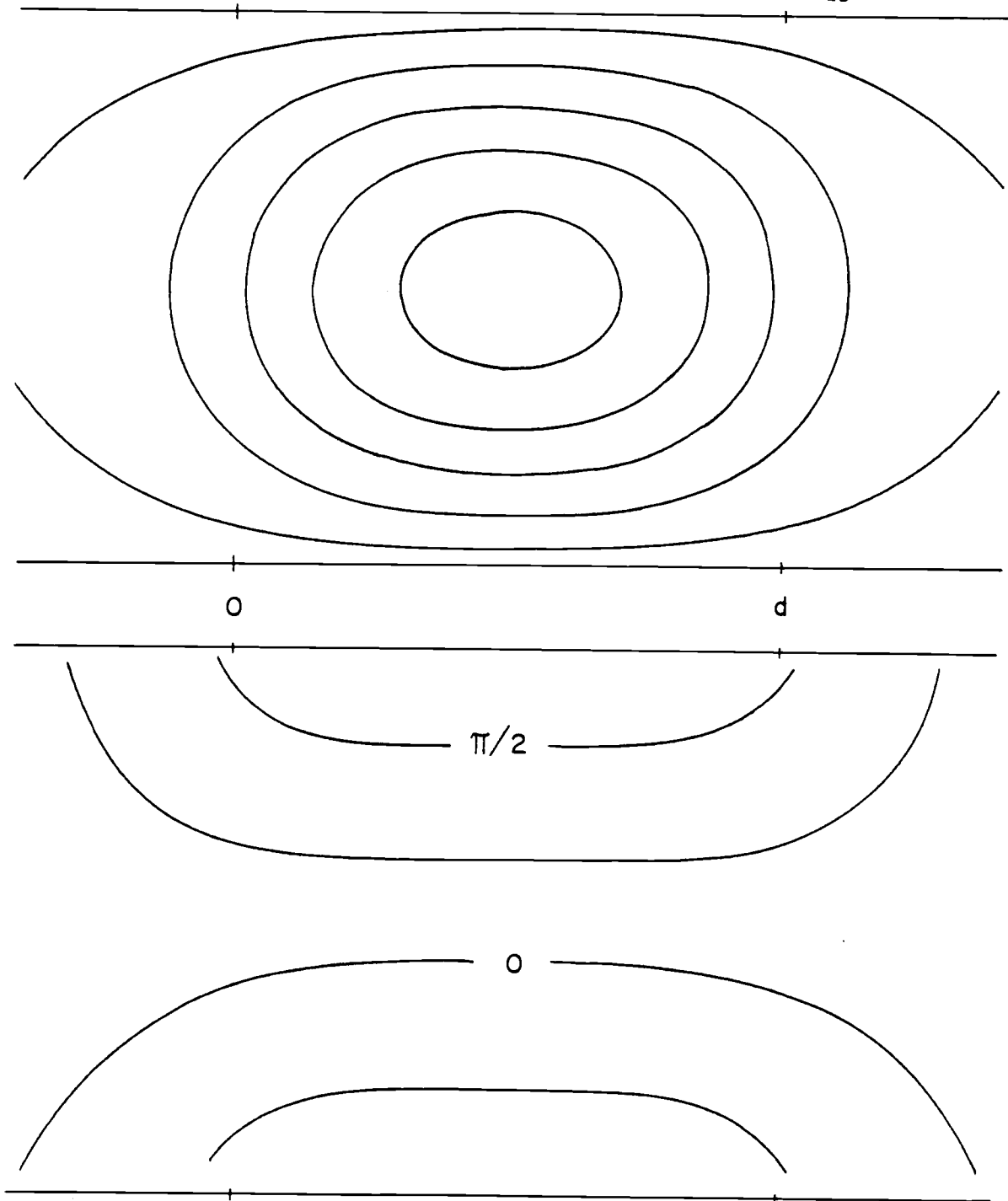


Figure 2a. Amplitude (top) and phase (bottom) of stream function for normal mode $\omega = 0.0652$ with $d/L = 1$, $\beta = 0$ and $h_1/h_0 = 0.6$. Amplitude is to within an arbitrary constant and is maximum at centre. Phase is to within an arbitrary constant and direction is for Northern Hemisphere.

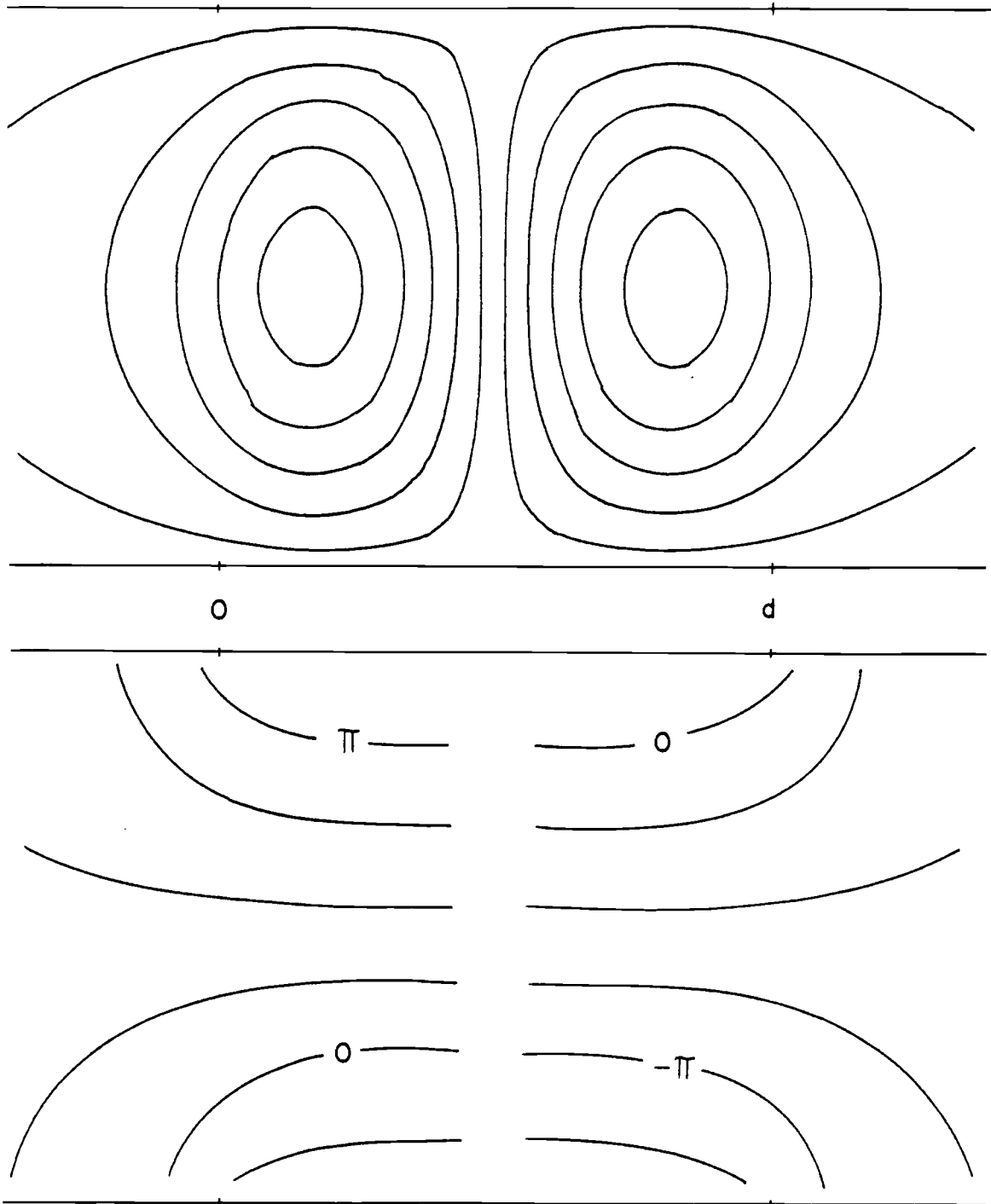


Figure 2b. Amplitude (top) and phase (bottom) of stream function for normal mode with $\omega = 0.0433$. The two amplitude maxima are out of phase. Other parameters are as in Figure 2a.

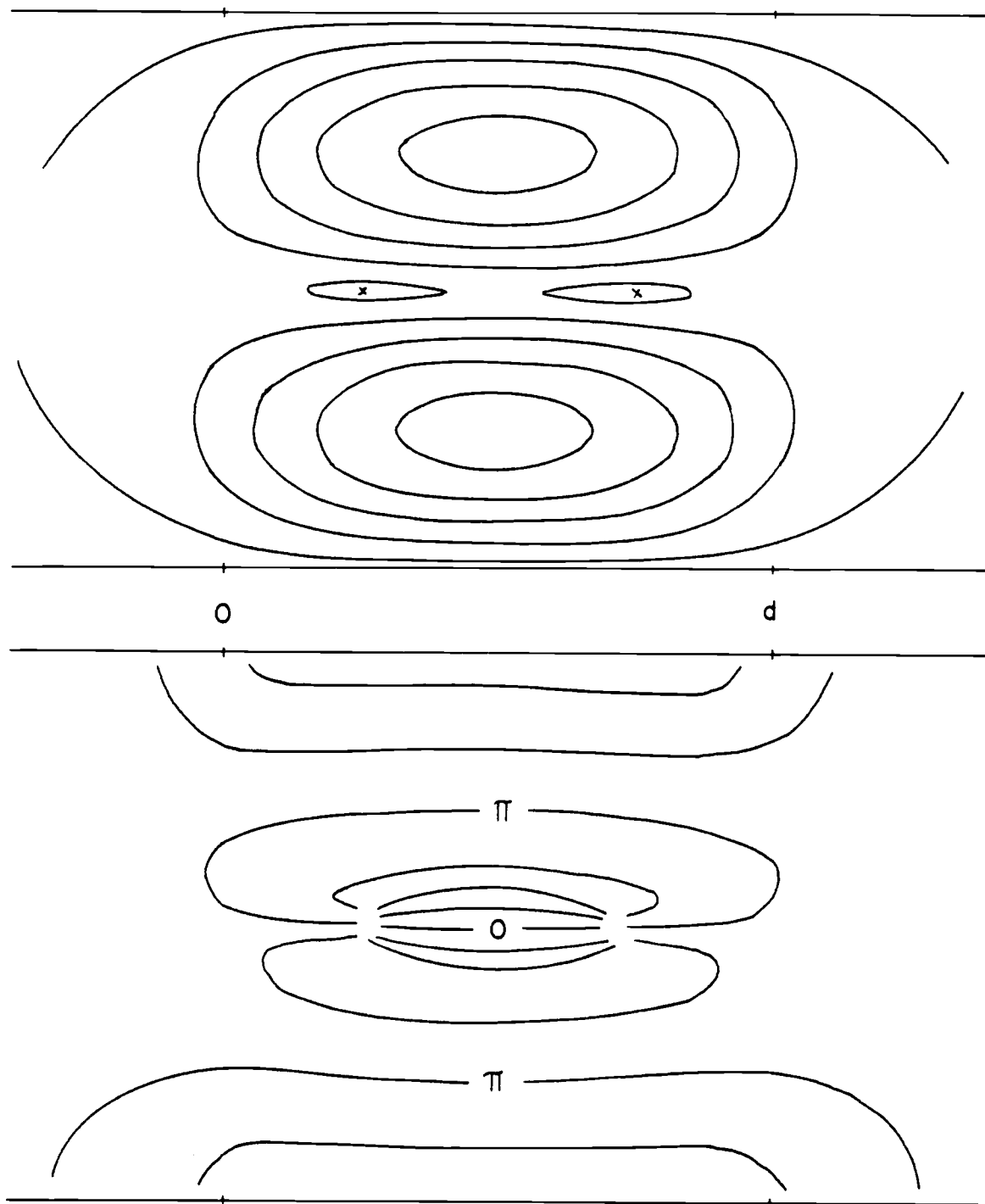


Figure 2c. Amplitude (top) and phase (bottom) of stream function for normal mode with $\omega = 0.0372$. The points marked \times are amphidromic points. Other parameters are as in Figure 2a.

function are drawn. They are characterized by integral numbers of amplitude maxima in the x and y directions. There is a phase propagation along depth contours to the left (right) in the Northern (Southern) Hemisphere when facing shallow water.

For beta non-zero it is found that complex eigenfrequencies result. Complex frequencies in this problem do not have physical relevance. If, however, the second term in (2.10) is neglected, it is found that real eigenfrequencies result. This term was neglected and in Figure 3 the phase for the gravest mode with weak beta, $\beta/b = 0.2$ is drawn. The amplitude is indistinguishable from the lowest mode with zero beta. There is a westward component to the phase propagation. One might compare Figures 2 and 3 with the 48.8 h mode calculated by Platzman (1975) (his Figure 3) which appears to be trapped by the South Scotia Ridge.

The channel model in this study has similarities to a sloping step in an infinite ocean and to a closed rectangular basin with sloping bottom (Veronis, 1966). It would be helpful to draw comparisons. Provided that $d/L \geq 1$, the modes calculated here resemble the modes which would exist if walls were placed at $x = 0, d$ in the sense that there is a one to one correspondence between modes with similar structure. The variation of eigenfrequencies with d/L as h_1/h_0 is kept constant is also similar. This is shown in Figure 4 for the lowest few modes. The dashed lines on the right are the basin eigenfrequencies.

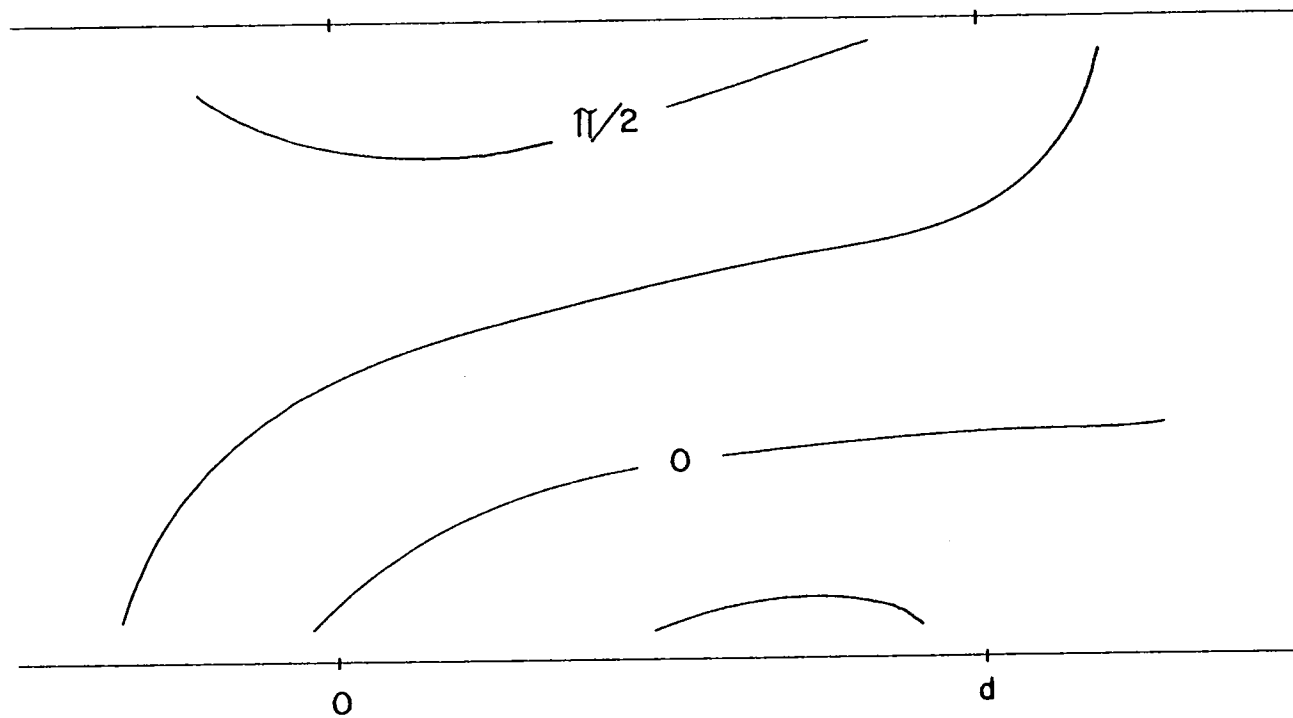


Figure 3. Phase of stream function of lowest mode, $\omega = 0.0666$ with $\beta/b = 0.2$, $d/L = 1$ and $h_1/h_0 = 0.6$.

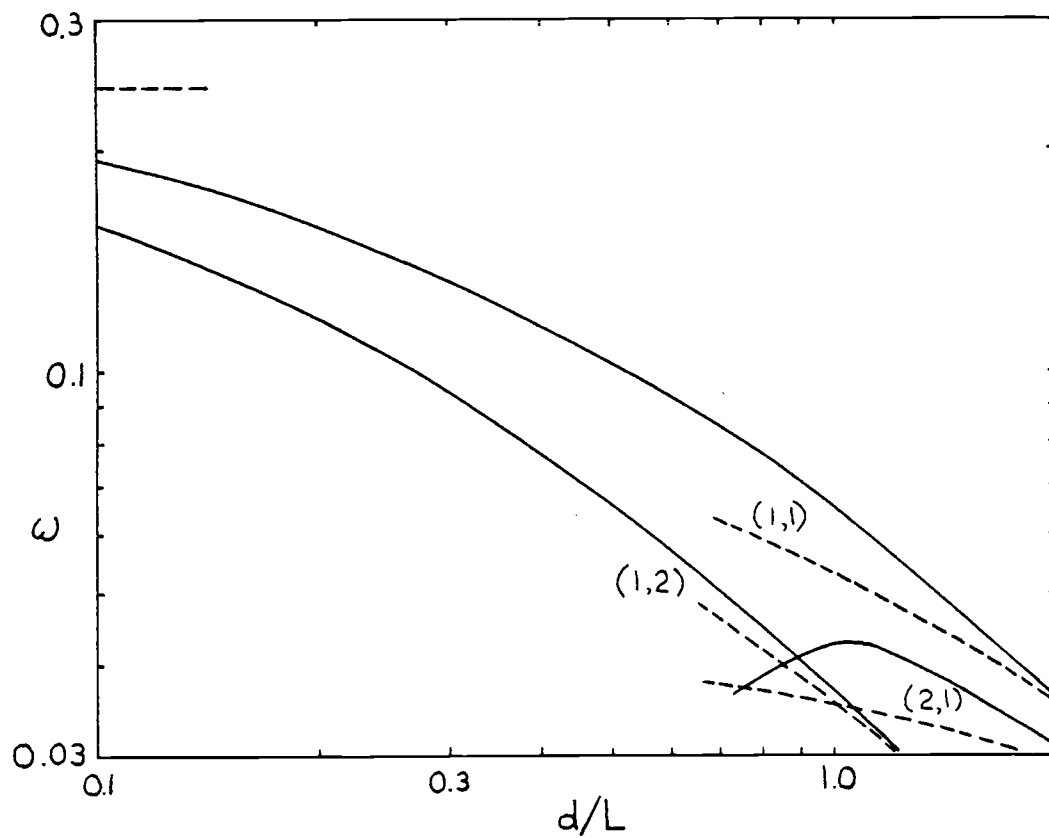


Figure 4. Frequencies of lowest normal modes as functions of d/L with $\beta = 0$ and $h_1/h_0 = 0.6$. Dashed lines at right are eigenfrequencies if walls are placed at $x = 0, d$. Dashed line at left is limiting frequency for a step discontinuity. The notation $(1,2)$ corresponds to a single amplitude maximum in the x direction, and two amplitude maxima in the y direction.

The resemblance begins to fail as d becomes smaller than L . The lowest x -modes (those with a single amplitude maximum in the x direction) have greatest eigenfrequencies for d/L small; higher x -modes have eigenfrequencies tending to zero. The currents for the lowest x -modes are no longer confined to the sloping region. This is evident in Figure 5 for the lowest normal mode with $d/L = 0.1$. Rhines (1969) and Buchwald and Adams (1968) have shown that the lowest mode trapped wave over a sloping step in an unbounded ocean has group velocity along the step but as the wavenumber component in the direction along the step is varied, the direction of group velocity does not reverse, (Longuet-Higgins (1968a) showed this was not true if free surface divergence is included). Waves with this property cannot form a normal mode. Thus the channel walls not only quantize the wavenumber but alter the behavior qualitatively.

A step discontinuity in an unbounded ocean with constant Coriolis parameter supports trapped waves decaying away from the step at the single frequency $\omega = (h_0 - h_1)/(h_0 + h_1)$ independent of wavenumber component along the step (Rhines, 1969). This frequency is indicated as the dashed line at the left of Figure 4. The limit of a step discontinuity is a degenerate one in the sense that all modes with a single amplitude maximum in the x -direction approach a single eigenfrequency.

If the forcing terms are non-zero the amplitude of the response would be unbounded at the eigenfrequencies. The depth

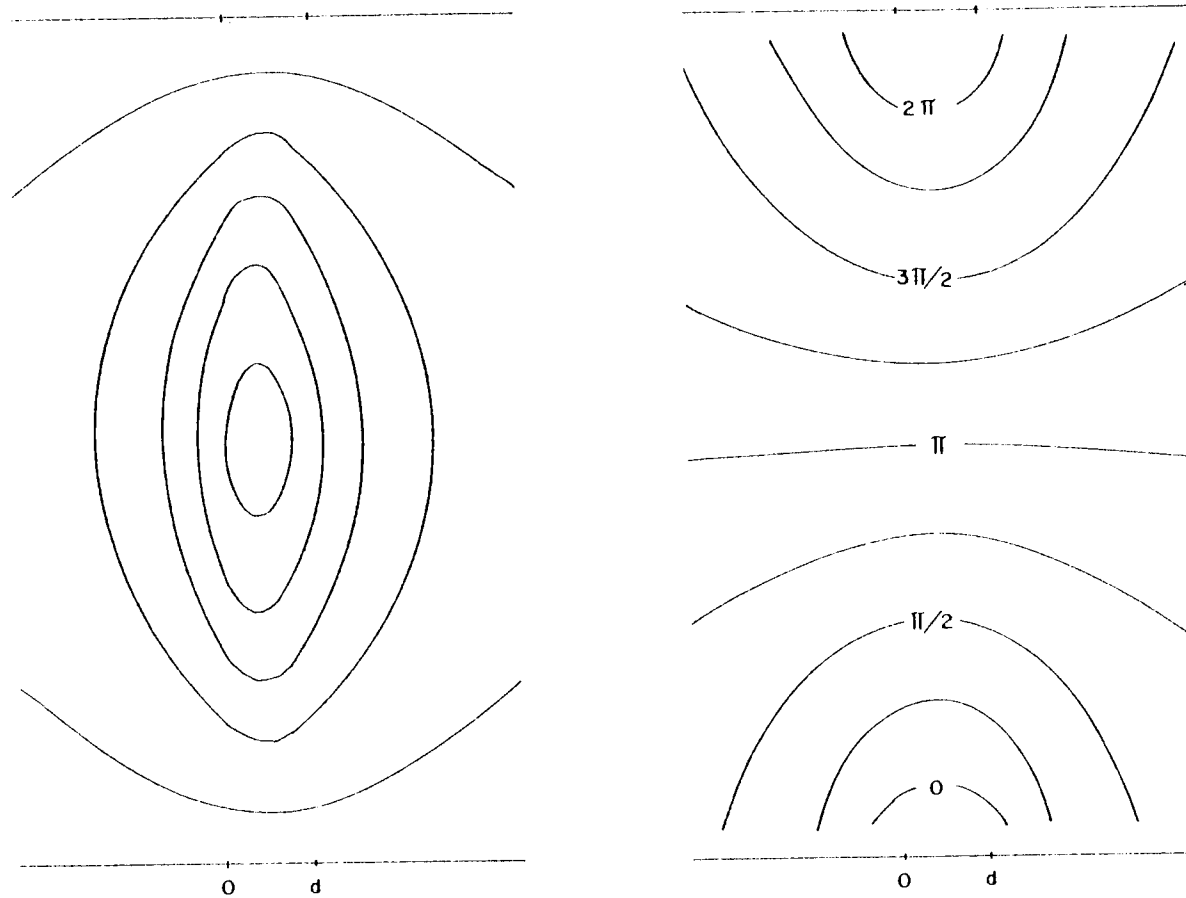


Figure 5. Amplitude (left) and phase (right) of stream function for lowest normal mode with $d/L = 0.1$, $\beta = 0$, $h_1/h_0 = 0.6$.

profile in this section was not used to study the response with $\omega < \beta L/2\pi$ for which Rossby waves may radiate energy. One reason is that the particular solution (3.7) becomes singular at the frequency at which a wave over the slope is resonant with the wind, both having zero x-wavenumber. A depth profile with discontinuities in slope is valid for long waves insensitive to details of the profile. In Drake Passage wave scales are restricted and may be less than significant topographic scales. A continuously varying slope is desirable and this is employed in the next two sections with short waves. The real justification for the short wave limit is that the resonant forcing mechanism is clarified.

4. Short wavelength limit, free waves

If the topography is considered to be smoothly varying and the wave scale is much smaller than both the topographic scale and the planetary scale, certain instructive analytical results may be obtained. This short wavelength, long period limit was described by Smith (1971). Let the depth vary on a long scale X defined $X = \epsilon x$ where $\epsilon \ll 1$, i.e. $h = h(X)$. Define $\tilde{\beta}$ as $\tilde{\beta} = \beta/\epsilon$ where $\tilde{\beta} = 0$ (1). Finally rescale frequency by defining $\tilde{\omega} = \omega/\epsilon$. Equation (2.10) becomes

$$\phi_{xx} + \phi_{yy} - \epsilon \frac{h'}{h} \phi_x + i \frac{\tilde{\beta}}{\tilde{\omega}} \phi_x + i \frac{h'}{\tilde{\omega}h} \phi_y = - i \frac{h'}{\tilde{\omega}h} \phi_y \quad (4.1)$$

where primes denote differentiation with respect to X . Henceforth we shall omit the tildes.

We expand

$$\begin{aligned} \phi(x,y) &= e^{-i \frac{h'}{2\omega h} y} \sum \phi_n(x) \sin(n\pi y/L) \\ - i \frac{h'}{\omega h} \phi_y &= e^{-i \frac{h'}{2\omega h} y} \sum \phi_n(X) \sin(n\pi y/L) \end{aligned} \quad (4.2)$$

and substitute in (4.1) to obtain

$$\begin{aligned} &\sum \left[\frac{d^2}{dx^2} \phi_n + i \frac{\beta}{\omega} \frac{d}{dx} \phi_n + \left(\frac{h'^2}{4\omega^2 h^2} - \frac{n^2 \pi^2}{L^2} \right) \phi_n \right. \\ &+ \epsilon P(X,y) \frac{d}{dx} \phi_n + \epsilon Q(X,y) \phi_n \left. \right] \sin(n\pi y/L) \\ &= \sum \phi_n(X) \sin(n\pi y/L) \end{aligned} \quad (4.3)$$

$$\text{where } P(X,y) = -\frac{i}{\omega} \left(\frac{h'}{h}\right)' y - \frac{h'}{h}$$

$$\text{and } Q(X,y) = \frac{\beta}{2\omega^2} \left(\frac{h'}{h}\right)' y + \varepsilon \left[-i \left(\frac{h'}{h}\right)'' \frac{y}{2\omega} - \frac{1}{4\omega^2} \left(\frac{h'}{h}\right)'^2 y^2 + \frac{i}{2\omega} \frac{h'}{h} \left(\frac{h'}{h}\right)' y \right].$$

With the further expansions

$$\begin{aligned} P(X,y) \sin(m\pi y/L) &= \sum_{n=1}^{\infty} P_{nm}(X) \sin(n\pi y/L) \\ Q(X,y) \sin(m\pi y/L) &= \sum_{n=1}^{\infty} Q_{nm}(X) \sin(n\pi y/L) \end{aligned} \quad (4.4)$$

the Fourier coefficients in (4.3) may be equated giving

$$\begin{aligned} \frac{d^2}{dx^2} \phi_n + i \frac{\beta}{\omega} \frac{d}{dx} \phi_n + \left(\frac{h'^2}{4\omega^2 h^2} - \frac{n^2 \pi^2}{L^2} \right) \phi_n + \varepsilon \sum_{m=1}^{\infty} \\ \left(P_{nm} \frac{d}{dx} \phi_m + Q_{nm} \phi_m \right) = \phi_n(X) \quad n = 1, 2, \dots \end{aligned} \quad (4.5)$$

Observe that the partial differential equation (4.1) has been reduced to a system of ordinary differential equations. They are coupled at $O(\varepsilon)$ and the coefficients in the equations are slowly varying. Asymptotic expansions to systems of equations such as (4.5) are described by Feshchenko, Shkil' and Nikolenko (1967, Chapter 6).

In this section we examine solutions to the homogeneous part of (4.5). The procedure we shall follow is to expand $\phi_n(x)$ in a power series in ε . The $O(1)$ balance of terms in (4.5) determines a

wavenumber which varies with the slowly varying topography. The $O(\epsilon)$ balance of terms in (4.5) determines first how the amplitude of a wave varies along the channel and secondly the nature of the coupling.

Assume a solution of the form

$$\phi_n(x) = A_n(X) e^{i\theta} \quad n = 1, 2, \dots \quad (4.6)$$

where

$$\frac{d}{dx}\theta = k(X) .$$

Let the amplitude $A_n(X)$ have an expansion

$$A_n(X) = \sum_{j=0}^{\infty} \epsilon^j A_{jn}(X) \quad n = 1, 2, \dots \quad (4.7)$$

Suppose that only a single term $n = \alpha$ in the Fourier series is non-zero at $O(1)$

$$A_{0n}(X) = A_{0\alpha}(X) \delta_{n\alpha} \quad n = 1, 2, \dots \quad (4.8)$$

($\delta_{n\alpha}$ is the Kronecker delta). The general solution is then a superposition.

With (4.6) substituted in (4.5) the result is

$$\begin{aligned} & \left[-k^2 - \frac{\beta}{\omega} k + \left(\frac{h'^2}{4\omega^2 h^2} - \frac{n^2 \pi^2}{L^2} \right) \right] A_n + \epsilon \left[i(2k + \frac{\beta}{\omega}) A'_n \right. \\ & \left. + ik'A_n \right] + i\epsilon k \sum_{m=1}^{\infty} P_{nm} A_m + \epsilon \sum_{m=1}^{\infty} Q_{nm} A_m + \epsilon^2 \sum_{m=1}^{\infty} P_{nm} A'_m = 0 \end{aligned} \quad (4.9)$$

The series (4.7) is substituted in (4.9) and the $O(1)$ balance of

terms gives

$$\left[-k^2 - \frac{\beta}{\omega} k + \left(\frac{h'^2}{4\omega^2 h^2} - \frac{n^2 \pi^2}{L^2} \right) \right] A_{0n} = 0. \quad (4.10)$$

From (4.8), $A_{0\alpha} \neq 0$ thus the wavenumber $k(X)$, must satisfy

$$k^2 + \frac{\beta}{\omega} k - \left(\frac{h'^2}{4\omega^2 h^2} - \frac{\alpha^2 \pi^2}{L^2} \right) = 0 \quad (4.11)$$

with roots k_{α_1} and k_{α_2} given by

$$\begin{aligned} k_{\alpha_1} &= -\frac{\beta}{2\omega} + q_{\alpha}(x)^{\frac{1}{2}} \\ k_{\alpha_2} &= -\frac{\beta}{2\omega} - q_{\alpha}(X)^{\frac{1}{2}} \end{aligned} \quad (4.12)$$

where $q_{\alpha}(X) = \frac{\beta^2}{4\omega^2} + \frac{h'^2}{4\omega^2 h^2} - \frac{\alpha^2 \pi^2}{L^2}$.

In this section we consider only the case $\omega < \beta L / 2\alpha\pi$ so that $q_{\alpha}(X)$ is positive everywhere, $k_{\alpha_1}(X)$ and $k_{\alpha_2}(X)$ are real and the solution is everywhere wavelike. The variation of $k_{\alpha_1}(X)$ and $k_{\alpha_2}(X)$ with X is sketched in Figure 6. The case $\omega > \beta L / 2\alpha\pi$ for which it is possible that $q_{\alpha}(X)$ is positive over the maximum topographic slope and negative elsewhere is discussed in the next section on the forced response. With $\omega < \beta L / 2\alpha\pi$, away from the topographic feature $h'(X) \rightarrow 0$ and (4.12) is simply a dispersion relation for Rossby waves in a channel. The x component of wavenumber k_{α_1} corresponds to the Rossby wave with longer wavelength and westward group velocity. The second root, k_{α_2} corresponds to the Rossby wave with eastward group velocity.

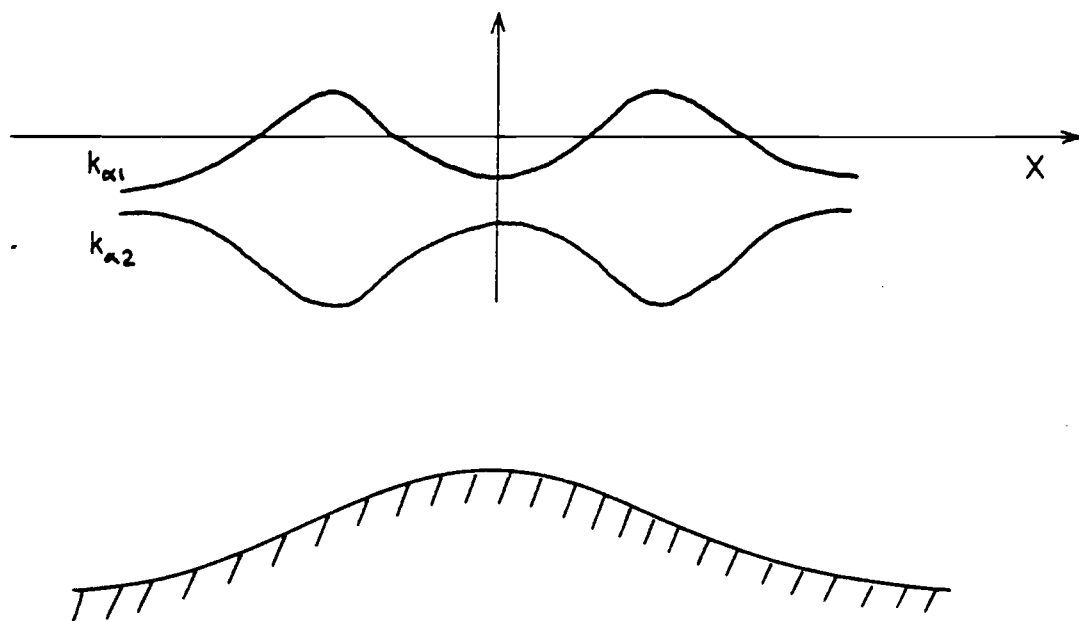


Figure 6. Variation of $k_{\alpha 1}(X)$ and $k_{\alpha 2}(X)$ for typical bottom topography in frequency range for which the solution is wavelike everywhere.

The $O(\epsilon)$ balance of terms in (4.9) is

$$\left[-k_{\alpha}^2 - \frac{\beta}{\omega} k_{\alpha} + \left(\frac{h'^2}{4\omega^2 h^2} - \frac{n^2 \pi^2}{L^2} \right) \right] A_{1n} + i \left(2k_{\alpha} + \frac{\beta}{\omega} \right) A'_{0n} + ik'_{\alpha} A_{0n} + ik_{\alpha} P_{n\alpha} A_{0\alpha} + Q_{n\alpha} A_{0\alpha} = 0 \quad (4.13)$$

The term in brackets vanishes for $n = \alpha$ which gives an equation for $A_{0\alpha}(X)$

$$i \left(2k_{\alpha} + \frac{\beta}{\omega} \right) A'_{0\alpha} + \left(ik'_{\alpha} + ik_{\alpha} P_{\alpha\alpha} + Q_{\alpha\alpha} \right) A_{0\alpha} = 0 \quad (4.14)$$

or

$$A_{0\alpha}(X) = \exp \left[- \int^X \frac{ik'_{\alpha} + ik_{\alpha} P_{\alpha\alpha} + Q_{\alpha\alpha}}{i(2k_{\alpha} + \beta/\omega)} dX \right] \quad (4.15)$$

For $n \neq \alpha$, the term in brackets in (4.13) is non-zero allowing the $O(\epsilon)$ corrections to be evaluated. We find

$$A_{1n}(X) = \frac{ik_{\alpha} P_{n\alpha} + Q_{n\alpha}}{k_{\alpha}^2 + \frac{\beta}{\omega} k_{\alpha} - \left(\frac{h'^2}{4\omega^2} - \frac{n^2 \pi^2}{L^2} \right)} A_{0\alpha}(X) \quad (4.16)$$

The higher order coefficients may be determined recursively in this manner.

Thus we have obtained a solution for a single non-zero term from the Fourier series (4.2) at $O(1)$. From (4.16), at higher order there are non-zero coefficients for $n \neq \alpha$. These terms vanish as $h'(X) \rightarrow 0$ from (4.16) and (4.4). Furthermore from (4.6) and (4.7) the solution at all orders is described by a single x component of wavenumber, either $k_{\alpha 1}(X)$ or $k_{\alpha 2}(X)$. This means that

an incident wave changes its form over the topographic feature but passes over it without a reflected wave and without energy scattered and radiated by waves of different wavenumber.

5. Short wavelength limit, forced waves

The inhomogeneous problem (4.5) is now examined. Only the leading order asymptotic approximation has been evaluated.

Consider the $n = \alpha$ term from the Fourier series in (4.5) with neglect of $O(\epsilon)$ terms

$$\frac{d^2}{dx^2} \phi_\alpha + i \frac{\beta}{\omega} \frac{d}{dx} \phi_\alpha + r_\alpha(X) \phi_\alpha = \phi_\alpha(X) \quad (5.1)$$

where

$$r_\alpha(X) = \frac{h'^2}{4\omega^2 h^2} - \frac{\alpha^2 \pi^2}{L^2} \quad \text{and} \quad q_\alpha(X) = \frac{\beta^2}{4\omega^2} + r_\alpha(X)$$

The response depends on the forcing frequency. Suppose that the maximum bottom slope exceeds the beta effect, $(h'/h)_{\max} > \beta$. Four frequency ranges can be distinguished by the zeros or absence of zeros in $r_\alpha(X)$ and $q_\alpha(X)$. They are defined in Table 1. We shall discuss the different cases in order of decreasing frequency. For sufficiently high frequency, $r_\alpha(X)$ is negative everywhere (frequency ranges I and II) and an approximate solution to (5.1) is

$$\phi_\alpha(X) = \phi_\alpha(X) / r_\alpha(X) \quad (5.2)$$

This is a response on the slowly varying topographic scale.

It is sketched in Figure 7 for $h(X) = h_0 \exp(-(1+X^2)^{-2})$.

The flow is nearly zonal. Vortex stretching over topography is balanced by an oscillating horizontal shear.

Table 1. Frequency ranges for different types of response.

I	$r_{\alpha}(X) < 0$ everywhere	$q_{\alpha}(X) < 0$ everywhere
II		$q_{\alpha}(X) > 0$ over topography
III	$r_{\alpha}(X) > 0$ over topography	$q_{\alpha}(X) > 0$ over topography
IV		$q_{\alpha}(X) > 0$ everywhere

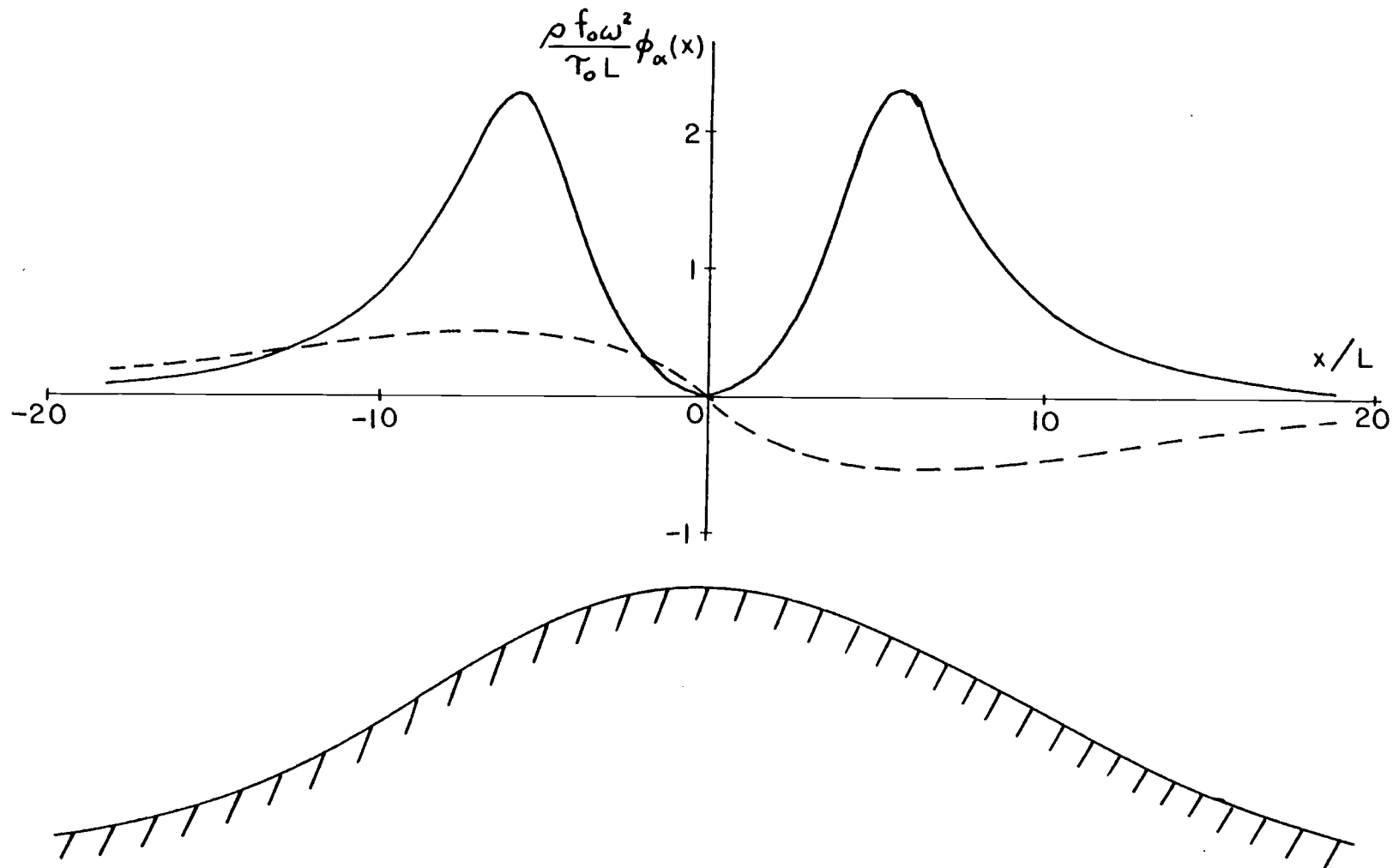


Figure 7. Nonresonant response, frequency range II. Real (solid line) and imaginary (dashed line) part of $\phi_\alpha(x)$ scaled by $\tau_0 L / \rho f_0 \omega^2$. Parameters are $\omega = 0.119$, $\beta L = 0.5$, $\epsilon = 0.1$, $\alpha = 1$ and $h(x) = h_0 \exp (-(1 + x^2)^{-1})$.

5.1 Trapped waves

The response (5.2) breaks down for frequency ranges III and IV for which $r_\alpha(X)$ crosses zero at several points. We let

$$\phi_\alpha(x) = \tilde{\phi}_\alpha(x) e^{-i\frac{\beta}{2\omega} x}$$

then (5.1) becomes

$$\frac{d^2}{dx^2} \tilde{\phi}_\alpha + q_\alpha(X) \tilde{\phi}_\alpha = e^{i\frac{\beta}{2\omega} x} \phi_\alpha(X)$$

which can be written

$$\frac{d^2}{dX^2} \tilde{\phi}_\alpha + \epsilon^{-2} q_\alpha(X) \tilde{\phi}_\alpha = \epsilon^{-2} e^{i\frac{\beta}{2\omega} \frac{X}{\epsilon}} \phi_\alpha(X) \quad (5.3)$$

In frequency range III, over the maximum bottom slope, $q_\alpha(X)$ is positive and free solutions are wavelike. Away from the topographic feature, $q_\alpha(X)$ is negative and solutions are decaying. The points at which $q_\alpha(X)$ are zero are known as turning points. Let us consider the typical case of two turning points, μ_1 and μ_2 with $\mu_1 < \mu_2$ so that $q_\alpha(X)$ is of the form

$$q_\alpha(X) = (X - \mu_1)(\mu_2 - X) f(X) \quad (5.4)$$

where $f(X) > 0$ everywhere.

We shall find solutions valid about each turning point then match them in the region of common validity which is $\mu_1 < X < \mu_2$. Considering first the turning point μ_1 we transform (5.3) into an

equation for which the solutions are known. This is the Langer transformation (Langer, 1949) which is outlined in Nayfeh (1973, Chapter 7). Let $\zeta_1(X)$ be defined by

$$\zeta_1' \zeta_1 = q_\alpha(X)^{1/2} \quad (5.5)$$

or

$$\begin{aligned} \frac{2}{3} \zeta_1^{3/2} &= \int_{\mu_1}^X \sqrt{(\xi - \mu_1)(\mu_2 - \xi)f(\xi)} \, d\xi \quad \mu_1 < X < \mu_2 \\ \frac{2}{3} (-\zeta_1)^{3/2} &= \int_X^{\mu_1} \sqrt{(\mu_1 - \xi)(\mu_2 - \xi)f(\xi)} \, d\xi \quad X < \mu_1 \end{aligned} \quad (5.6)$$

Note that the term under the radical in the first integral of (5.6) becomes negative and hence the definition becomes invalid for $X > \mu_2$. We now define a new dependent variable $Z_1(\zeta_1)$ as

$$Z_1(\zeta_1) = \zeta_1^{1/2} \tilde{\phi}_\alpha \quad (5.7)$$

The transformed (5.4) is

$$\frac{d^2}{d\zeta_1^2} Z_1 + \epsilon^{-2} \zeta_1 Z_1 = \epsilon^{-2} g(\zeta_1) \quad (5.8)$$

where

$$g(\zeta_1) = \frac{e^{i\frac{\beta}{2\omega} \frac{X}{\epsilon}} \phi_\alpha(X)}{\zeta_1^{3/2}} \quad (5.9)$$

We recognize the homogeneous part of (5.8) as the Airy equation.

The complementary solution which vanishes as $X \rightarrow -\infty$ is

$$Z_1 = a \operatorname{Ai}(-\epsilon^{-2/3} \zeta_1)$$

where a is a constant. A particular solution can be constructed if we write

$$g(\zeta_1) = g(0) + [g(\zeta_1) - g(0)]$$

A solution satisfying $(g(\zeta_1) - g(0))$ on the right of (5.8) and which is uniformly valid about $X = \mu_1$ is

$$Z_1 = \frac{g(\zeta_1) - g(0)}{\zeta_1}$$

The solution which satisfies $g(0)$ on the right side of (5.8) and which is bounded as $X \rightarrow -\infty$ is

$$Z_1 = -\epsilon^{-2/3} \pi g(0) \operatorname{Gi}(-\epsilon^{-2/3} \zeta_1)$$

(See Abramowitz and Stegun (1965), Section 10.4 for an outline of the properties of Gi).

The complete solution is then

$$Z_1 = a \operatorname{Ai}(-\epsilon^{-2/3} \zeta_1) + \frac{g(\zeta_1) - g(0)}{\zeta_1} - \epsilon^{-2/3} \pi g(0) \operatorname{Gi}(-\epsilon^{-2/3} \zeta_1)$$

Making use of (5.9) and (5.5) we find that $\tilde{\phi}_\alpha$ is given by

$$\begin{aligned} \bar{\phi}_\alpha &= \frac{a}{\zeta_1^{1/2}} \text{Ai}(-\epsilon^{-2/3} \zeta_1(X)) + \frac{1}{q_\alpha} \left[e^{i\frac{\beta}{2\omega} \frac{X}{\epsilon}} \phi_\alpha(X) \right. \\ &\quad \left. - \frac{e^{i\frac{\beta}{2\omega} \frac{\mu_1}{\epsilon}} \phi_\alpha(\mu_1) \zeta_1^{3/2}}{(\mu_2 - \mu_1)^{1/2} f(\mu_1)^{1/2}} \right] - \frac{\epsilon^{-2/3} \pi e^{i\frac{\beta}{2\omega} \frac{\mu_1}{\epsilon}} \phi_\alpha(\mu_1) \text{Gi}(-\epsilon^{-2/3} \zeta_1)}{(\mu_2 - \mu_1)^{1/2} f(\mu_1)^{1/2} \zeta_1^{1/2}} \end{aligned} \quad (5.10)$$

The asymptotic behavior of (5.10) is

$$\bar{\phi}_\alpha \sim \frac{e^{i\frac{\beta}{2\omega} \frac{X}{\epsilon}} \phi_\alpha(X)}{q_\alpha(X)} \quad \text{as } X \rightarrow -\infty$$

and

$$\begin{aligned} \bar{\phi}_\alpha &\sim \frac{a\epsilon^{1/6}}{\pi^{1/2} q_\alpha^{1/4}} \sin\left(\frac{2}{3} \epsilon^{-1} \zeta_1^{3/2} + \pi/4\right) \\ &\quad - \frac{\pi^{1/2} e^{i\frac{\beta}{2\omega} \frac{\mu_1}{\epsilon}} \phi_\alpha(\mu_1)}{\epsilon^{1/2} (\mu_2 - \mu_1)^{1/2} f(\mu_1)^{1/2} q_\alpha^{1/4}} \cos\left(\frac{2}{3} \epsilon^{-1} \zeta_1^{3/2} + \pi/4\right) \quad \text{as } X \rightarrow \infty \end{aligned} \quad (5.11)$$

In a similar fashion we can construct a solution valid about the turning point μ_2 by defining

$$\begin{aligned} \frac{2}{3} \zeta_2^{3/2} &= \int_X^{\mu_2} \sqrt{(\xi - \mu_1)(\mu_2 - \xi)f(\xi)} d\xi \quad \mu_1 < X < \mu_2 \\ \frac{2}{3} (-\zeta_2)^{3/2} &= \int_{\mu_2}^X \sqrt{(\xi - \mu_1)(\xi - \mu_2)f(\xi)} d\xi \quad X > \mu_2 \end{aligned} \quad (5.12)$$

The complementary solution is

$$\tilde{\phi}_\alpha = \frac{b}{\zeta_2^{1/2}} \text{Ai}(-\epsilon^{-2/3} \zeta_2)$$

where b is a constant. The particular solution is

$$\begin{aligned} \tilde{\phi}_\alpha = & - \frac{\epsilon^{-2/3} \pi e^{i\frac{\beta}{2\omega} \frac{\mu_2}{\epsilon}} \phi_\alpha(\mu_2)}{(\mu_2 - \mu_1)^{1/2} f(\mu_2)^{1/2} \zeta_2^{1/2}} \text{Gi}(-\epsilon^{-2/3} \zeta_2) \\ & + \frac{1}{q_\alpha(X)} \left[e^{i\frac{\beta}{\omega} \frac{X}{\epsilon}} \phi_\alpha(X) - \frac{e^{i\frac{\beta}{2\omega} \frac{\mu_2}{\epsilon}} \phi_\alpha(\mu_2)}{(\mu_2 - \mu_1)^{1/2} f(\mu_2)^{1/2}} \zeta_2^{3/2} \right] \end{aligned} \quad (5.13)$$

The asymptotic behavior of (5.13) is

$$\tilde{\phi}_\alpha \sim \frac{e^{i\frac{\beta}{2\omega} \frac{X}{\epsilon}} \phi_\alpha(X)}{q_\alpha(X)} \quad \text{as } X \rightarrow \infty$$

and

$$\begin{aligned} \tilde{\phi}_\alpha \sim & \frac{\epsilon^{1/6} b}{\pi^{1/2} q_\alpha^{1/4}} \sin\left(\frac{2}{3} \epsilon^{-1} \zeta_2^{3/2} + \pi/4\right) \\ & - \frac{\pi^{1/2} e^{i\frac{\beta}{2\omega} \frac{\mu_2}{\epsilon}} \phi_\alpha(\mu_2)}{\epsilon^{1/2} (\mu_2 - \mu_1)^{1/2} f(\mu_2)^{1/2} q_\alpha^{1/4}} \cos\left(\frac{2}{3} \epsilon^{-1} \zeta_2^{3/2} + \pi/4\right) \quad \text{as } X \rightarrow -\infty \end{aligned} \quad (5.14)$$

The solutions (5.10) and (5.13) are both valid in $\mu_1 < X < \mu_2$.

The asymptotic forms (5.11) and (5.14) are set equal giving

$$\begin{aligned}
 & a \sin\left(\frac{2}{3} \epsilon^{-1} \zeta_1^{3/2} + \pi/4\right) - b \sin\left(\frac{2}{3} \epsilon^{-1} \zeta_2^{3/2} + \pi/4\right) \\
 &= \frac{\pi e^{i\frac{\beta}{2\omega} \frac{\mu_1}{\epsilon}} \phi_\alpha(\mu_1)}{\epsilon^{1/3} (\mu_2 - \mu_1)^{1/2} f(\mu_1)^{1/2}} \cos\left(\frac{2}{3} \epsilon^{-1} \zeta_1^{3/2} + \pi/4\right) \\
 &- \frac{\pi e^{i\frac{\beta}{2\omega} \frac{\mu_2}{\epsilon}} \phi_\alpha(\mu_2)}{\epsilon^{1/3} (\mu_2 - \mu_1)^{1/2} f(\mu_2)^{1/2}} \cos\left(\frac{2}{3} \epsilon^{-1} \zeta_2^{3/2} + \pi/4\right) \quad (5.15)
 \end{aligned}$$

We write

$$\begin{aligned}
 \Delta &= \frac{2}{3} \epsilon^{-1} (\zeta_1^{3/2} + \zeta_2^{3/2}) + \pi/2 \\
 &= \epsilon^{-1} \int_{\mu_1}^{\mu_2} \sqrt{(\xi - \mu_1)(\mu_2 - \xi)f(\xi)} \, d\xi + \pi/2
 \end{aligned}$$

so that

$$\frac{2}{3} \epsilon^{-1} \zeta_2^{3/2} + \pi/4 = \Delta - \left(\frac{2}{3} \epsilon^{-1} \zeta_1^{3/2} + \pi/4\right)$$

From (5.15) we may evaluate a and b as

$$a + b \cos \Delta = - \frac{\pi e^{i\frac{\beta}{2\omega} \frac{\mu_2}{\epsilon}} \phi_\alpha(\mu_2)}{\epsilon^{1/3} (\mu_2 - \mu_1)^{1/2} f(\mu_2)^{1/2}} \sin \Delta$$

$$\begin{aligned}
b \sin \Delta = & - \frac{\pi e^{i\frac{\beta}{2\omega} \frac{\mu_1}{\varepsilon}} \phi_\alpha(\mu_1)}{\varepsilon^{1/3} (\mu_2 - \mu_1)^{1/2} f(\mu_1)^{1/2}} \\
& + \frac{\pi e^{i\frac{\beta}{2\omega} \frac{\mu_1}{\varepsilon}} \phi_\alpha(\mu_2)}{\varepsilon^{1/3} (\mu_2 - \mu_1)^{1/2} f(\mu_2)^{1/2}} \cos \Delta
\end{aligned} \tag{5.16}$$

The coefficient b from (5.16) becomes unbounded when $\sin(\Delta) = 0$ or

$$\int_{\mu_1}^{\mu_2} \sqrt{(\xi - \mu_1)(\mu_2 - \xi) f(\xi)} \, d\xi = \varepsilon(m - \frac{1}{2})\pi \tag{5.17}$$

where m is an integer. This is the condition for free waves to be trapped by topography. From the behavior of A_i we see that m in (5.17) is the number of amplitude maxima in the x direction for the stream function. Trapped free waves over slowly varying topography have been described previously by Longuet-Higgins (1968a) and by Rhines and Bretherton (1973). The innovation here is that an expression for the forced response away from resonance has been obtained.

5.2 Propagating waves

The leading order asymptotic approximation for frequency range IV is now described. In this frequency range there are no turning points and $q_\alpha(X)$ is positive everywhere. Free waves at these frequencies were discussed in Section 4. We write a solu-

tion to (5.1) of the form

$$\phi_{\alpha}(x) = A(x)e^{i\theta_1} + B(x)e^{i\theta_2} \quad (5.18)$$

where

$$\frac{d}{dx} \theta_i = k_{\alpha i}(x) \quad i = 1, 2$$

and where $k_{\alpha i}$ are defined in (4.12). Note that (5.18) differs from (4.6) in that the amplitude in the latter expression is a slowly varying function, whereas $A(x)$ and $B(x)$ in (5.18) vary on the x scale. We substitute (5.16) in (5.1) and neglect $O(\epsilon)$ terms with the result

$$\begin{aligned} \phi_{\alpha}(x) = & e^{i\theta_1} \int_x^{\infty} \frac{\phi_{\alpha}(\epsilon\xi) e^{-i\theta_1(\xi)} d\xi}{i(k_{\alpha 2}(\epsilon\xi) - k_{\alpha 1}(\epsilon\xi))} \\ & + e^{i\theta_2} \int_{-\infty}^x \frac{\phi_{\alpha}(\epsilon\xi) e^{-i\theta_2(\xi)} d\xi}{i(k_{\alpha 2}(\epsilon\xi) - k_{\alpha 1}(\epsilon\xi))} \end{aligned} \quad (5.19)$$

There are two constants of integration in (5.19). Recall that $k_{\alpha 1}$ away from the topographic feature corresponds to the Rossby wave with westward group velocity. Thus the integral multiplying $e^{i\theta_1}$ is chosen to vanish as $x \rightarrow \infty$. Similarly the integral multiplying $e^{i\theta_2}$ is chosen to vanish as $x \rightarrow -\infty$.

In both integrals in (5.19) ϕ_{α} , $k_{\alpha 1}$ and $k_{\alpha 2}$ are slowly

varying functions. The dominant contributions to the integrals arise from points of stationary phase, X_0 , defined by

$$\frac{d}{dx} \theta_1 = k_{\alpha 1}(X_0) = 0$$

which are the zeros of $k_{\alpha 1}$. From (4.12) and Figure 6 it can be seen that $k_{\alpha 2}(X)$ corresponding to the Rossby wave with eastward group velocity does not have zeros. The first term in (5.19) was claimed by Nayfeh (1973) to be the dominant term in an asymptotic approximation to the solution of a second order inhomogeneous differential equation with no turning points.

At the points of stationary phase the x component of wavenumber of the free waves coincides with the x wavenumber of the forcing which is uniform. Thus we have a form of resonant excitation. Energy is then radiated by a Rossby wave to the west. We have considered up to this point the special case of uniform wind forcing. A traveling disturbance of wind stress curl with oscillations on the x scale characterized by the slowly varying wavenumber $\lambda(X)$ could be represented by replacing $\phi_{\alpha}(X)$ in (5.1) by $\phi_{\alpha}(X)e^{i\theta}$ where $\frac{d}{dx} \theta = \lambda(X)$.

Points of stationary phase in (5.19) would be defined by

$$\frac{d}{dx} (\theta - \theta_1) = 0$$

or

$$k_{\alpha 1}(X_0) = \lambda(X_0)$$

Thus the region of forcing is about points where the x wavenumber

of a free wave coincides with $\lambda(X)$. An eastward traveling disturbance has positive $\lambda(X)$. Since from Figure 6 only $k_{\alpha 1}(X)$ assumes positive values, an eastward moving disturbance forces a response in which energy is radiated by a Rossby wave to the west of the bottom feature.

To illustrate the response in frequency range IV (5.19) has been integrated numerically for $h(X) = h_0 \exp(-(1 + X^2)^{-1})$ and uniform wind and is drawn in Figure 8. Only the first term in (5.19) is included. The features of Figure 8 are decay to the east of the bottom feature, a complicated eddy structure over it and a Rossby wave to the west. The calculation was repeated over a range of frequencies and the amplitude of the stream function of the Rossby wave, well to the west of the topographic feature, is plotted against forcing frequency in Figure 9. In this model the rate of energy propagation by the Rossby wave is balanced by the topographic stress acting with the zonal flow. The frequency dependence in Figure 9 reflects the varying phase relations of (5.19) over topography.

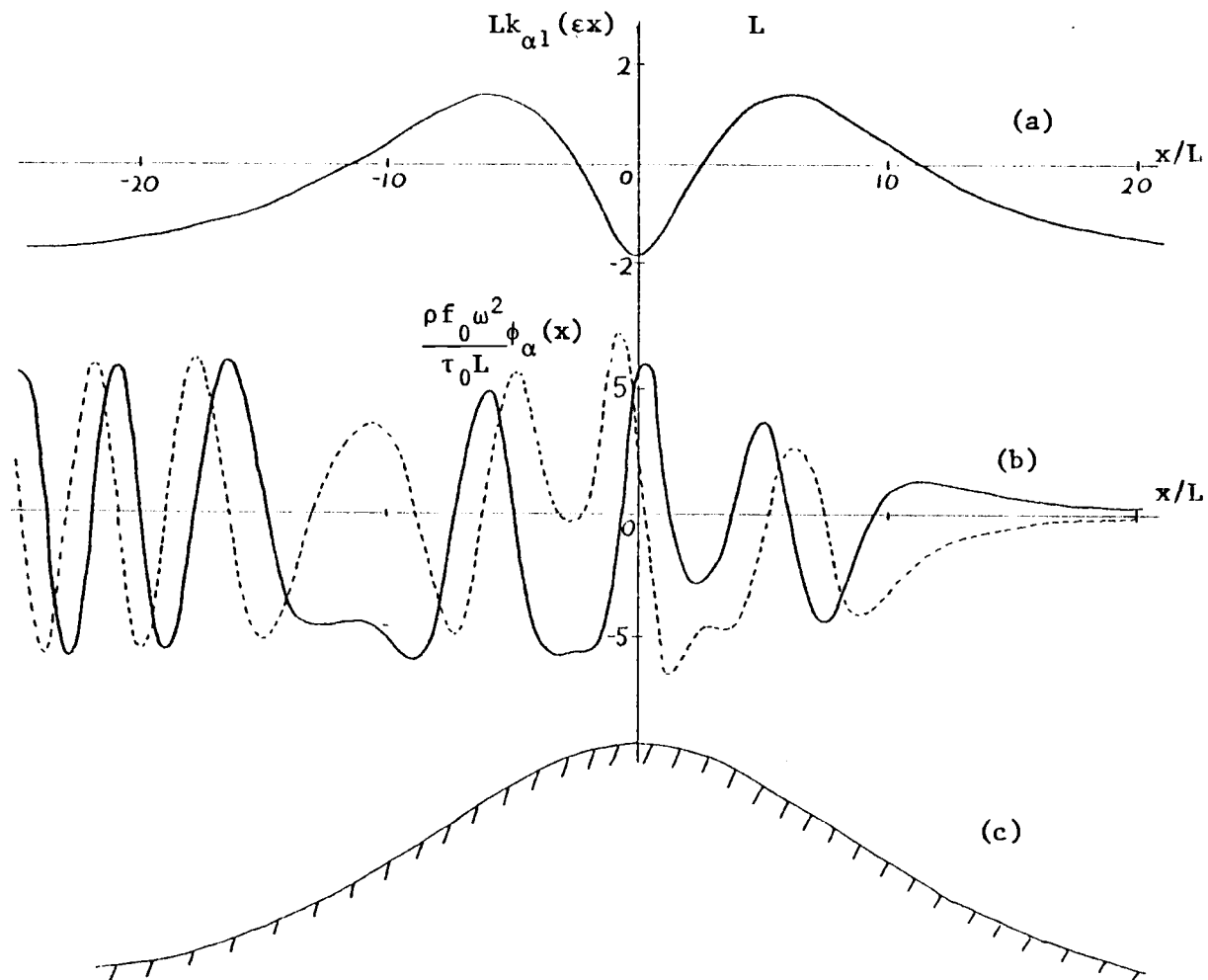


Figure 8. Resonant response, frequency range IV. (a) Variation of wavenumber, $k_{\alpha 1}(x)$. (b) Real (solid line) and imaginary (dashed line) part of $\phi_{\alpha}(x)$ scaled by $\tau_0 L / \rho f_0 \omega^2$. (c) Sketch of bottom profile. $\omega = 0.0696$, other parameters as in Figure 7.

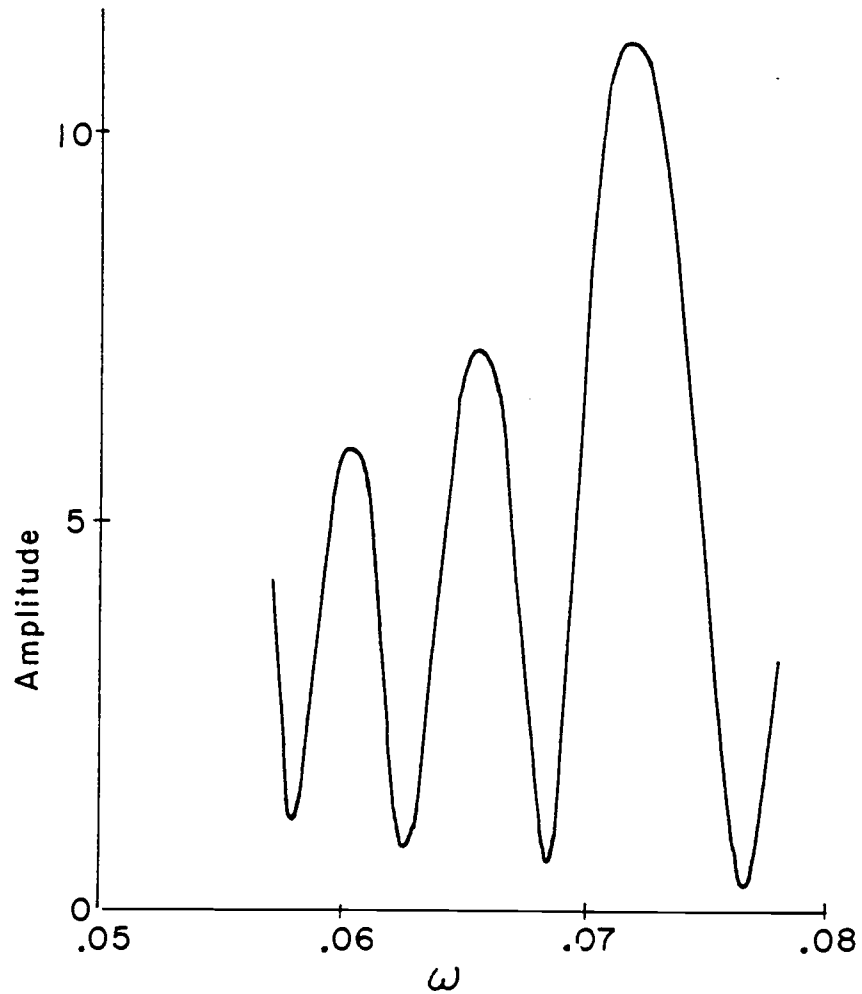


Figure 9. Stream function amplitude of Rossby wave (far to west of bottom feature) scaled by $\tau_0 L / \rho f_0 \omega^2$ as a function of ω in frequency range IV. Parameters as in Figure 7.

6. Summary of barotropic model

If the Drake Passage region has normal modes in the frequency range of maximum atmospheric forcing then this study should be relevant despite neglect of stratification, mean flow and non-linearity. The channel walls in the model play an important part in wave trapping by limiting the scale of motion. Actually there is communication between Drake Passage and the large Pacific basin, however the fastest waves in the basin have scale exceeding the Passage width. This mismatch of scales could reduce the efficiency for wave energy to escape.

It would be of interest to extend the analysis of forced radiating waves over slowly varying topography to a stratified fluid. Recent studies in the Pacific Ocean at about 40°N (Bernstein and White, 1977, and Roden, 1977) find baroclinic eddies in the western region, a quiet regime in the east and a rather abrupt transition. This is suggestive of forcing on a seasonal time scale and bottom topography playing a role in the spatial inhomogeneity. A model treating bottom topography as a small amplitude perturbation (Rhines, 1970) would result in waves of the scale of the topography. In the slowly varying model there is a separation of scales between the waves and topography by definition, but it should be realized that waves which have neither the x-scale of the topography nor of the wind may be excited.

7. Formulation of instability problem

We discuss now the two layer problem and modify the notation. We consider two layers of homogeneous, incompressible fluid again in a zonal channel of width L on a beta plane. With coordinates x^* eastward, y^* poleward and z^* up, the channel walls are located at $y^* = 0, L$ (asterisks denote dimensional variables). At an initial time, a north-south step is imposed at $x^* = 0$. The initial depth is H and the step height is h^* . For simplicity we choose the layer depths to be equal, each being $H/2$ when the fluid is at rest. When the fluid is in motion the interface is displaced an amount η^* . The system is sketched in Figure 10.

With the beta plane approximation, $f = f_0 + \beta^*y^*$. A natural length scale associated with the stratification is the internal radius of deformation defined

$$L_D = \frac{(g'H/2)^{1/2}}{f_0} \quad . \quad \text{Here } g' = \frac{\rho_2 - \rho_1}{\rho_2} \quad g \ll g$$

where g is the acceleration of gravity, ρ_1 and ρ_2 are the densities (subscript 1 refers to an upper layer quantity, subscript 2 to a lower layer quantity). We scale horizontal length by L_D . A characteristic horizontal velocity is the magnitude of the initial velocity difference between upper and lower layers $U = |U_1^* - U_2^*|$. We shall refer to this quantity as the shear. Since we are concerned with cases in which instability

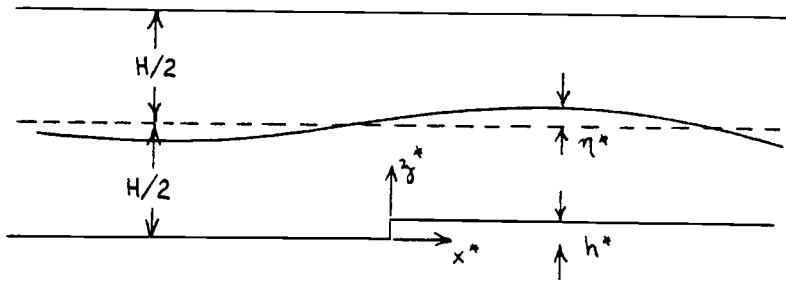


Figure 10. The two-layer model.

is possible, U is non-zero and the scaling is valid. Vertical length is scaled by H , vertical velocity by UH/L_D and the time by L_D/U . The nondimensional dynamic pressures are written as

$$p_1 = \left[p_1^* - \rho_1 g(H - z^*) \right] / (\rho_1 U f_0 L_D)$$

$$\text{and } p_2 = \left[p_2^* - \rho_2 g(H/2 - z^*) - \rho_1 gH/2 \right] / (\rho_2 U f_0 L_D)$$

The interface displacement is scaled by Uf_0L_D/g' . Continuity of pressure at the interface is expressed by the condition

$$\eta = p_2 - p_1 .$$

Nondimensional equations of momentum and continuity are

$$R(u_{nt} + \underline{q}_n \cdot \nabla_n u_n) - (1 + R\beta y)v_n = -p_{nx} \quad (7.1a)$$

$$R(v_{nt} + \underline{q}_n \cdot \nabla_n v_n) + (1 + R\beta y)u_n = -p_{ny} \quad (7.1b)$$

$$0 = p_{nz} \quad (7.1c)$$

$$\nabla \cdot \underline{q}_n = 0 \quad n = 1, 2 \quad (7.1d)$$

where $\underline{q}_n = (u_n, v_n, w_n)$. We have assumed hydrostatic balance and have neglected viscosity. The nondimensional parameters in (7.1) are a Rossby number, $R = Uf_0/L_D$ and a measure of the relative importance of beta and shear $\beta = \beta^* L_D^2 / U$.

Boundary conditions at the rigid top, the interface and the bottom are

$$w_1 = 0 \quad z = 1 \quad (7.2a)$$

$$w_n = \frac{1}{2}R (\eta_t + u_n \eta_x + v_n \eta_y) \quad z = \frac{1}{2} \quad (7.2b)$$

$$w_2 = \frac{1}{2}R \hat{h} U_2 h_x \quad z = 0 \quad (7.2c)$$

where \hat{h} is a measure of the step height. At the channel walls, $v_n = 0$ at $y = 0, L/L_D$.

The parameter range we consider is

$$R \ll 1, \beta \leq 0(1), \hat{h} \ll 1, L_D/L \leq 0(1).$$

We expand in powers of R

$$u_n = u_n^{(0)} + R u_n^{(1)} + \dots$$

$$v_n = v_n^{(0)} + R v_n^{(1)} + \dots$$

$$w_n = R w_n^{(1)} + \dots$$

$$p_n = p_n^{(0)} + R p_n^{(1)} + \dots$$

The $0(1)$ balance is

$$v_n^{(0)} = p_{nx}^{(0)} \quad (7.3a)$$

$$u_n^{(0)} = -p_{ny}^{(0)} \quad (7.3b)$$

$$0 = p_{nz}^{(0)} \quad (7.3c)$$

$$u_{nx}^{(0)} + v_{ny}^{(0)} = 0 \quad (7.3d)$$

The $0(1)$ horizontal velocities in each layer are independent of depth. We form a vorticity equation for each layer, integrate in the vertical making use of (7.2) and write horizontal velocities and

interface displacement in terms of pressure to obtain the quasi-geostrophic potential vorticity equations.

$$(\partial/\partial t - p_{1y}\partial/\partial x + p_{1x}\partial/\partial y)(\nabla^2 p_1 + \beta y + p_2 - p_1) = 0 \quad (7.4a)$$

$$(\partial/\partial t - p_{2y}\partial/\partial x + p_{2x}\partial/\partial y)(\nabla^2 p_2 + \beta y - p_2 + p_1) = p_{2y}\hat{h}h_x \quad (7.4b)$$

The superscripts denoting pressure as an $O(R^0)$ term have been dropped in (7.4).

The step is represented as

$$h(x) = H(x) H(t)$$

$$\text{or } h_x(x) = \delta(x) H(t)$$

where $H(x)$ and $H(t)$ are Heaviside functions. We suppose that initially there is a uniform zonal flow, U_1 and U_2 in each layer. With the scaling we have chosen, $U_1 - U_2 = \pm 1$.

We decompose pressure into a part representing the zonal flow and a part representing the small amplitude disturbance which is a series in the cross-channel eigenfunctions,

$$p_n(x, y, t) = -U_n y + \sum_{j=1}^{\infty} \phi_n^{(j)}(x, t) \sin(j\pi L_D y/L) \quad (7.5)$$

Note that $|\phi_n^{(j)}| = O(\hat{h}) \ll 1$. We write \hat{h} as

$$\hat{h} = \frac{4\hat{h}}{\pi} \sum_{j \text{ odd}} \frac{1}{j} \sin(j\pi L_D y/L)$$

$$= \sum_{j \text{ odd}} \hat{h}^{(j)} \sin(j\pi L_D y/L) \quad (7.6)$$

Substituting (7.5) and (7.6) into (7.4) and neglecting nonlinear terms in $\phi_n^{(j)}$ we obtain for a given cross-channel mode,

$$(\partial/\partial t + U_1 \partial/\partial x)((\partial^2/\partial x^2 - \ell^2)\phi_1 + \phi_2 - \phi_1) + (\beta \pm 1)\phi_{1x} = 0 \quad (7.7a)$$

$$\begin{aligned} & (\partial/\partial t + U_2 \partial/\partial x)((\partial^2/\partial x^2 - \ell^2)\phi_2 - \phi_2 + \phi_1) + (\beta \mp 1)\phi_{2x} \\ & = -U_2 \hat{h} h_x \end{aligned} \quad (7.7b)$$

The superscripts identifying the particular cross-channel mode have been dropped and $j\pi L_D/L$ has been replaced by ℓ . The upper sign is for positive shear, the lower for negative shear. By assuming the topographic scale as $O(\hat{h})$ topographic waves have been eliminated. The modification of the stability of the flow by topography also is neglected.

8. A criterion for the transformed solution

As we have indicated, the steady form of (7.7) does not define a unique solution unless boundary conditions at infinity are prescribed. The solution, in the linearized formulation, may not even be bounded if instabilities develop. We impose the step at $t = 0$ and require that prior to $t = 0$ there be zero disturbance.

The equations for the Laplace transform $\phi_n(x,s)$ of $\phi_n(x,t)$ from (7.7) are

$$(s + U_1 \partial / \partial x) [(\partial^2 / \partial x^2 - \lambda^2) \phi_1 + \phi_2 - \phi_1] + (\beta \pm 1) \phi_{1x} = 0 \quad (8.1a)$$

$$(s + U_2 \partial / \partial x) [(\partial^2 / \partial x^2 - \lambda^2) \phi_2 - \phi_2 + \phi_1] + (\beta \mp 1) \phi_{2x} \\ = - \frac{U_2 \hat{h} \delta(x)}{s} \quad (8.1b)$$

We employ the delta function formalism here. This is equivalent to matching solutions across the step at $x = 0$ so that ϕ_n, ϕ_{nx} and ϕ_{1xx} are continuous. There is a discontinuity in ϕ_{2xx} of $-\hat{h}/s$. Solutions to (8.1) are of the form $\phi_n(x,s) = A(s)e^{m(s)x}$ where $m(s)$ satisfies

$$[(s + U_1 m)(m^2 - \lambda^2 - 1) + (\beta \pm 1)m] [(s + U_2 m)(m^2 - \lambda^2 - 1) \\ + (\beta \mp 1)m] - (s + U_1 m)(s + U_2 m) = 0 \quad (8.2)$$

The inverse transform is given by integrals of the form

$$\frac{1}{2\pi i} \int_{\gamma-i\infty}^{\gamma+i\infty} A(s) e^{m(s)x + st} ds \quad (8.3)$$

where the contour is taken to the right of all singularities. The solution must formally vanish for $t < 0$. With t negative, the contour is closed by a large semi-circle in the positive real s half-plane. By Jordan's lemma and Cauchy's theorem it can be seen that if $\text{Re}(m(s))$ is negative on the semi-circle, the integral (3.3) vanishes only if the root $m(s)$ applies to the region $x > 0$. If $\text{Re}(m(s))$ is positive on the semi-circle, then $m(s)$ applies to the region $x < 0$ only. The criterion we use for determining in which region a root $m(s)$ applies is identical to that used by Thacker (1976).

McIntyre (1968) considered the initial value problem for a single layer flow over a step on a beta plane. Our criterion is also identical to that of McIntyre. In fact, our problem is simply a generalization of the single layer flow to two layers. McIntyre demonstrated that the single layer contains no instabilities. There are instabilities for two layers and we discuss them in the next section.

9. Transient solution on f plane

We examine first the transient behavior on the f plane by setting $\beta = 0$ in (8.2)

$$[(s + U_1 m)(s + U_2 m)(m^2 - \ell^2 - 2) - m^2] (m^2 - \ell^2) = 0 \quad (9.1)$$

Without loss of generality, we have taken shear positive.

Equation (9.1) may be used to express s as a function of m

$$s = -U_2 m - \frac{1}{2}m \pm \frac{1}{2}m \frac{(-m^2 + \ell^2 - 2)^{\frac{1}{2}}}{(-m^2 + \ell^2 + 2)^{\frac{1}{2}}} \quad (9.2)$$

U_1 has been replaced by $U_2 + 1$ in (9.2). Normal modes for temporal instability are of the form $e^{mx + st}$ with m purely imaginary and s complex with positive real part. Unstable modes have low wavenumber $\text{Im}(m)^2 + \ell^2 < 2$ with maximum growth at $\text{Im}(m)^2 = 2(\ell^2 + 2)^{\frac{1}{2}} - (\ell^2 + 2)$ (see Pedlosky (1964b) for further details).

There are six roots $m(s)$ to (9.1) given by $m = \pm \ell$ and $m_j(s)$, $j = 1$ to 4. Contours of the real and imaginary parts of $m_j(s)$ on the complex s plane have been calculated from (9.2) and are drawn in Figure 11 for $U_2 = 0.3$ and $\ell^2 = 0.25$. The temporally unstable waves are those along the $\text{Re}(m_1) = 0$ contour in the positive real s half-plane. It can be seen that m_1, m_2, m_3 and $-\ell$ have negative real part on a large semi-circle in the positive real s half-plane and thus by the criterion established in the previous section describe the solution in $x > 0$. The roots

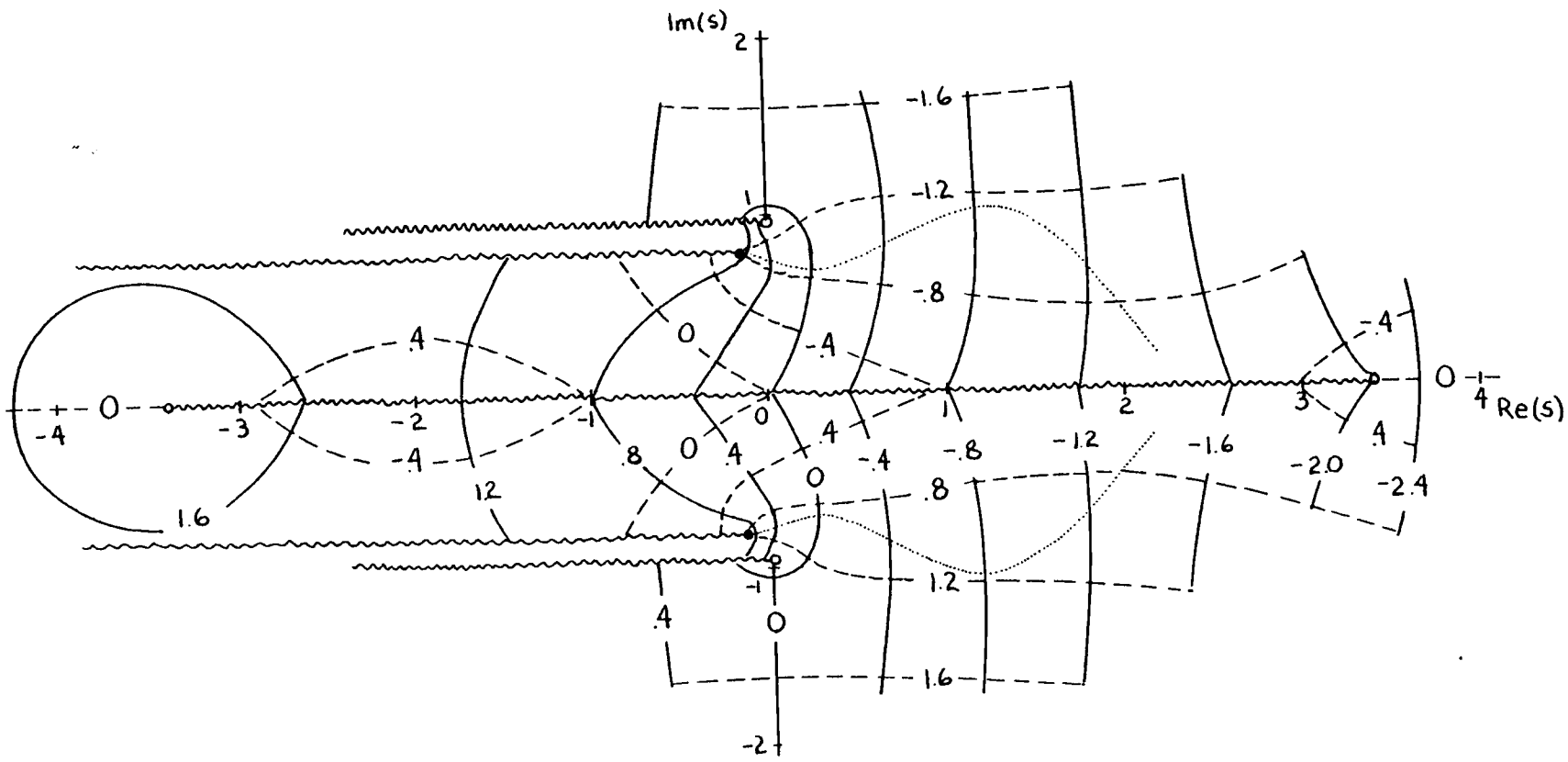


Figure 11a. The root $m_1(s)$, $U_2 = 0.3$, $\beta = 0$, $l^2 = 0.25$. Contours of real (solid lines) and imaginary (dashed lines) parts of $m_1(s)$ drawn on the complex s plane. Closed circles (\bullet) are branch points of the full solution, open circles (\circ) are branch points for a root $m_j(s)$. The dotted lines are loci of saddle points.

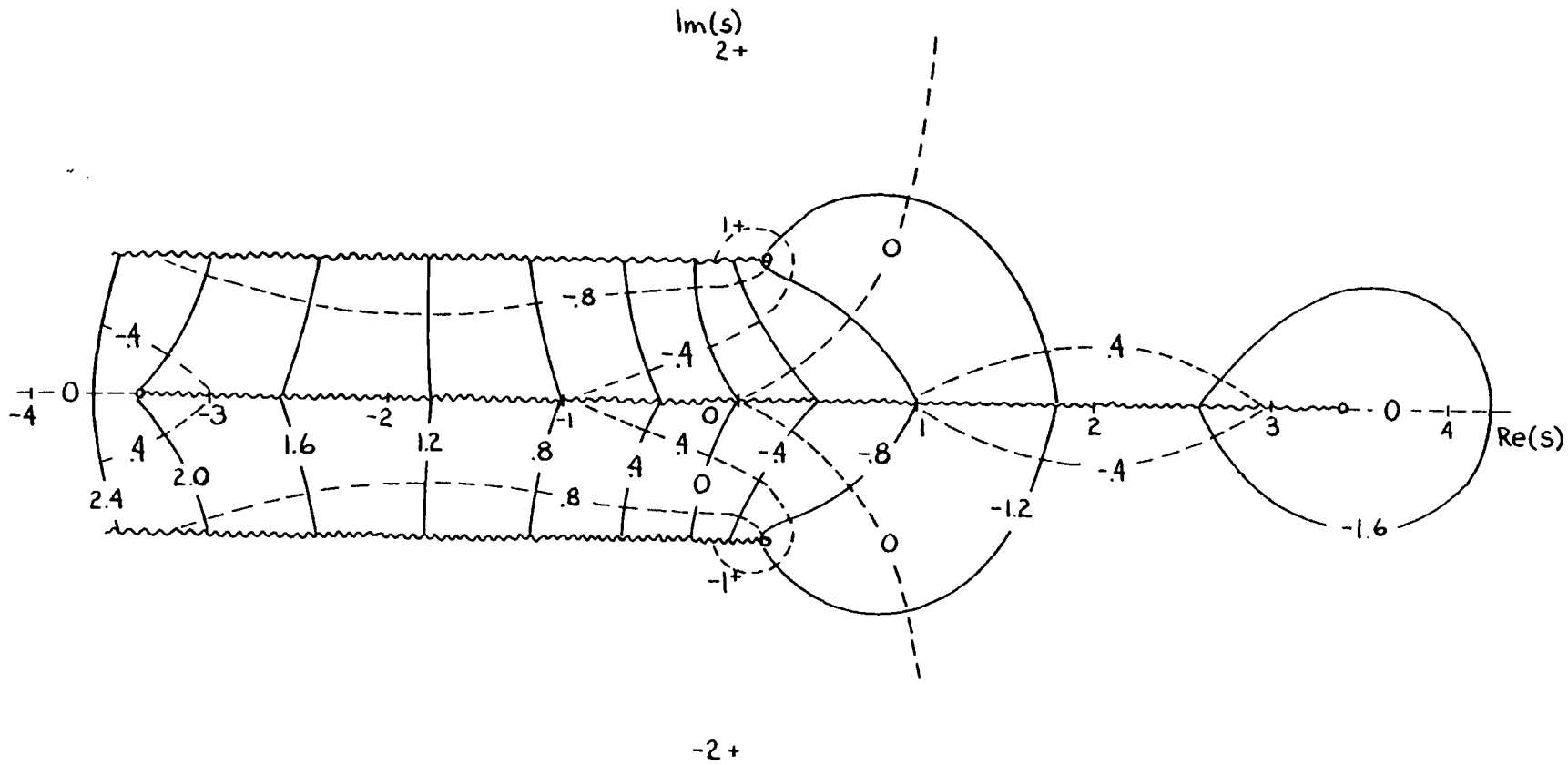


Figure 11b. The root $m_2(s)$.

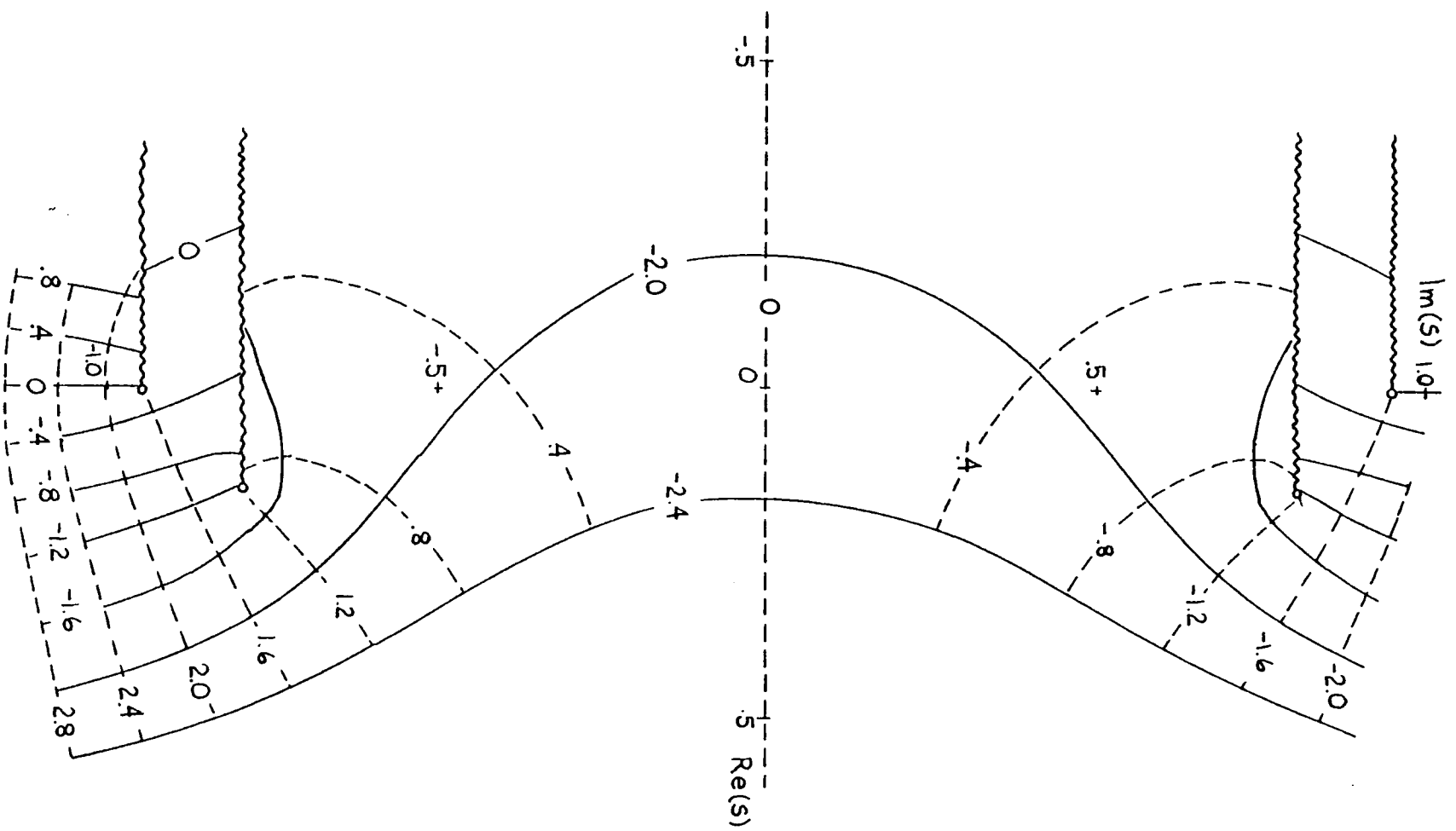


Figure 11c. The root $m_3(s)$.

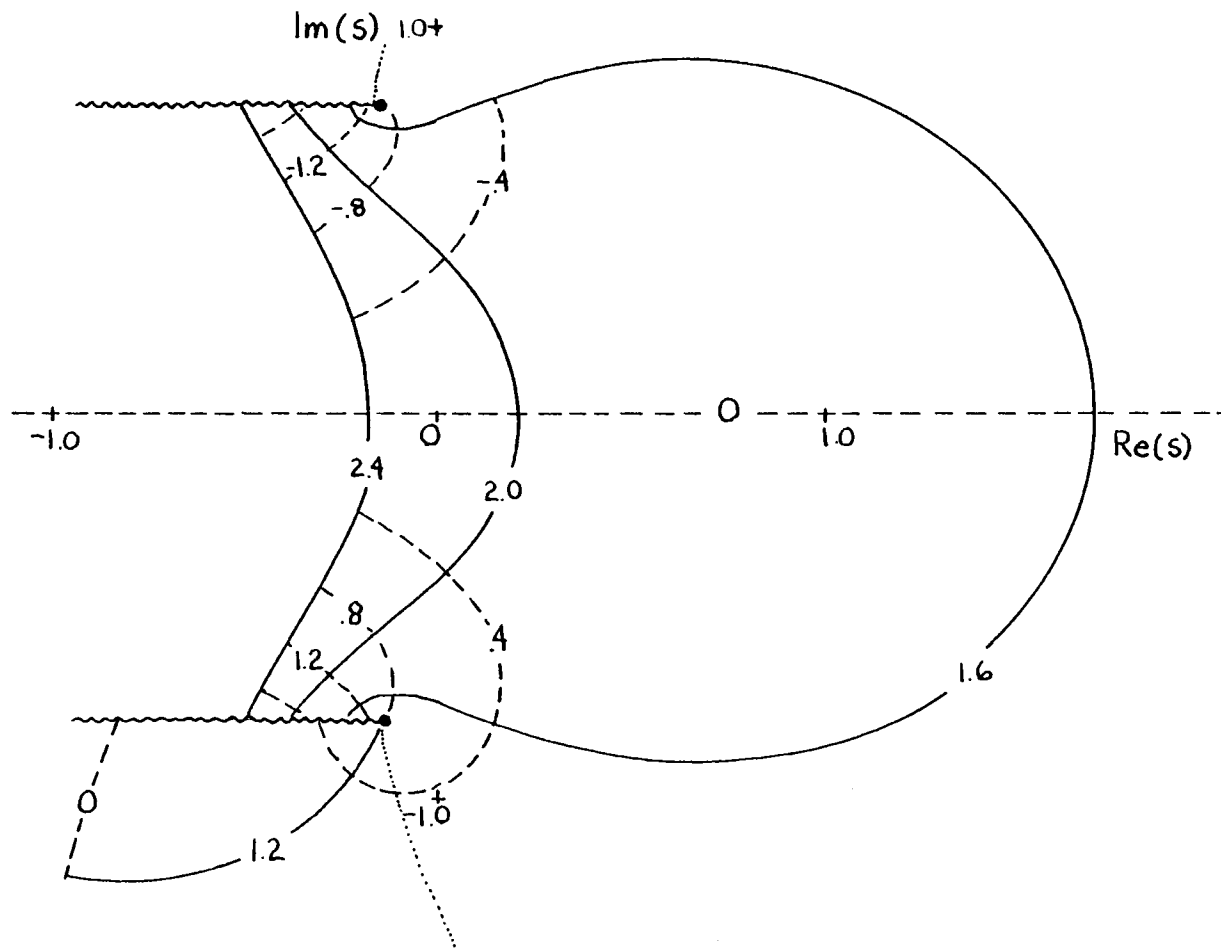


Figure 11d. The root $m_4(s)$. The dotted lines are loci of saddle points.

m_4 and ℓ describe the solution in $x < 0$. The solution to (8.1) is

$$\begin{aligned}
 \phi_1(x,s) &= \frac{(s + U_1 m_1) \hat{h} e^{m_1 x}}{s U_1 (m_1 - m_2) (m_1 - m_3) (m_1 - m_4) (m_1^2 - \ell^2)} \\
 &+ \frac{(s + U_1 m_2) \hat{h} e^{m_2 x}}{s U_1 (m_2 - m_1) (m_2 - m_3) (m_2 - m_4) (m_2^2 - \ell^2)} \\
 &+ \frac{(s + U_1 m_3) \hat{h} e^{m_3 x}}{s U_1 (m_3 - m_1) (m_3 - m_2) (m_3 - m_4) (m_3^2 - \ell^2)} \\
 &- \frac{(s - U_1 \ell) \hat{h} e^{-\ell x}}{2s \ell U_1 (m_1 + \ell) (m_2 + \ell) (m_3 + \ell) (m_4 + \ell)} \quad x > 0 \\
 \phi_1(x,s) &= \frac{(s + U_1 m_4) \hat{h} e^{m_4 x}}{s U_1 (m_4 - m_1) (m_4 - m_2) (m_4 - m_3) (m_4^2 - \ell^2)} \\
 &+ \frac{(s + U_1 \ell) \hat{h} e^{\ell x}}{2s \ell U_1 (m_1 + \ell) (m_2 + \ell) (m_3 + \ell) (m_4 + \ell)} \quad x < 0
 \end{aligned} \tag{9.3}$$

A similar expression can be obtained for ϕ_2 . The coefficient of $e^{m_j x}$ is that of (9.3) multiplied by $[-(m_j^2 - \ell^2 - 1)$

$-m_j / (s + U_1 m_j)]$ which is obtained from (8.1a).

The roots $m_j(s)$ are analytic functions of s except at branch points. The open circles in Figure 11 are branch points for an individual root $m_j(s)$ but not for $\phi_1(x,s)$ as a whole. For example,

along the branch cut between $s = \pm 3.42$ any contour of $m_1(s)$ is continuous with a corresponding contour of $m_2(s)$. Thus if a circuit of 2π is followed about the branch point $s = 3.42$, one moves from the Riemann surface of $m_1(s)$ onto that of $m_2(s)$ and from the Riemann surface of $m_2(s)$ onto that of $m_1(s)$. From (9.3), however, $\phi_1(x,s)$ does not change its value if m_1 and m_2 are interchanged. The closed circles in Figure 11 are branch points of $\phi_1(x,s)$. The foregoing argument concerning which branch points of $m_j(s)$ are also branch points of $\phi_1(x,s)$ is equivalent to arguments of Thacker (1976). If s is considered a function of m , at saddle points, $ds/dm = 0$. These saddle points are the branch points for m considered a function of s .

The transform $\phi_1(x,s)$ is now inverted resulting in integrals of the form (8.3). We obtain asymptotic approximations for $\phi_1(x,t)$, valid for long time. The exponent of (8.3) is written as $m(s)x + st = (m(s)x/t + s)t$. For a given speed x/t , a saddle point of $m(s)x/t + s$ at s_0 is defined by

$$\frac{dm}{ds} \frac{x}{t} + 1 = 0 \quad (9.4)$$

As $t \rightarrow \infty$ the asymptotic approximation to (8.3) is

$$\frac{A(s_0)}{(2\pi |d^2m/ds^2|_x)^{1/2}} \exp [(m(s_0)x/t + s_0)t + i(\theta - \pi/2)] \quad (9.5)$$

where θ is the angle of the path of steepest descent through s_0 .

Writing (9.4) as $-ds/dm = x/t$ we see that we may interpret $-ds/dm$ as a group velocity. (Since we do not explicitly integrate (8.3) we can regard m as a function of s or s as a function of m from (9.1), whichever proves more convenient). Note that $-ds/dm$ has this interpretation only when it is real. It is at this stage which our solution differs from Thacker (1976). In Thacker's solution the dominant asymptotic contribution for fixed x and $t \rightarrow \infty$ arose from branch points of $\Phi_1(x,s)$. These branch points are saddle points of $mx/t + s$ for the particular value of $x/t \rightarrow 0$. The saddle point method thus includes Thacker's solution as a special case.

The behavior of (9.5) is dominated by the real part of the exponential. The growth rate, defined as $\text{Re}(mx/t + s)$ at the saddle point corresponding to x/t , is a function of x/t . If it is positive, the wave which propagates at x/t is growing. Since $U_1 - U_2 = 1$, the nondimensional shear is fixed and the effect of varying U_2 is simply to translate the growth curve without change of shape. This can be seen by making the transformation $\tilde{s}(m) = s + U_2 m$ in (9.2). The function $\tilde{s}(m)$ is independent of U_2 and saddle points of $m\tilde{x}/t + \tilde{s}$ can be found for a given \tilde{x}/t . The growth rate, $\text{Re}(m\tilde{x}/t + \tilde{s} - U_2 m)$ is unchanged for the transformation if $\tilde{x}/t = x/t - U_2$, a speed relative to the lower layer flow. The growth rate, aside from the translation, depends only on ℓ . The lower layer mean flow, U_2 , enters into the complete solution

in a non-trivial manner through the coefficients of the exponentials in (9.3).

We can consider m and \tilde{s} related by

$$\tilde{s}(m) = -\frac{1}{2}m \pm \frac{1}{2}m \frac{(-m^2 + \ell^2 - 2)^{\frac{1}{2}}}{(-m^2 + \ell^2 + 2)^{\frac{1}{2}}} \quad (9.6)$$

which will permit a classification of the transient behavior according to the growth rate at $x/t - U_2 = 0$. The growth rate at $x/t - U_2 = 0$ arises from a saddle point of $m(\tilde{s})x/t + \tilde{s}$ with $d\tilde{s}/dm = 0$ and is simply $\text{Re}(\tilde{s})$ evaluated at the saddle point. Again, points at which $d\tilde{s}/dm$ is zero are equivalently branch points of $m(\tilde{s})$. We set $d\tilde{s}/dm$ equal to zero from (9.6) which leads to

$$m^6 - (\ell^2 + 2)m^4 - (\ell^2 + 2)^2 m^2 + (\ell^2 + 2)(\ell^2 - 2) = 0 \quad (9.7)$$

This is a cubic equation for the value of $m^2(\tilde{s})$ at branch points; the effect of the transformation to \tilde{s} has been a reduction in the order of the equation determining branch points. The roots of (9.7) can be determined explicitly and their positions on the \tilde{s} plane are qualitatively distinct depending on whether ℓ^2 is less than, equal to or greater than $11/8$. Positions of the branch points of $m(\tilde{s})$ on the \tilde{s} plane for the three cases are sketched in Figure 12. As in the solution (9.3), there are points which are branch points only of $m(\tilde{s})$ (represented in Figure 12 by open circles) and there are branch points (closed circles) of the transient solution. In the Appendix it is shown that only

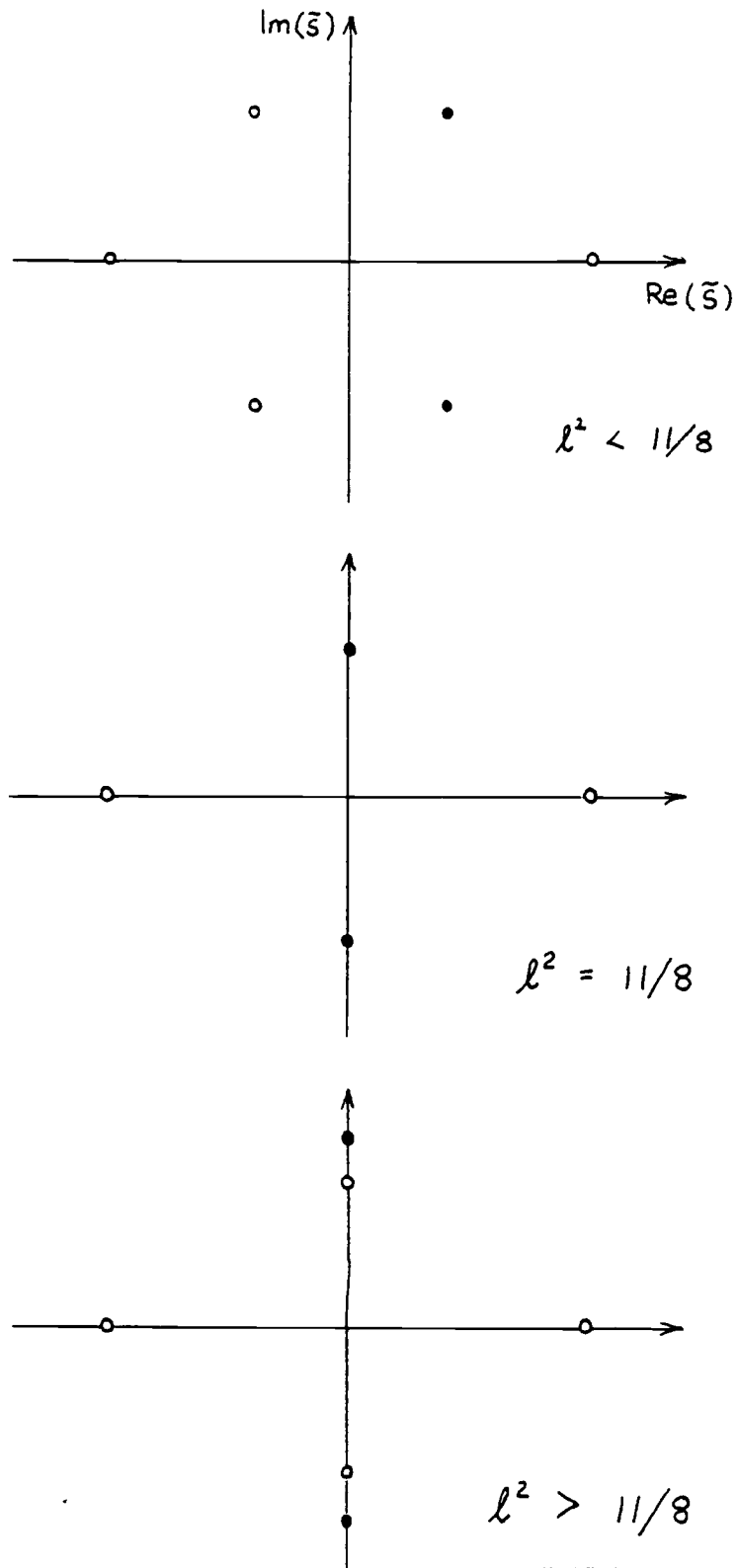


Figure 12. Positions of branch points of $m_j(\bar{s})$ for three values of l^2 . Closed circles (\bullet) are branch^j points of the full solution, open circles (\circ) are branch points for a root $m_j(\bar{s})$.

branch points for the transformed stream function give asymptotic contributions. For ℓ^2 less than $11/8$ branch points of the transient are complex with positive $\text{Re}(\tilde{s})$. For ℓ^2 greater than or equal to $11/8$ branch points for the transient lie along the imaginary s axis. Thus, the growth rate is positive for ℓ^2 less than $11/8$ and is zero, corresponding to algebraic asymptotic behavior, for ℓ^2 equal to or greater than $11/8$.

The procedure for obtaining the asymptotic solution is first to plot contours of $m(s)$ as in Figure 11. (Contours of $m(\tilde{s})$ would give growth rates, but the complete solution is obtained from (9.3) in which s is used.) From contours of $m(s)$, the loci of $-ds/dm$ real, which are saddle points of $m(s)x/t + s$, can be observed. These are sketched as dotted lines in Figure 11a (for $-ds/dm$ positive) and in Figure 11d (for $-ds/dm$ negative). The loci pass through the branch points of $\phi_1(x,s)$ at which $ds/dm = 0$. There are additional saddle points, but it is shown in the Appendix that they do not result in asymptotic contributions. Once the saddle point is located, the corresponding values of $-ds/dm$ and growth rate are calculated.

Growth rates for the three cases are drawn in Figure 13a. The common feature of the three curves is that there is an interval of $x/t - U_2$ for which the dominant asymptotic contribution is a growing wave. The wave with maximum growth rate propagates at $x/t - U_2 = 0.5$, the mean of the upper and lower layer speeds.

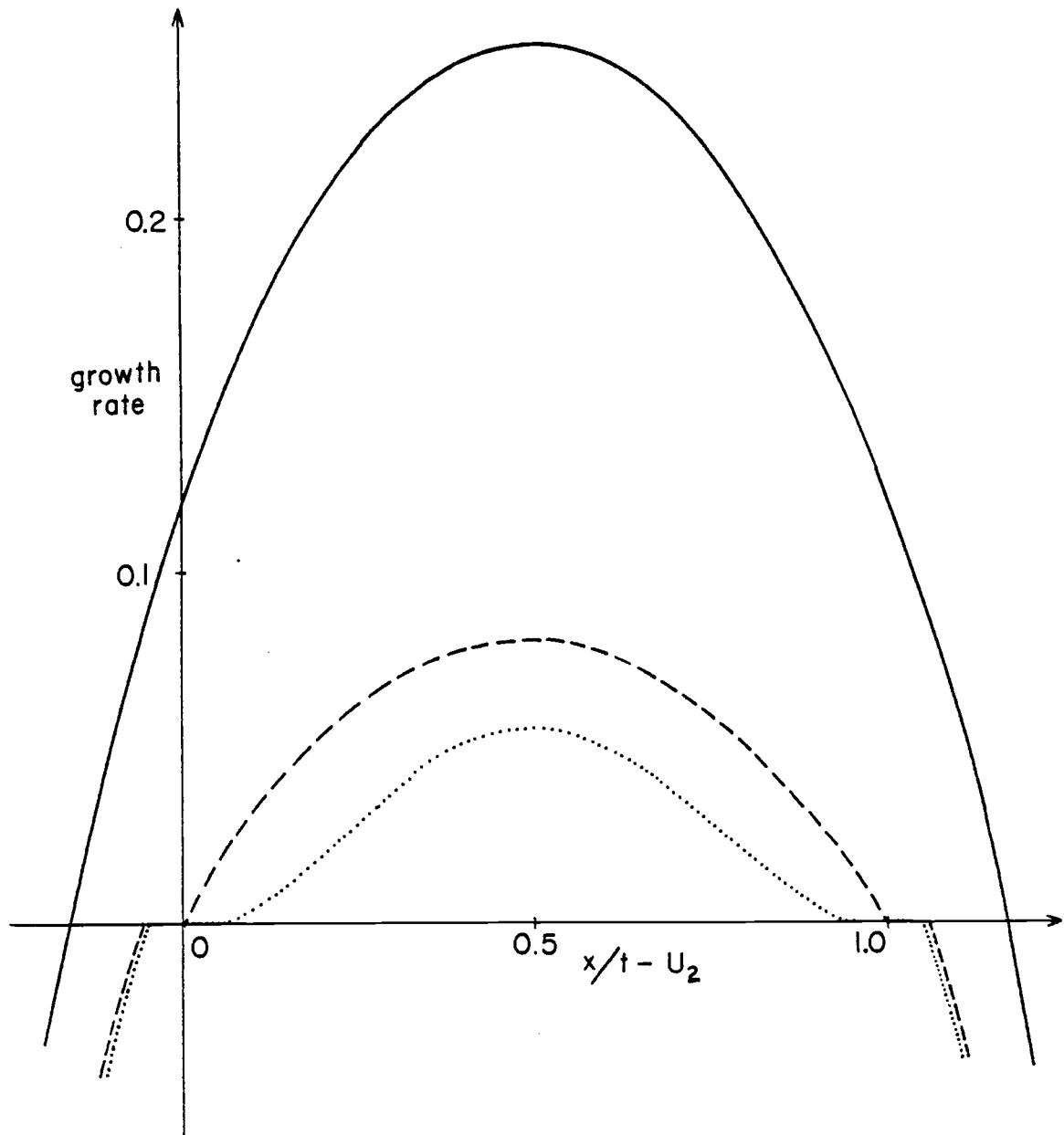


Figure 13a. Growth rates for $l^2 = 0.25$ (solid line), $l^2 = 11/8$ (dashed line) and $l^2 = 1.56$ (dotted line) on f plane.

The symmetry about $x/t - U_2 = 0.5$ is an effect of assuming layer depths equal. The value of m for the fastest growing wave is purely imaginary and this is the wave maximum temporal growth rate. This result was shown by Gaster (1968) and Pedlosky (1976). This means that there is a growing transient excited whenever conditions for temporal instability are met (in this case, whenever $\ell^2 < 2$).

For the case $\ell^2 = 0.25$ the growth rate is positive for $-0.16 < x/t - U_2 < 1.16$. For $x/t - U_2 < 0.16$ and $x/t - U_2 > 1.16$ the asymptotic behavior is exponential decay. Thus if $U_2 < 0.16$ a growing wave propagates upstream of the step. The incoming flow is altered and the instability prevents a steady state from being reached. If $U_2 > 0.16$ the trailing edge of the growing wave propagates downstream of the step. In the region between the tail of the growing transient and the step, the transient decays and we shall see in the next section that the steady state is established in this region.

In Figure 13b additional features of the asymptotic solution for $\ell^2 = 0.25$ are shown. The top curve in Figure 13b is again the growth rate. Below that is the phase speed relative to U_2 which is $-\text{Im}(s)/\text{Im}(m) - U_2$. Finally the amplitude and phase of the ratio of lower to upper layer disturbance stream function, ϕ_2/ϕ_1 , are shown.

For $11/8 < \ell^2 < 2$ the region of positive growth is confined

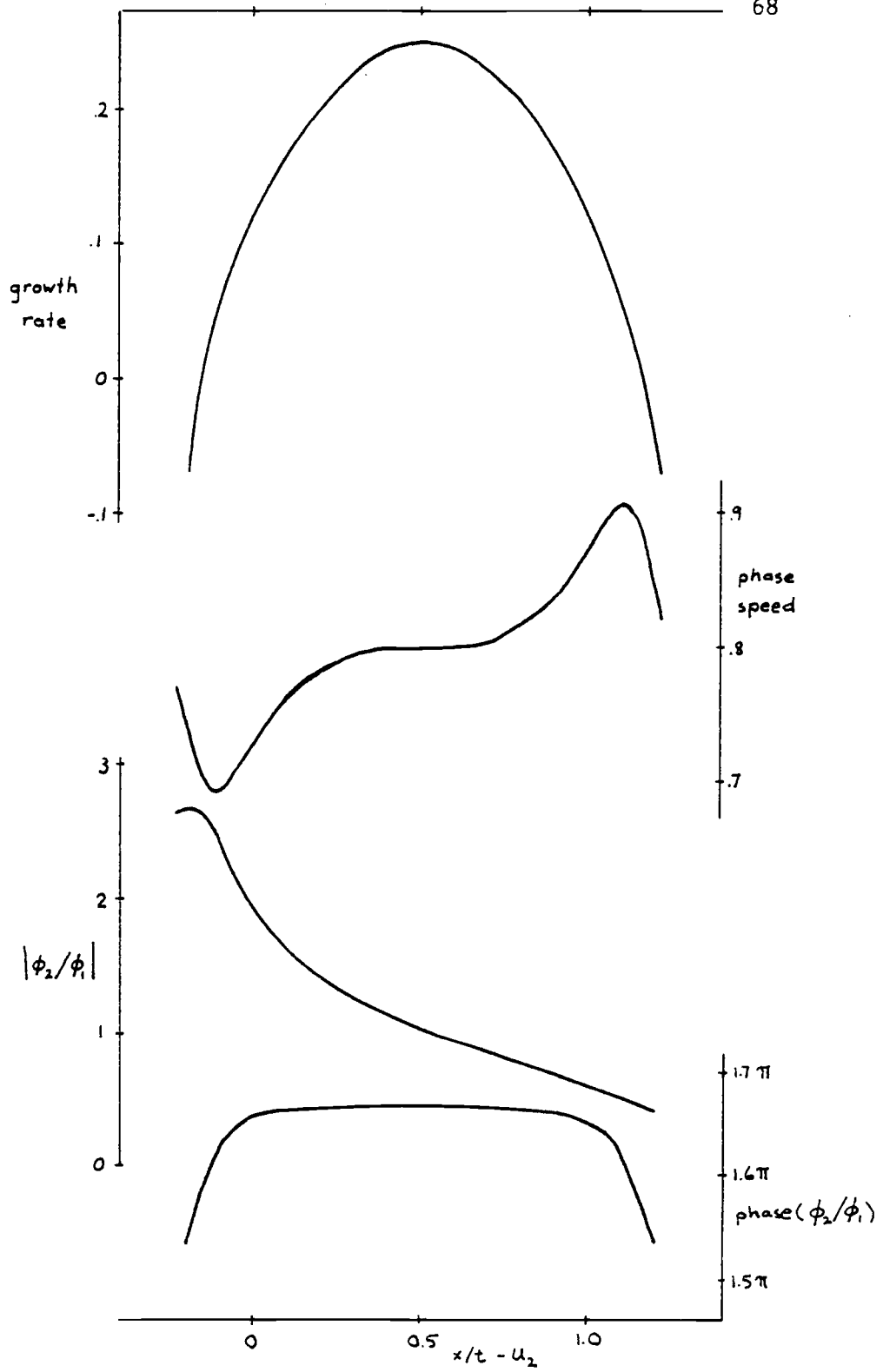


Figure 13b. Growth rate, phase speed relative to U_2 , amplitude and phase of ϕ_2/ϕ_1 for $l^2 = 0.25$ on f plane.

$0 < x/t - U_2 < 1$. U_2 is required only to be arbitrarily small and positive for the growing disturbance to be advected completely downstream. Note that for the two cases $\ell^2 = 11/8$ and $\ell^2 = 1.56$, preceding and trailing the growing portion of the transient, there are regions with zero growth rate. These are waves which arise from the neutral part of the dispersion relation. It is convenient when discussing neutrally stable waves to let $k = \text{Im}(m)$, $\tilde{\omega} = -\text{Im}(\tilde{s})$ and examine that part of (9.6) for which m and s are purely imaginary. This leads to

$$\tilde{\omega} = \frac{1}{2}k \pm \frac{1}{2}k \frac{(k^2 + \ell^2 - 2)^{1/2}}{(k^2 + \ell^2 + 2)^{1/2}} \quad (9.8)$$

$$\text{and } d\tilde{\omega}/dk = \frac{1}{2} \pm \frac{k^4 + 2(\ell^2 + 2)k^2 + \ell^4 - 4}{(k^2 + \ell^2 + 2)^{3/2} (k^2 + \ell^2 - 2)^{1/2}} \quad (9.9)$$

for $k^2 + \ell^2 > 2$.

Observe that $\tilde{\omega}$ is a frequency in a frame of reference moving with the lower layer speed.

The neutral part of the dispersion relation is sketched in Figure 14 together with $d\tilde{\omega}/dk$ for $\ell^2 = 0.25$, $\ell^2 = 11/8$ and $\ell^2 = 1.56$. In each case, at $k^2 = 2 - \ell^2$, $d\tilde{\omega}/dk$ is unbounded. As $k \rightarrow \infty$, $d\tilde{\omega}/dk \rightarrow 1$ for the upper branch and $d\tilde{\omega}/dk \rightarrow 0$ for the lower branch. The result of the saddle point method is that there is a neutral wave contribution to the asymptotic when inflection points develop in $\tilde{\omega}(k)$. These are zeros of $d\tilde{\omega}^2/dk^2$ given by

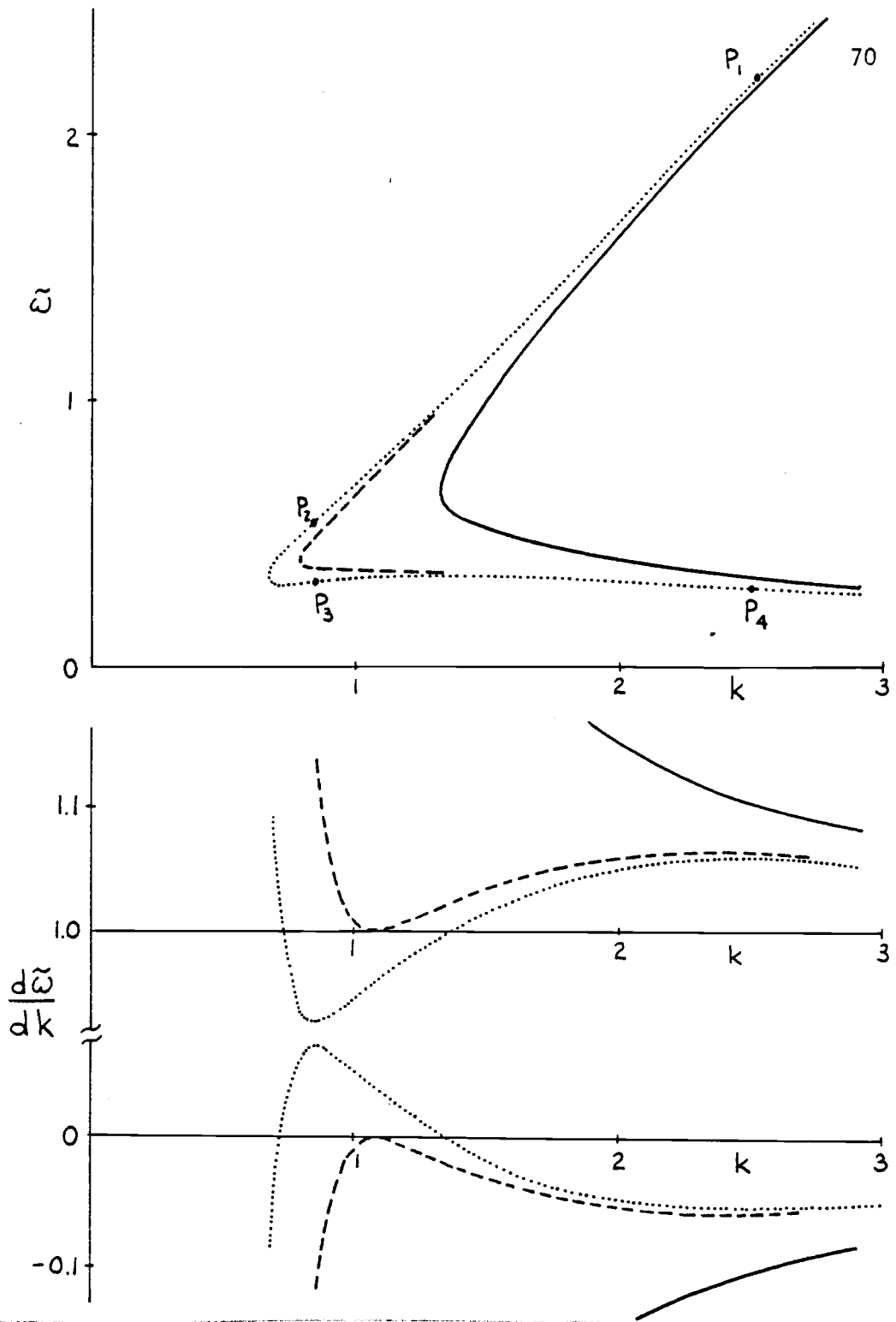


Figure 14. Plot of $\tilde{\omega}$ (upper figure) and $d\tilde{\omega}/dk$ (lower figure) versus k for $\ell^2 = 0.25$ (solid line), $\ell^2 = 11/8$ (dashed line) and $\ell^2 = 1.56$ (dotted line). The points P_1 to P_4 are inflection points of $\tilde{\omega}(k)$.

$$k^2 = \ell^2 + 2 \pm 2[(\ell^2 + 2)(\ell^2 - 1)]^{1/2} \quad (9.10)$$

so that they occur for real values of k when $\ell^2 > 1$.

For example, in Figure 14 for $\ell^2 = 1.56$, the four inflection points from (9.10) are labelled P_j , $j = 1$ to 4. It is found that only those waves to the right of P_2 and P_3 make asymptotic contributions, which propagate at $-0.054 < x/t - U_2 < 0.064$ and $0.94 < x/t - U_2 < 1.054$. The asymptotic decay at the inflection points is $t^{-1/3}$, and is $t^{-1/2}$ at other points from the neutral dispersion relation. Note that the two points of zero $d\tilde{\omega}/dk$ correspond to the branch points along the imaginary \tilde{s} axis in Figure 12 for $\ell^2 > 11/8$.

In the case $\ell^2 = 11/8$ the two values of k at which the lower branch of $d\tilde{\omega}/dk$ is zero have coalesced into a single value of k . Only those waves to the right of this k make asymptotic contributions with propagation speed $-0.059 < x/t - U_2 < 0$ and $1.0 < x/t - U_2 < 1.059$. For $1 < \ell^2 < 11/8$ there are contributions from the neutral dispersion curve, but growth rates at $x/t - U_2 = 0, 1$ are positive. For $\ell^2 < 1$ no part of the neutral dispersion curve makes an asymptotic contribution.

We note that when instability is present ($\ell^2 < 2$) there are saddle points of $m(\tilde{s})x/t + \tilde{s}$ for m and s purely imaginary with $|-ds/dm| = |d\tilde{\omega}/dk|$ arbitrarily large. These saddle points do not contribute to the asymptotic behavior and propagation speeds for the disturbance are bounded.

10. The steady state on the f plane

On inversion of (9.3) the transient arises from integration along the steepest descent contour. The steady solution results from the pole $s = 0$. It is found that the steepest descent path is deformed to the left of $s = 0$ for $x/t - U_2 < 0.5$. The steady state is thus established in this region. The residue of (9.3) from $s = 0$ is

$$\begin{aligned} \phi_1(x) &= -\frac{\hat{h}}{m_3 m_4 \ell^2} + \frac{\hat{h} e^{m_3 x}}{m_3 (m_3 - m_4) (m_3^2 - \ell^2)} \\ &+ \frac{\hat{h} e^{-\ell x}}{2\ell^2 (m_3 + \ell) (m_4 + \ell)} \quad x > 0 \\ \phi_1(x) &= \frac{\hat{h} e^{m_4 x}}{m_4 (m_4 - m_3) (m_4^2 - \ell^2)} - \frac{\hat{h} e^{\ell x}}{2\ell^2 (m_3 + \ell) (m_4 + \ell)} \\ &\quad x < 0 \end{aligned} \tag{10.1a}$$

$$\begin{aligned} \phi_2(x) &= -\frac{(U_1(\ell^2 + 1) - 1) \hat{h}}{U_1 m_3 m_4 \ell^2} - \frac{U_1(m_3^2 - \ell^2 - 1) + 1}{U_1 m_3 m_4 \ell^2} \hat{h} e^{m_3 x} \\ &+ \frac{(U_1 - 1) \hat{h} e^{-\ell x}}{U_1 2\ell^2 (m_3 + \ell) (m_4 + \ell)} \quad x > 0 \end{aligned}$$

$$\phi_2(x) = \frac{U_1(m_4^2 - \ell^2 - 1) + 1}{U_1 m_4 (m_4 - m_3) (m_4^2 - \ell^2)} \hat{h} e^{m_4 x}$$

$$- \frac{(U_1 - 1) \hat{h} e^{\ell x}}{2\ell^2 U_1 (m_3 - \ell)(m_4 - \ell)} \quad x < 0 \quad (10.1b)$$

In (10.1) m_3 and m_4 are evaluated at $s = 0$. The root $m_3(0)$ is real and negative and $m_4(0)$ real and positive so that these roots describe disturbances which decay from the step. They are the roots of (9.1) with $s = 0$,

$$U_1 U_2 (m^2 - \ell^2 - 2) - 1 = 0 \quad (10.2)$$

or

$$m^2 = \frac{1}{U_1 U_2} + \ell^2 + 2 .$$

Observe that as $U_2 \rightarrow 0$, $|m_3(0)|$ and $|m_4(0)| \rightarrow \infty$ and $\phi_j(x) \rightarrow 0$. From Figure 11 $m_1(0)$ and $m_2(0)$ are both zero. There is a net deflection of the streamlines. The $m = 0$ disturbance is formally established for x/t less than $U_2 + 0.5$. The speed $x/t = U_2 + 0.5$ might be interpreted as a signal velocity but note that this value is within the growing transient. We shall comment further on signal velocity in the next section.

The flow over the step is sketched in Figure 15. The deflection of streamlines can be understood by remembering that for positive shear the basic interface slope is upwards towards the positive y direction. Vortex columns in the lower layer are displaced in the positive y direction as they are advected over the

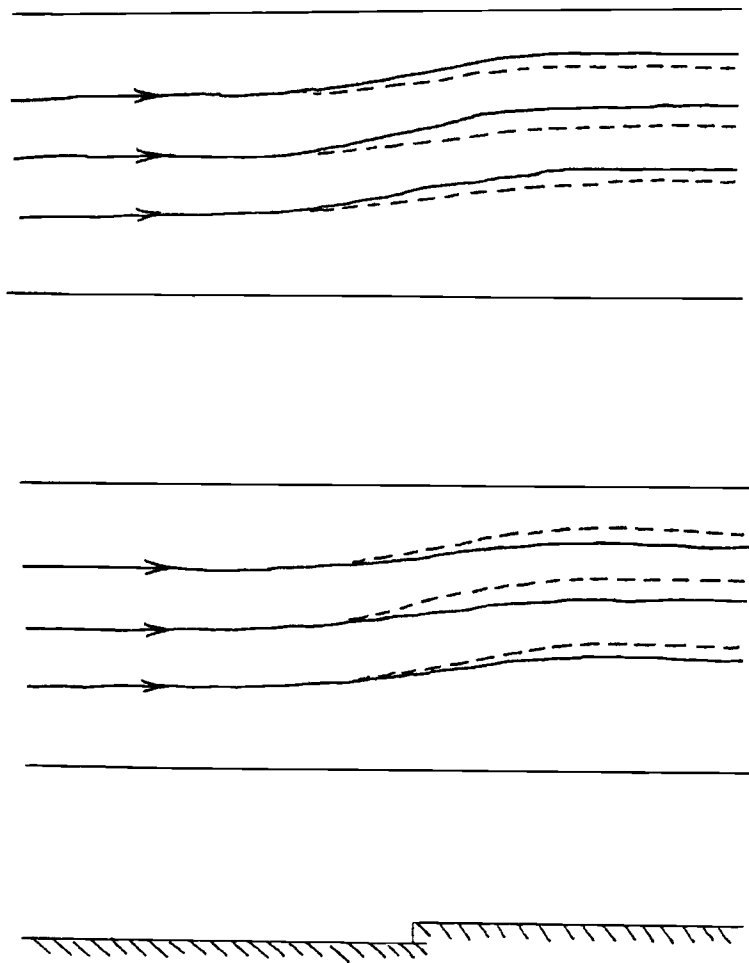


Figure 15. Flow on f plane. Solid lines are streamlines in upper layer, dashed lines are streamlines in lower layer for $\ell \ll 1$ (top) and $\ell \gtrsim 1$ (bottom).

step. Far downstream, where the decaying solutions can be neglected, the ratio of the lower to upper layer perturbation stream functions is

$$\phi_2/\phi_1 = \ell^2 + U_2/U_1 \quad (10.3)$$

This is positive when U_1 and U_2 are both positive. For $\ell^2 \ll 1$ the ratio is the ratio of the initial zonal velocities. The streamlines in the upper and lower layers are nearly identical. For $\ell^2 \gg 1$, the interface acts as a rigid surface confining the disturbance to the lower layer. Recall that ℓ is a ratio of the internal radius of deformation to a cross-channel wave scale. As the wave scale is decreased from a large value to where it is comparable to the internal radius, the effect of stratification is to increasingly attenuate the disturbance with height. This result was demonstrated by Hogg (1973) and McCartney (1975) for Taylor columns.

deSzoeker (1972) has shown that if the upper and lower layer flows are in opposite directions, there exists a steady solution which is wavelike. These are the solutions of (10.2) with m purely imaginary. Our results show these solutions have validity only if $\ell^2 > 2$ and no unstable wave is produced. A growing wave would alter the incoming flow in at least one of the layers.

The steady solution, for the two layers, in contrast to Hogg(1976) for continuously varying vertical shear, is bounded

in space. Let us imagine, for a laboratory flow, a forcing mechanism initiated at $t = 0$ and subsequently oscillating at frequency σ ,

$$\delta(x) H(t) \cos \sigma t.$$

The term on the right of (8.1b) would be the Laplace transform

$$\delta(x) \frac{s}{s^2 + \sigma^2} .$$

The steady state solution would be the residue from poles at $s = \pm i\sigma$. Observe from Figure 11a, that along the imaginary s axis between branch points at $\pm i .95$, $\text{Re}(m_1(s))$ is positive. The steady state in this case would be a wave with frequency σ and spatial growth downstream.

We have shown that at those saddle points of $mx/t + s$ which give an asymptotic contribution for the transient, $-ds/dm$ may be interpreted as a group velocity. We wish to illustrate with the case of oscillatory forcing that at $s = \pm i\sigma$, $\text{Re}(-ds/dm)$ (ds/dm is complex in general) cannot be interpreted as a group velocity. We illustrate this by showing that the sign of $\text{Re}(-ds/dm)$ at $\pm i\sigma$ does not give the correct direction for the steady state response. Suppose that $\sigma = 0.5$. From Figure 11a for the root $m_4(s)$, we see that ds/dm is complex and $\text{Re}(-ds/dm)$ is positive at $s = \pm i 0.5$. However $m_4(s)$ represents a decaying response in the region $x < 0$.

11. The beta effect

11.1 General considerations

We now discuss the modifications to the previous results when β is non-zero. From (8.2), we may express s as

$$s = -U_2 m - \frac{1}{2} \operatorname{sgn}(U_1 - U_2) m + \frac{\beta m (-m^2 + \ell^2 + 1)}{(-m^2 + \ell^2)(-m^2 + \ell^2 + 2)} \\ \pm \frac{m [(-m^2 + \ell^2)^4 - 4(-m^2 + \ell^2)^2 + 4\beta^2]^{\frac{1}{2}}}{2(-m^2 + \ell^2)(-m^2 + \ell^2 + 2)} \quad (11.1)$$

It may be observed that for temporal instability β is required to be less than 1. The range of wavenumbers for temporally unstable waves is then

$$2(1 - (1 - \beta^2)^{\frac{1}{2}}) < (\operatorname{Im}(m)^2 + \ell^2)^2 < 2(1 + (1 - \beta^2)^{\frac{1}{2}}) \quad (11.2)$$

There are six roots $m_j(s)$ to (8.2). Branch points for $m_j(s)$ are found by setting $ds/dm = 0$ in (11.1) and occur at six values of m^2 . We shall not attempt an exhaustive investigation of the dependence on the parameters β and ℓ , rather, we shall illustrate several types of behavior.

Growth rates as a function of $x/t - U_2$ for positive shear, $\beta = 0.5$ and various ℓ are plotted in Figure 16. From (11.1) it can be seen that s for westward shear is related to s for eastward

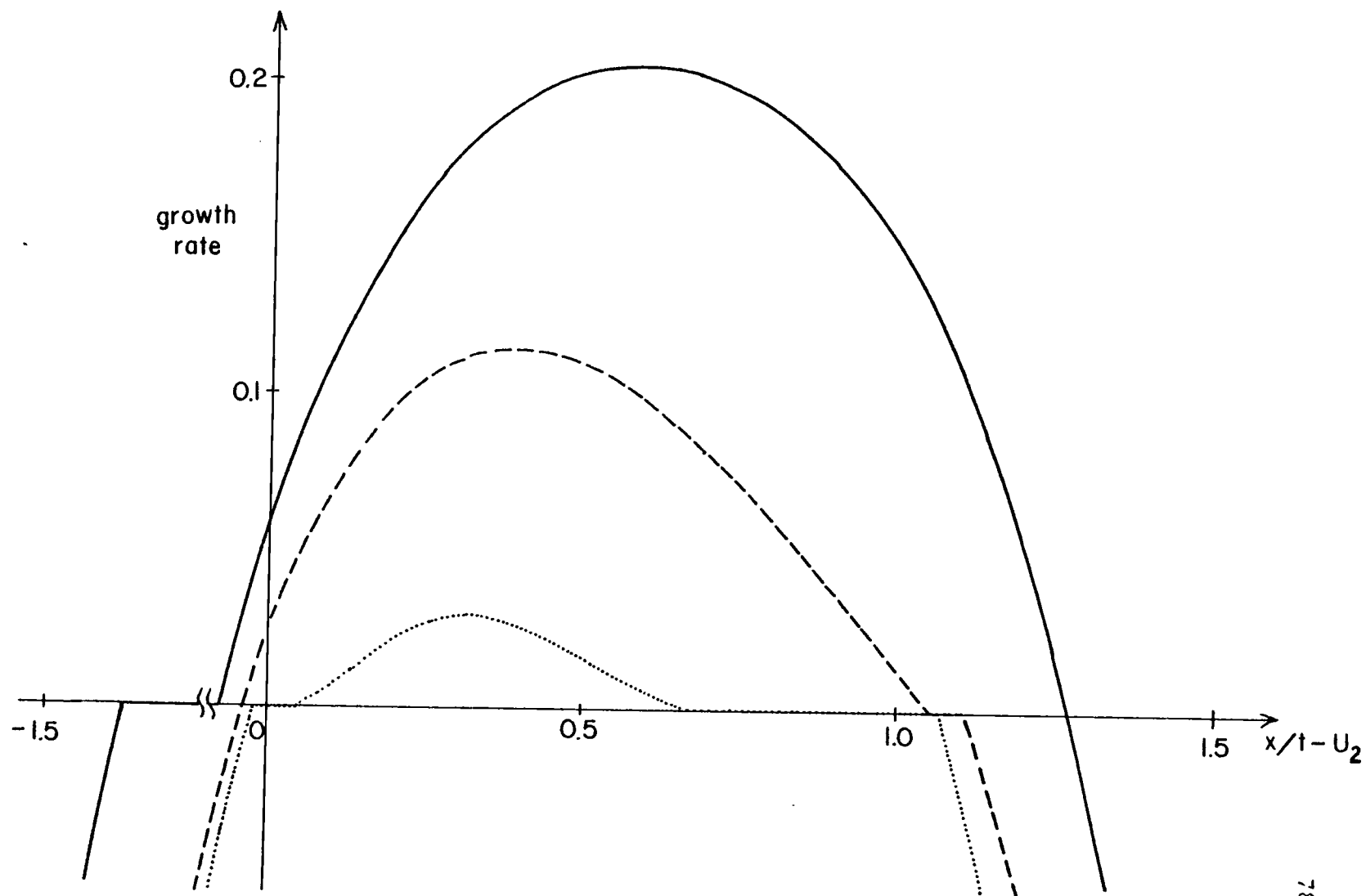


Figure 16. Growth rates for $l^2 = 0.25$ (solid line), $l^2 = 1.0$ (dashed line) and $l^2 = 1.69$ (dotted line) with $\beta = 0.5$.

shear by

$$s^{(m)}_{\text{westward shear}} = s^{(m)}_{\text{eastward shear}} + m$$

and

$$ds/dm_{\text{westward shear}} = ds/dm_{\text{eastward shear}} + 1$$

By substituting these relations into the definition of growth rate, it is seen that growth rates for westward shear can be obtained from Figure 16 by shifting the curves one unit to the left. For example the growth rate at $x/t - U_2 = 1$ in Figure 16 is the growth rate for $x/t - U_2 = 0$ for westward shear. This relationship between growth rate for eastward shear and westward shear is a simplification of taking equal layer depths.

The three curves of Figure 16 show that the wave with maximum growth propagates in the direction of the shear, in a reference frame moving with U_2 . Growth rates of the maximum are smaller than with $\beta = 0$. A qualitative distinction between the curves in Figure 16 is the different manner in which neutral waves contribute. A second distinction is whether there is positive growth rate at $x/t - U_2 = 0, 1$.

11.2 Low wavenumber neutral modes

In discussing the differences in the transient growth rates and in the steady states it is useful to consider the neutral part of the dispersion relation. We again substitute

$\tilde{\omega} = -\text{Im}(s + U_2 m)$ and $k = \text{Im}(m)$ in (11.1) to obtain

$$\begin{aligned} \tilde{\omega} &= \frac{1}{2} \text{sgn}(U_1 - U_2)k - \frac{\beta k(k^2 + \ell^2 + 1)}{(k^2 + \ell^2)(k^2 + \ell^2 + 2)} \\ &\pm \frac{k[(k^2 + \ell^2)^4 - 4(k^2 + \ell^2)^2 + 4\beta^2]^{\frac{1}{2}}}{(k^2 + \ell^2)(k^2 + \ell^2 + 2)} \end{aligned} \quad (11.3)$$

for the neutral stability regions $(k^2 + \ell^2)^2 < 2(1 - (1 - \beta^2)^{\frac{1}{2}})$ and $(k^2 + \ell^2)^2 > 2(1 + (1 - \beta^2)^{\frac{1}{2}})$. Taking $\text{sgn}(U_1 - U_2) = -1$, westward shear, it is found that $\tilde{\omega}/k$ is always negative. The phase speed is westward relative to the lower layer flow and stationary waves are not possible when both layer flows are westward. For eastward shear, $\tilde{\omega}/k$ is negative with the negative sign before the discriminant for $0 < (k^2 + \ell^2)^2 < 2(1 - (1 - \beta^2)^{\frac{1}{2}})$ and with the positive sign for $\beta^2 < (k^2 + \ell^2)^2 < 2(1 + (1 - \beta^2)^{\frac{1}{2}})$. Thus for both layer flows eastward, a stationary wave is possible.

The neutral part of the dispersion curve for $\beta = 0.5$, $\ell^2 = 0.25$ is shown in Figure 17. The waves between 0 and P_1 contribute to the asymptotic transient for $-1.38 < x/t - U_2 < -0.08$ in Figure 17. U_2 must exceed 0.08 for a steady state to be reached.

The six roots $m_j(s)$ are sketched in Figure 18 for eastward shear, $U_2 = 0.2$, $\beta = 0.5$, and $\ell^2 = 0.25$. The roots $m_j(s)$, $j=1$ to 4 apply to $x > 0$, roots $m_5(s)$ and $m_6(s)$ apply to $x < 0$. For the steady solution there is a stationary wave downstream of the step

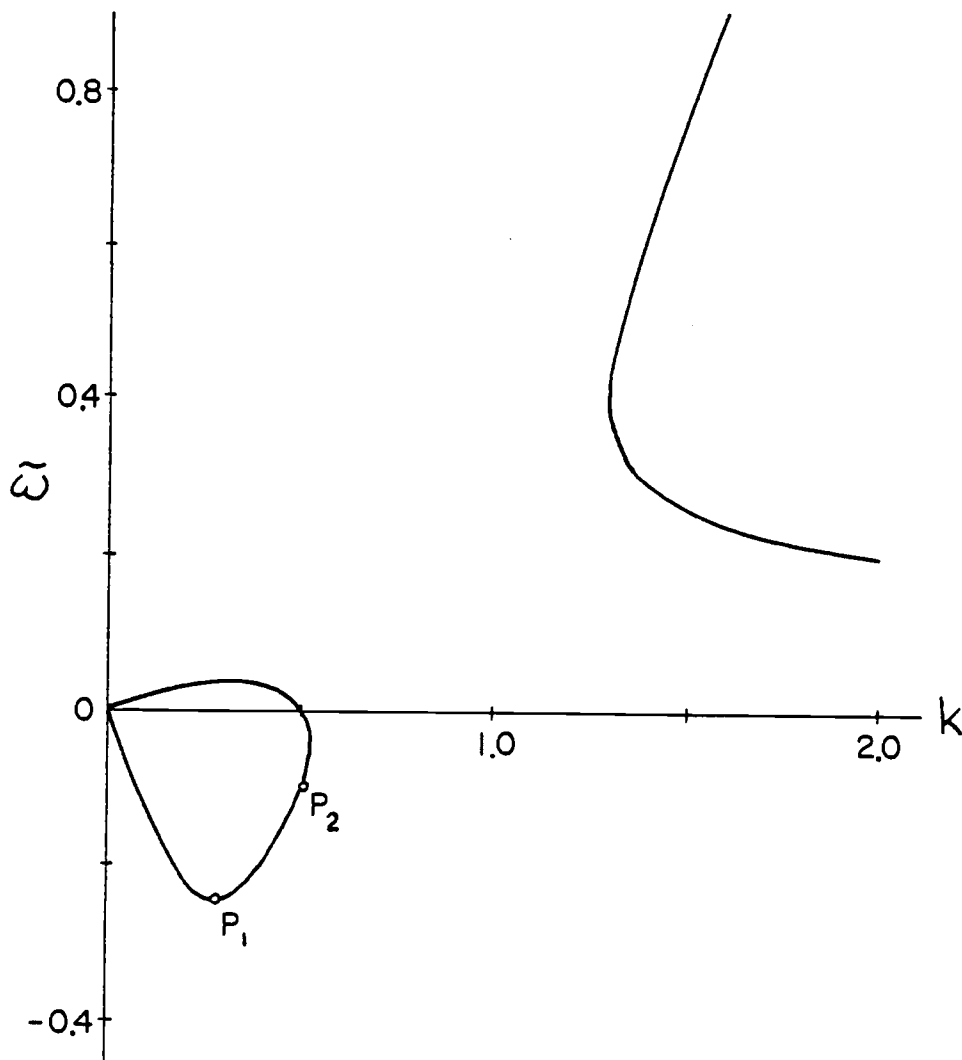


Figure 17. Neutral part of dispersion relation, $\beta = 0.5$, $\ell^2 = 0.25$.
 Points between 0 and P_1 contribute to asymptotic transient.
 Stationary wave when $U_2 = 0.2$ arises from P_2 .

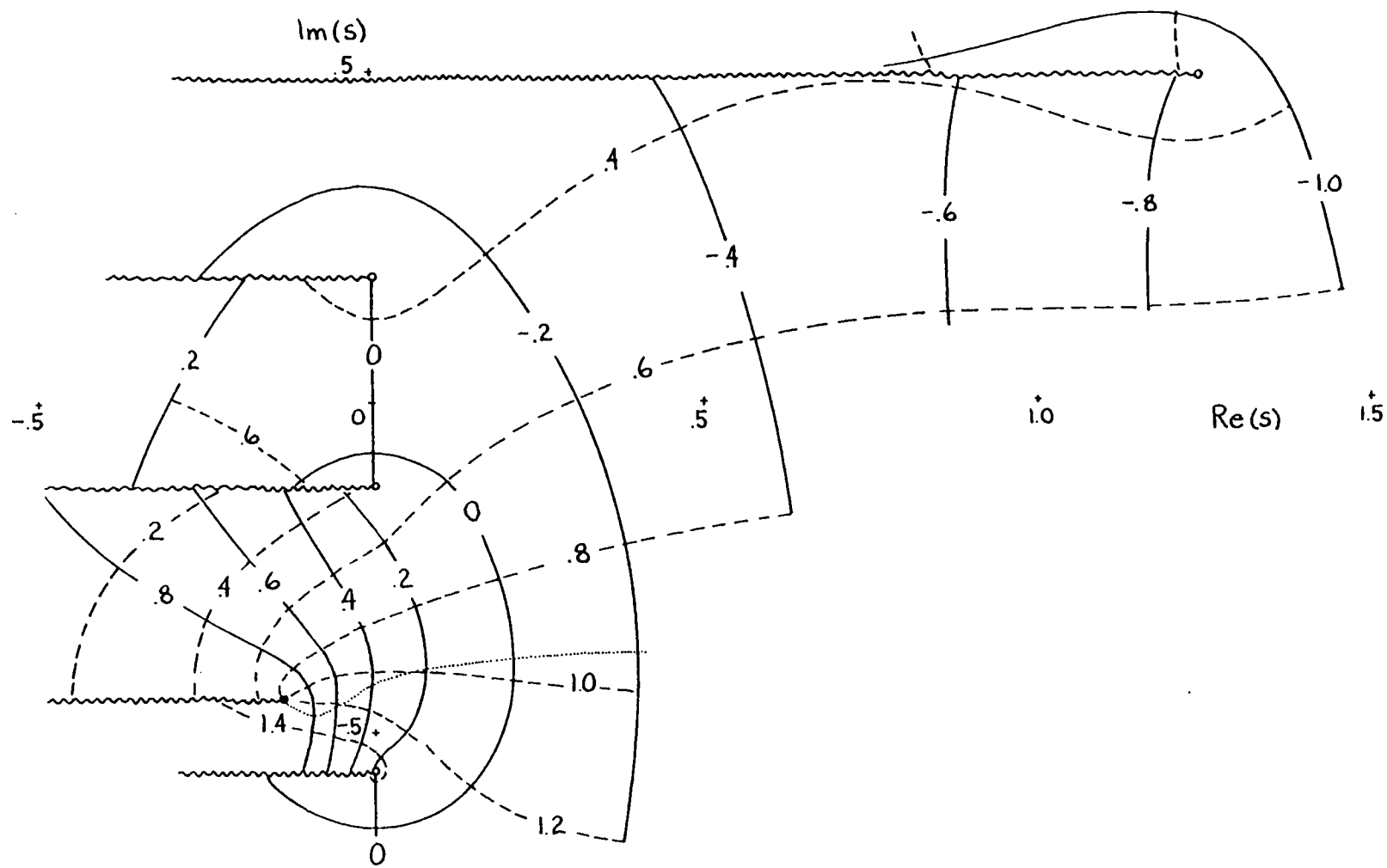


Figure 18a. The root $m_1(s)$, $U_2 = 0.2$, $\beta = 0.5$, $\ell^2 = 0.25$. Contours of real (solid lines) and imaginary (dashed lines) parts of $m_1(s)$ drawn on complex s plane. Closed circle (•) is a branch point for full solution, open circles (o) are branch points for a root $m_j(s)$ only. Dotted line is locus of saddle points.

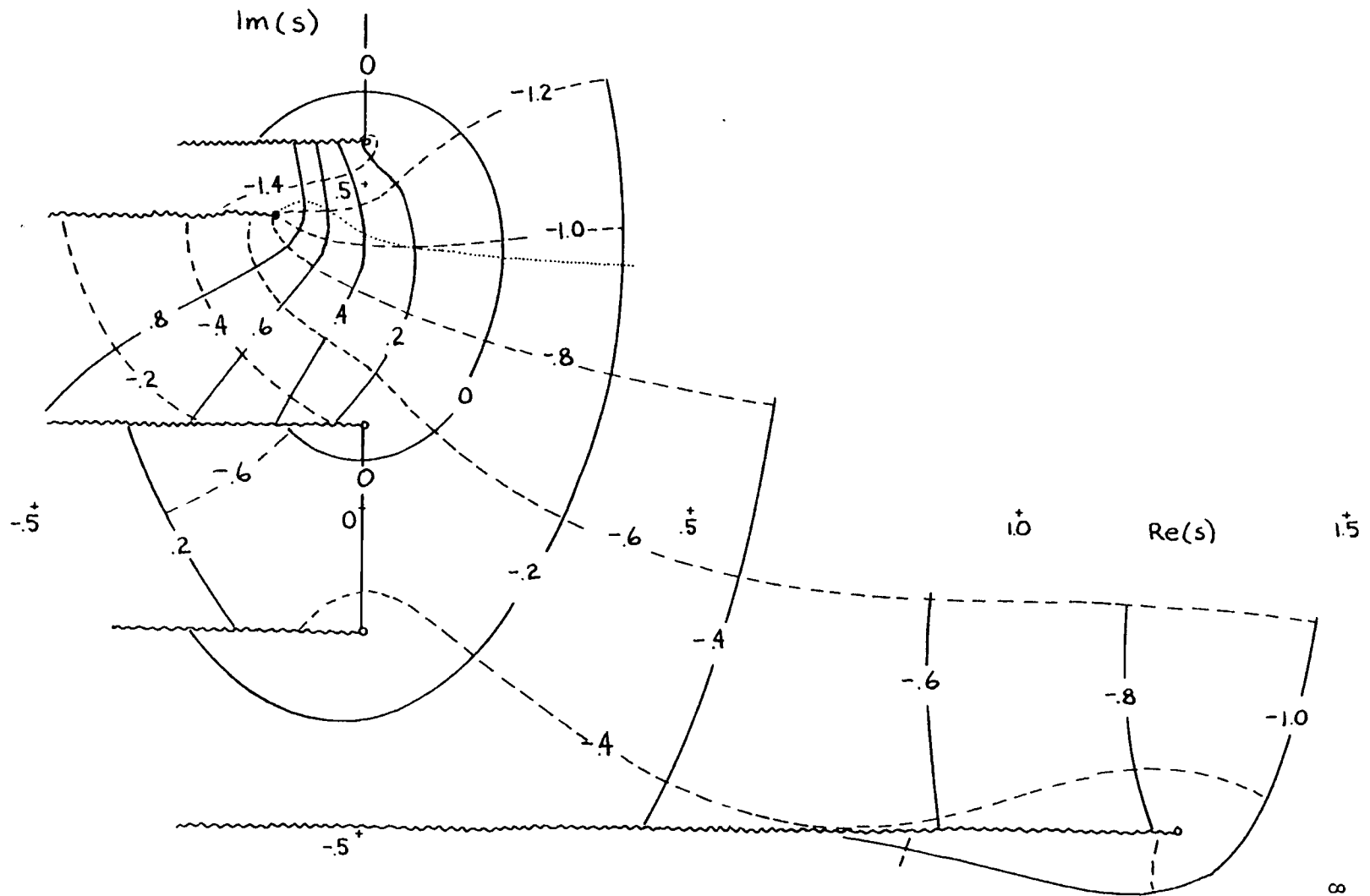


Figure 18b. The root $m_2(s)$.

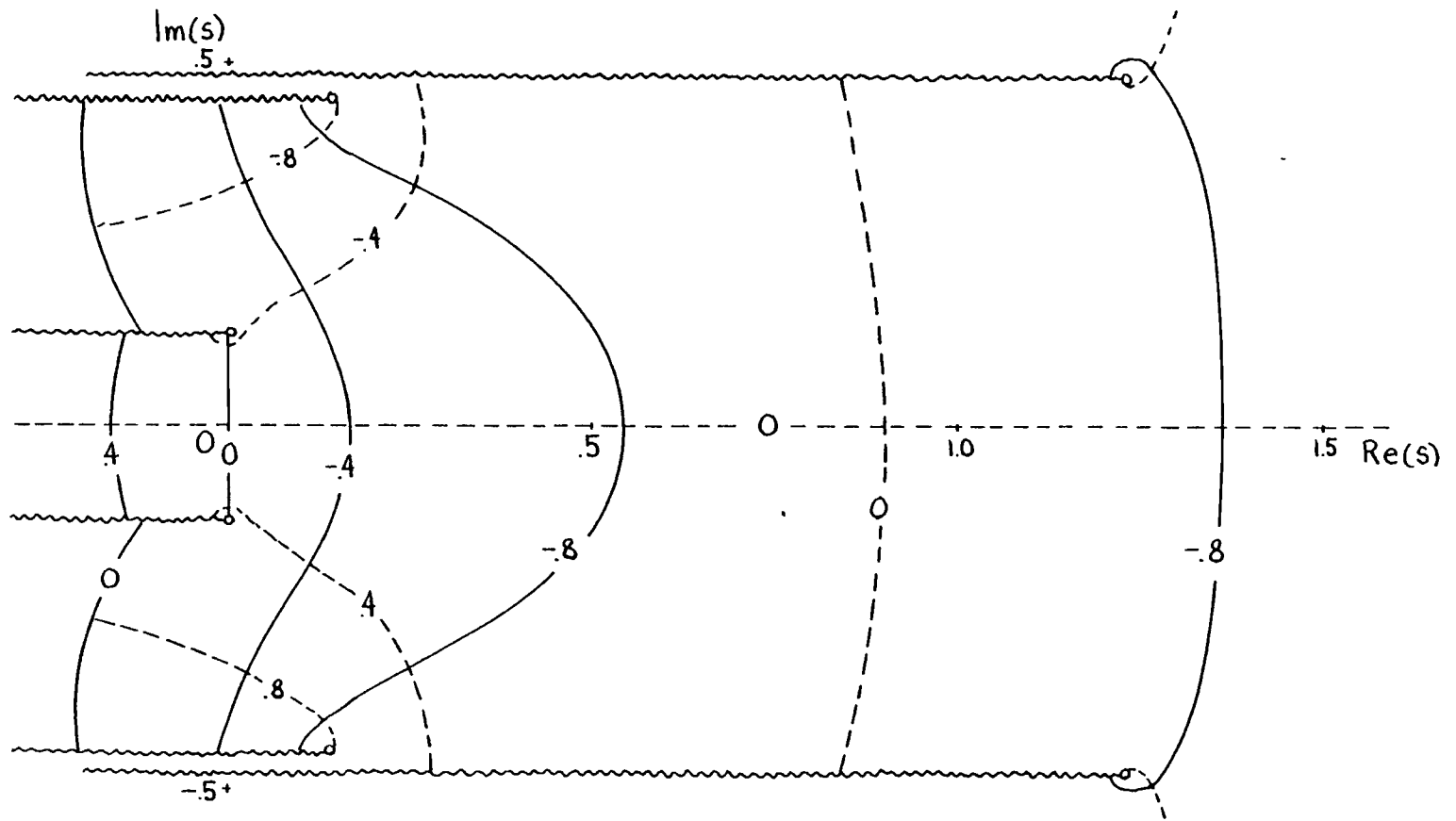


Figure 18c. The root $m_3(s)$.

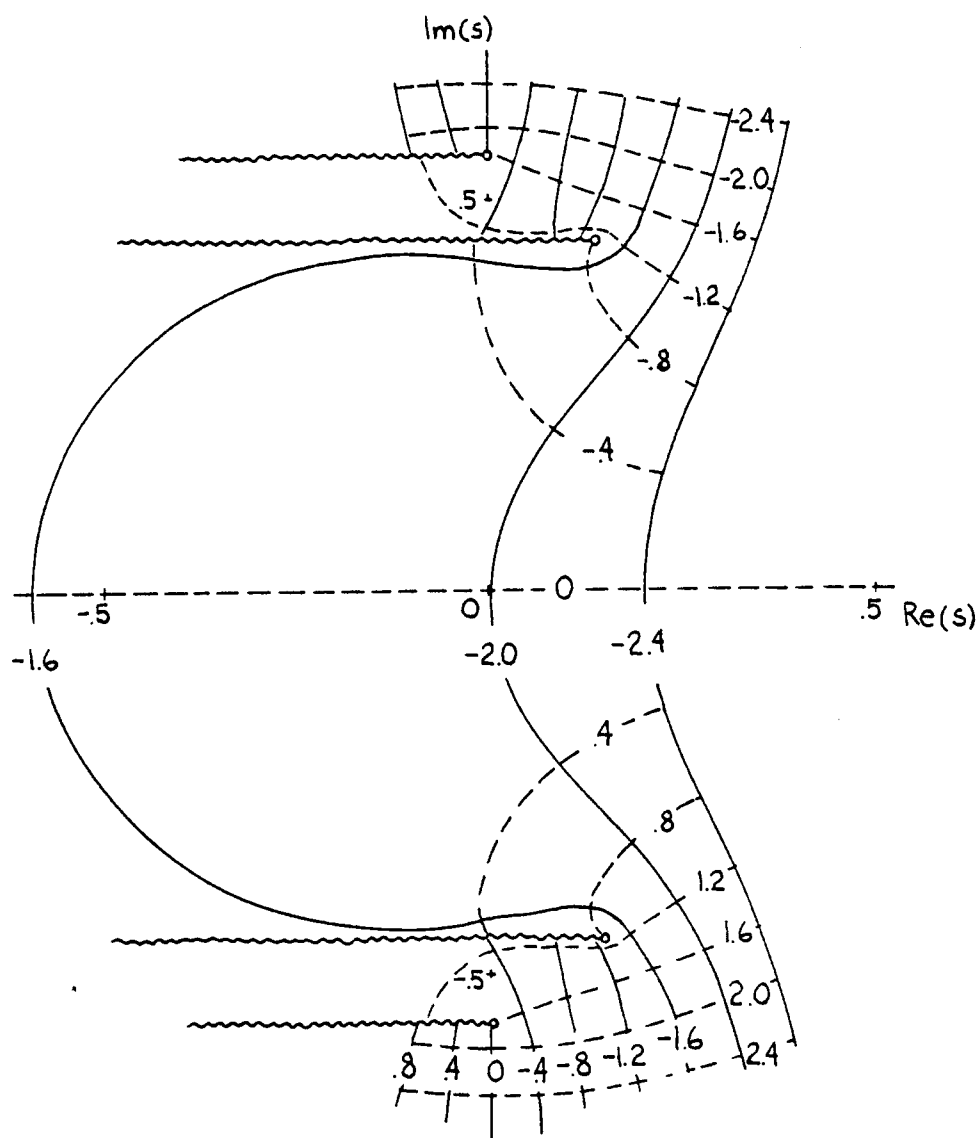


Figure 18d. The root $m_4(s)$.

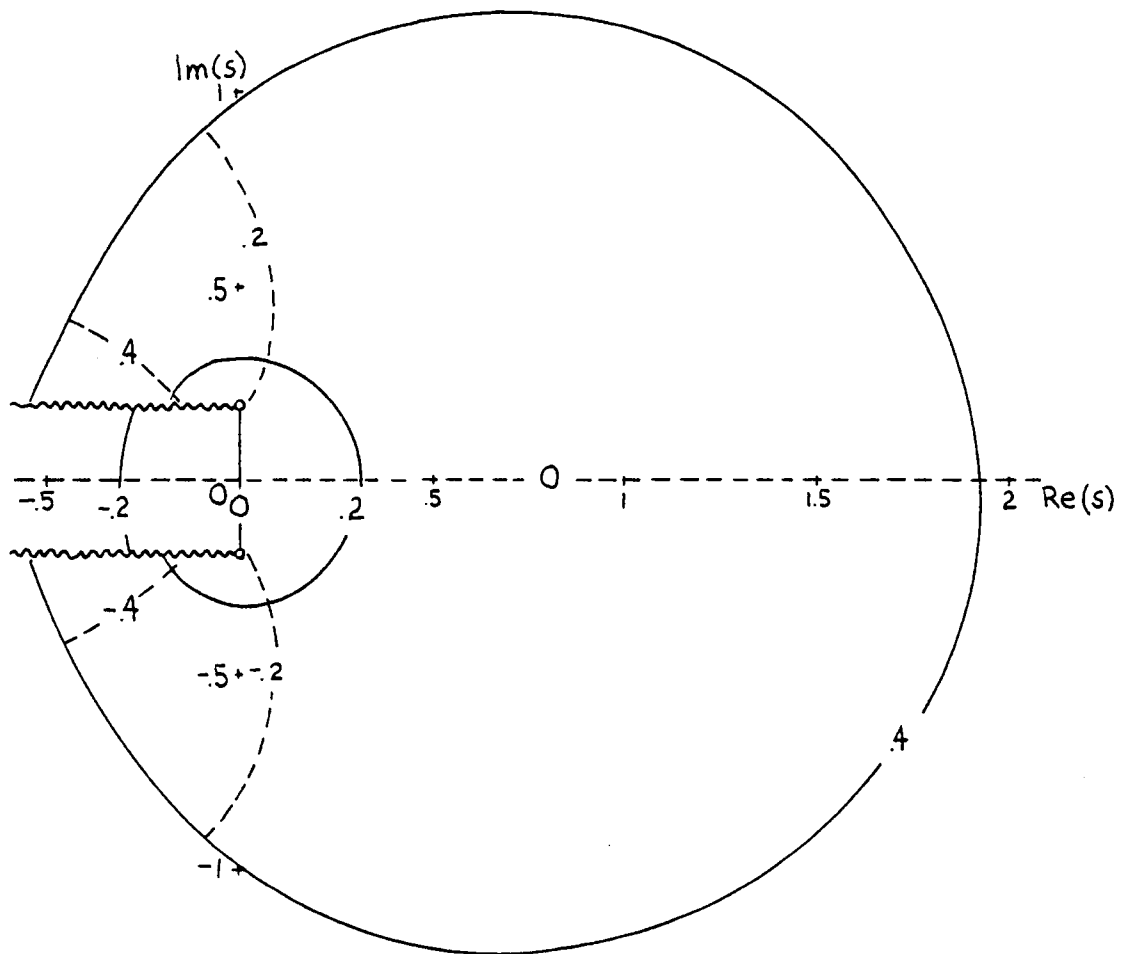


Figure 18e. The root $m_5(s)$.

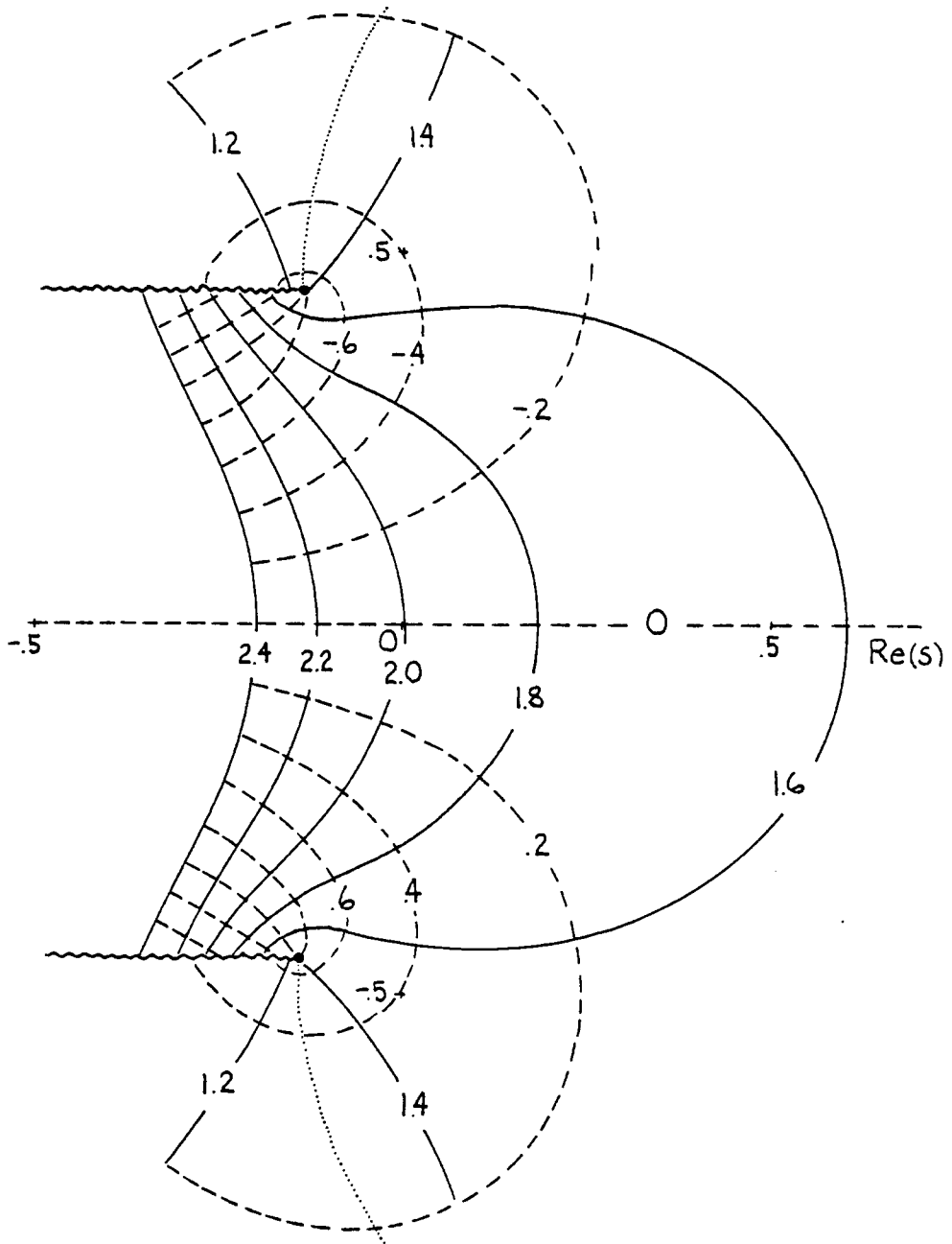


Figure 18f. The root $m_6(s)$.

given by $m_1(0)$ and $m_2(0)$. The wavenumber, k_0 , of the stationary wave is obtained from (11.3) by setting $\omega/k = -U_2$ and is

$$k_0^2 + \ell^2 = -\frac{1}{2} (N_1 + N_2) + \frac{1}{2} [(N_1 - N_2)^2 + 4]^{\frac{1}{2}} \quad (11.4)$$

where

$$N_1 = -\frac{\beta}{U_1} + \frac{U_2}{U_1}$$

and

$$N_2 = -\frac{\beta}{U_1} + \frac{U_1}{U_2}.$$

The stationary wave arises from the point P_2 on the neutral dispersion curve in Figure 17. At P_2 $d\bar{\omega}/dk = 1.84$. From Figure 16, $x/t - U_2 = 1.84$ is in the region of exponential decay ahead of the transient. From the saddle point method the contour is deformed across the pole at $s = 0$ for $x/t - U_2 < 0.10$. Thus, as found by Gadgil (1976), group velocity of the stationary wave is not equivalent to the signal velocity for the steady solution. Note from Figure 16 that $x/t - U_2 = 0.10$ is in the region of positive growth so that similarly to the f plane example, the interpretation of $x/t - U_2 = 0.10$ as a signal velocity is obscured.

Roots $m_3(0)$ and $m_5(0)$ are zero and represent disturbances independent of x which have propagated far upstream and downstream. Decaying solutions are represented by $m_4(0)$ and $m_6(0)$. The steady solution is

$$\begin{aligned}
\phi_1(x) &= \frac{\hat{h}}{k_0^2(k_0^2 + m_4^2)(k_0^2 + m_6^2)} \cdot \\
&\cdot [(k_0^2 - m_4 m_6) \cos k_0 x + k_0(m_4 + m_6) \sin k_0 x] \\
&+ \frac{\hat{h}}{m_4 m_6 k_0^2} + \frac{\hat{h} e^{m_4 x}}{m_4(m_4^2 + k_0^2)(m_4 - m_6)} \quad x > 0 \\
\phi_1(x) &= -\frac{\hat{h}}{m_4 m_6 k_0^2} - \frac{\hat{h} e^{m_6 x}}{m_6(m_6^2 + k_0^2)(m_6 - m_4)} \quad (11.5)
\end{aligned}$$

The ratio of the lower to upper layer stream function amplitudes for the stationary wave part is

$$\phi_2/\phi_{1_{\text{wave}}} = k_0^2 + \ell^2 - \frac{\beta}{U_1} + \frac{U_2}{U_1} \quad (11.6)$$

Equation (11.6) is identical to an expression derived by McCartney (1975) for ϕ_2/ϕ_1 far downstream of a bottom feature with non-linear terms taken into account. When $k_0^2 + \ell^2$ from (11.5) is substituted in (11.6) it can be shown that $\phi_2/\phi_{1_{\text{wave}}} \rightarrow U_2/U_1$ as $\beta \rightarrow 0$ and that for $\beta > 0$, $\phi_2/\phi_{1_{\text{wave}}}$ exceeds U_2/U_1 when U_1 and U_2 are both positive.

11.3 High wavenumber neutral modes

For the higher cross-channel modes, ℓ^4 exceeds $2(1 - (1 - \beta^2)^{\frac{1}{2}})$ and the low wavenumber neutral modes disappear. Cross-channel modal numbers $\ell^2 = 1.0$ and $\ell^2 = 1.69$ are in this range. The growth curves in Figure 16 for these values of ℓ^2 show an asymptotic

contribution from neutral waves to the east of the growing portion. In Figure 19 $d\tilde{\omega}/dk$ is drawn for $\ell^2 = 1.0$ and the neutral wave portion of the dispersion relation. As in the f plane case, there are inflection points for the upper branch and neutral waves are found in the interval $1.08 \leq x/t - U_2 \leq 1.11$. The lower branch of $\tilde{\omega}(k)$ contains no inflection points and makes no asymptotic contribution. Neutral waves to the west, for $\ell^2 = 1.69$ arise from the lower branch of the neutral dispersion curve. For $\ell^2 = 1.69$, the growth rates at $x/t - U_2 = 0, 1$ are zero hence an arbitrarily small U_2 advects the growing disturbance downstream. The steady state in both cases is a displacement of stream lines downstream of the step.

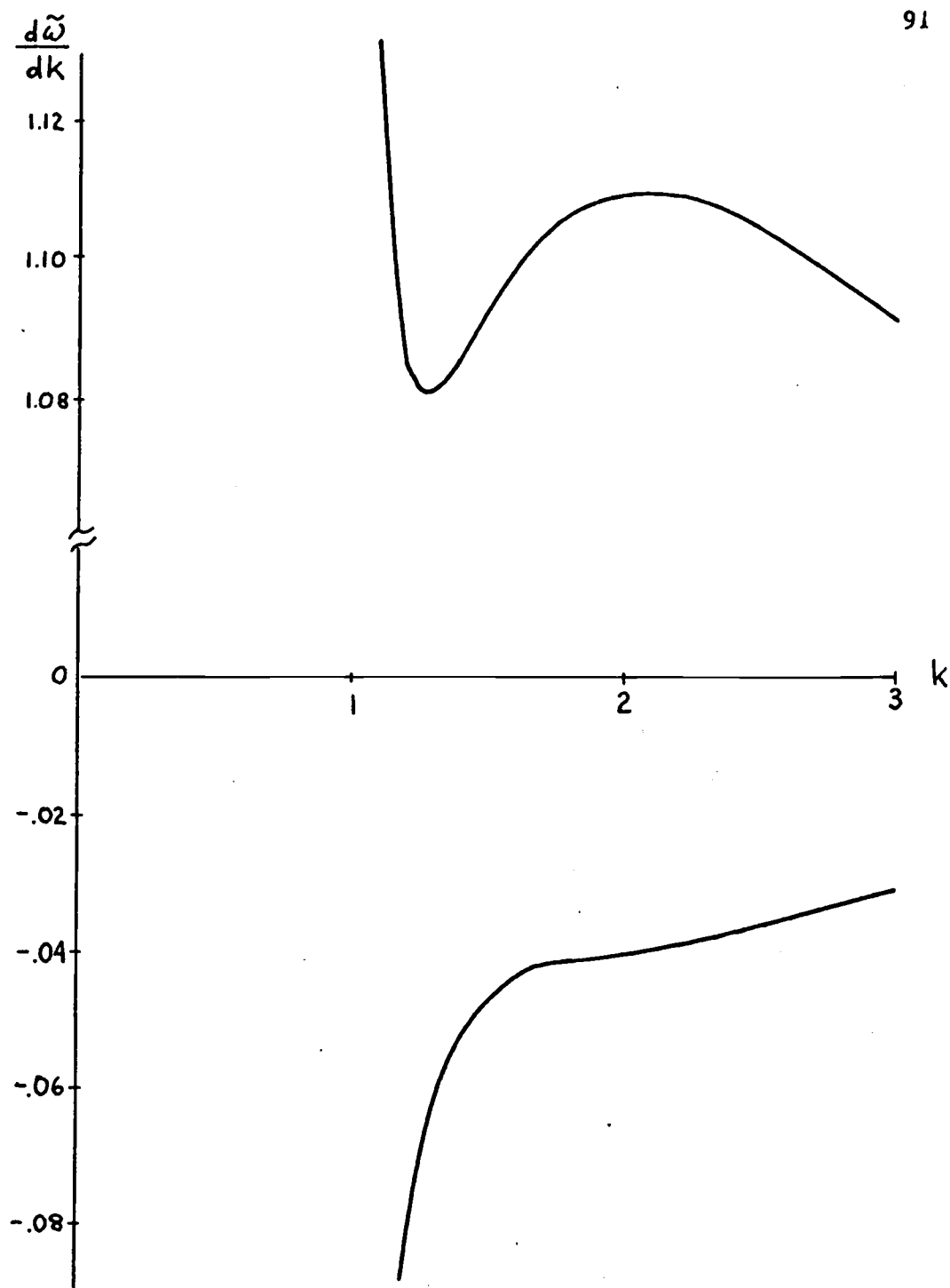


Figure 19. $d\tilde{\omega}/dk$ as a function of k in neutral part of dispersion relation $\beta = 0$, $\ell^2 = 1$. Points on upper curve to right of minimum contribute to asymptotic transient.

12. Summary of instability problem

The steady ($\sigma = 0$) solutions for the two layers are bounded. The extension of the initial value problem to continuously varying vertical shear is not a trivial one. Pedlosky (1964a) considered an initial value problem of the Eady system. The Eady modes are solutions to the vertical eigenvalue problem but do not form a complete set. Pedlosky found that the continuous spectrum, solutions with a delta function behavior in the vertical, was needed to describe the behavior from an initial state although the long time behavior was dominated by the unstable Eady modes.

The question of whether there is a meaningful signal velocity for the establishment of the stationary wave was raised by Gadgil (1976). In the examples we have examined the stationary wave is formally established at a speed at which a growing wave is propagating. The stationary wave, which is bounded is not observed until the growing part of the transient has passed. Thus it appears that the trailing edge of the growing transient has more relevance as a speed for the establishment of the steady solution.

APPENDIX

The saddle point method for the asymptotic approximation to the solution is outlined here. We have a sum of integrals of the form

$$\frac{1}{2\pi i} \int A(s) e^{(m_j(s)x/t + s)t} ds$$

where x/t is given, $t \rightarrow \infty$ and $m_j(s)$ is one of the roots of (8.2). We show that not all the saddle points, i.e. those points satisfying

$$\frac{dm_j}{ds} \frac{x}{t} + 1 = 0$$

give asymptotic contributions.

We illustrate with several examples from the case $U_2 = 0.3$, $\beta = 0$ and $\ell^2 = 0.25$ for which the four roots $m_j(s)$ are drawn in Figure 11. The contour C , for the inversion of the transformed solution, can be deformed into \hat{C} as shown in Figure 20. From contour \hat{C} , it is observed that branch points for the full solution (the closed circles in Figure 11) dominate for x fixed and $t \rightarrow \infty$. The growth rate is $\text{Re}(s)$ at the branch point, and is negative.

For values of x/t non-zero, it is necessary to examine the individual roots to evaluate growth rates. From the growth rate curve in Figure 13a for $\beta = 0$, $\ell^2 = 0.25$, the asymptotic solution decays exponentially for $x/t - U_2 < -0.16$. Thus, with $U_2 = 0.3$

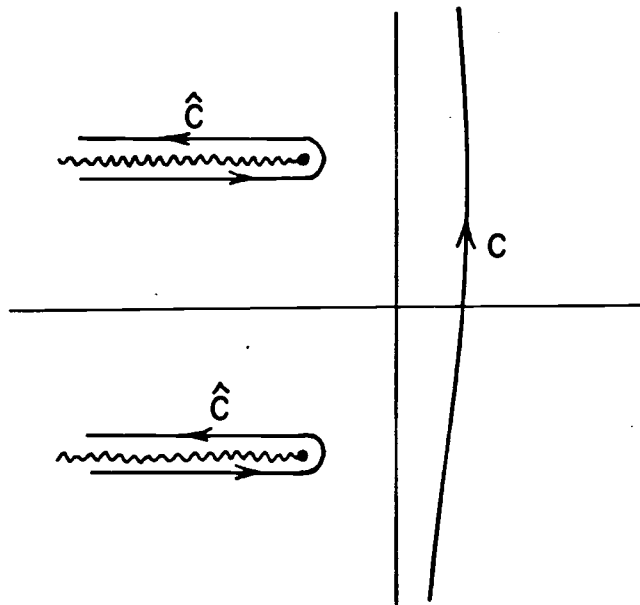


Figure 20. Contour on complex s plane for inversion of Laplace transform.

there is a decay for $x/t < 0.14$. To illustrate how this result was arrived at, we have drawn integration contours for a typical value of x/t in the range $0 < x/t < 0.14$ in Figure 21. The sign of $\text{Re}(m_j(s)x/t + s)$ and branch cuts for $m_j(s)$, $j = 1-3$ are indicated. There is symmetry about the $\text{Re}(s)$ axis and only the lower half s plane is drawn. Saddle points occur at P_1, P_2, P_3 and P_4 . Since the integral along C equals the integral along \hat{C} (plus residues of any poles between the two) then contours C_2 and C_2' , C_3 and C_3' and C_4 and C_4' must cancel one another. Note that C could have been chosen to pass through P_3 without deforming about the pair of branch points on the real s axis to give the integral for $m_1(s)$. However, if this were done, the integrals from $m_2(s)$ and $m_3(s)$ could not be evaluated. This is the reason for the choice of contours in Figure 22. Saddle points P_2, P_3 and P_4 are irrelevant. Note that at P_2 , $m_1(s)$ and s are purely imaginary, but this neutral wave gives no asymptotic contribution. The contour C_1 is the path of the steepest descent through P_1 , giving the asymptotic form (9.5). P_1 is in a region of negative $\text{Re}(m_1(s)x/t + s)$ resulting in negative growth rate.

From Figure 13a there is positive growth for $-0.16 < x/t - U_2 < 1.16$. Integration contours for a typical value of x/t in $0.14 < x/t < 1.46$ are drawn in Figure 22. Again the integration along C_2 and C_2' cancels. Along C_3 and C_4 the integral is exponentially small. The asymptotic approximation arises from the

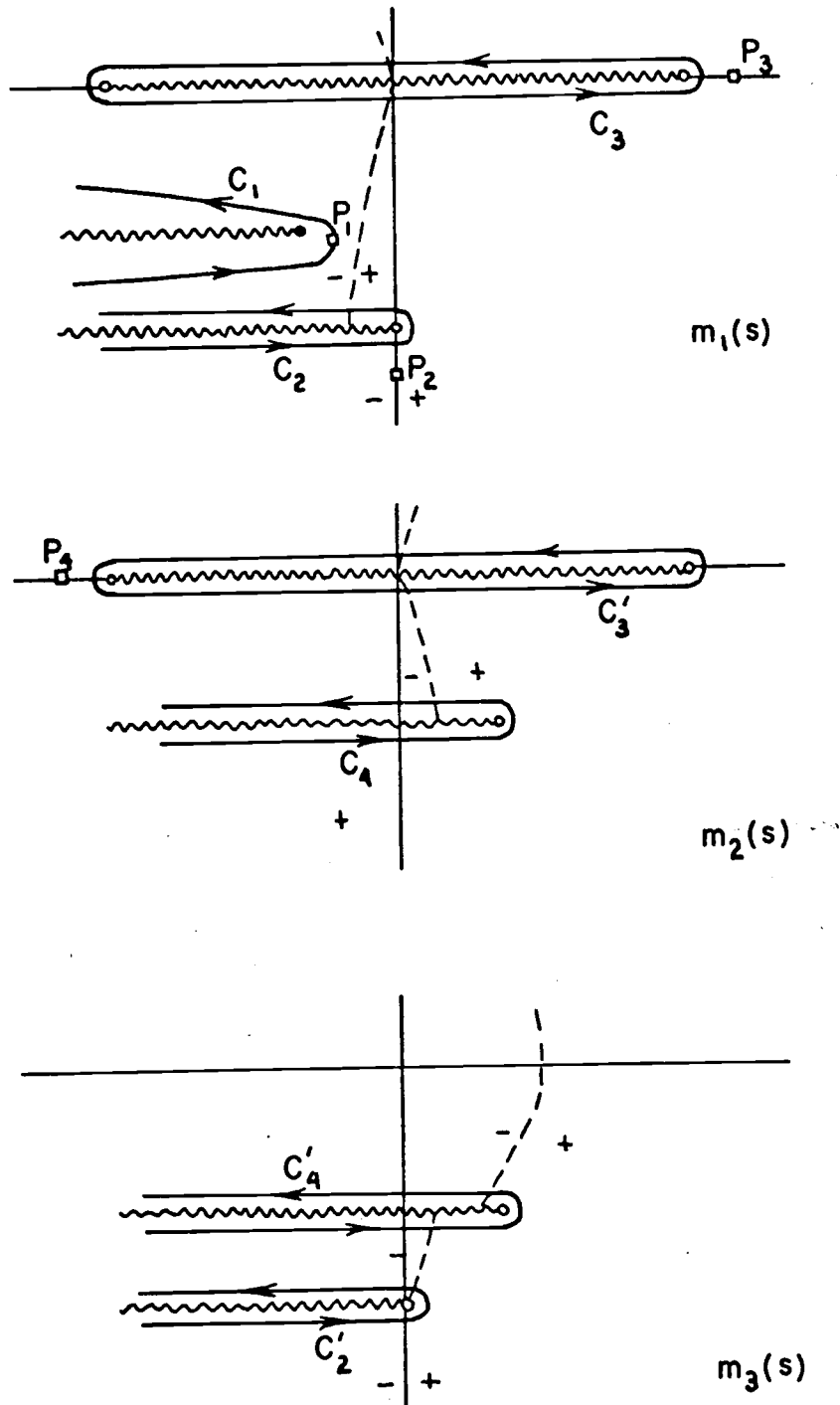


Figure 21. Typical contour for $0 < x/t < 0.14$ for the three downstream roots. Saddle points of $m_j x/t + s$ are denoted by \square . The regions of positive and negative $\text{Re}(m_j x/t + s)$ are indicated.

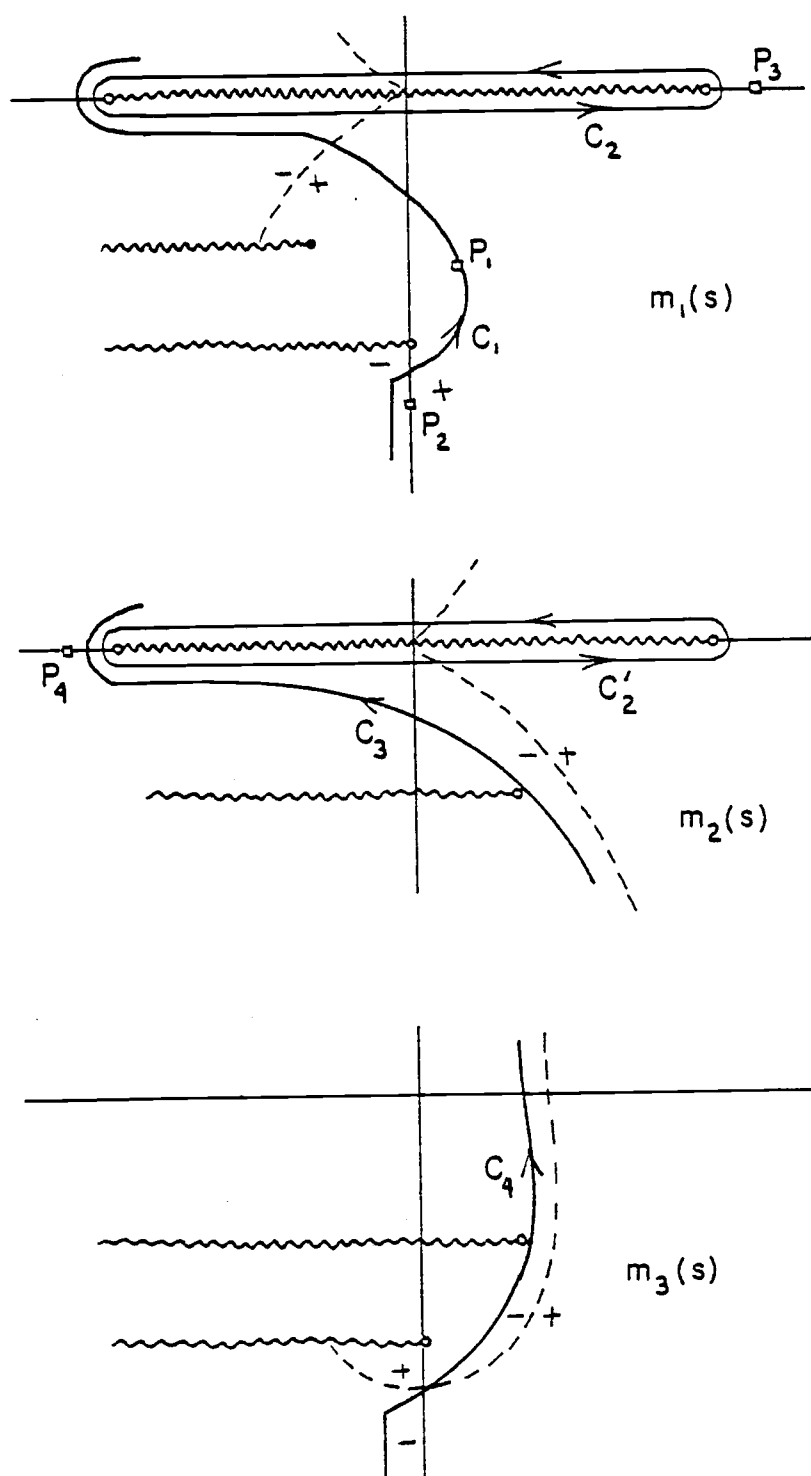


Figure 22. Typical contour for $0.14 < x/t < 1.46$.

saddle point, P_1 , for which the growth is positive. P_2 is a point of stationary phase for a neutral wave and gives negligible contribution relative to P_1 .

Integration contours for a typical value of $x/t > 1.46$ are drawn in Figure 23. Contours encircling the branch cut along the real s axis for $m_1(s)$ and $m_2(s)$ were shown to result in zero net contribution. Recalling that $m_1(s)$ is continuous with $m_2(s)$ across the branch cut, it can be verified that the contours C_2 and C_2' in Figure 24 also must cancel. P_2 is again the neutral wave but any contour through P_2 must pass through a region in which $\text{Re}(m_1(s)x/t + s)$ is positive. Thus the asymptotic form of the integral is not obtained from P_2 . The asymptotic approximation is found from the steepest descent path through P_1 , resulting in a negative growth rate. It should be verified in a particular calculation that the integral along C_3 , for which $\text{Re}(m_3(s)x/t + s)$ is negative but there is no saddle point, is exponentially small relative to the integral along C_1 .

For $x/t < 0$, there is a single root $m_4(s)$ describing the solution, and the saddle point method is straightforward. The steady solution results from the pole $s = 0$. For $x/t > U_2 + 0.5$, the steepest descent contours are found to pass to the right of $s = 0$ and there is no contribution from the pole. For $x/t < U_2 + 0.5$, the steepest descent paths pass to the left of $s = 0$ and the steady state is set up in this region.

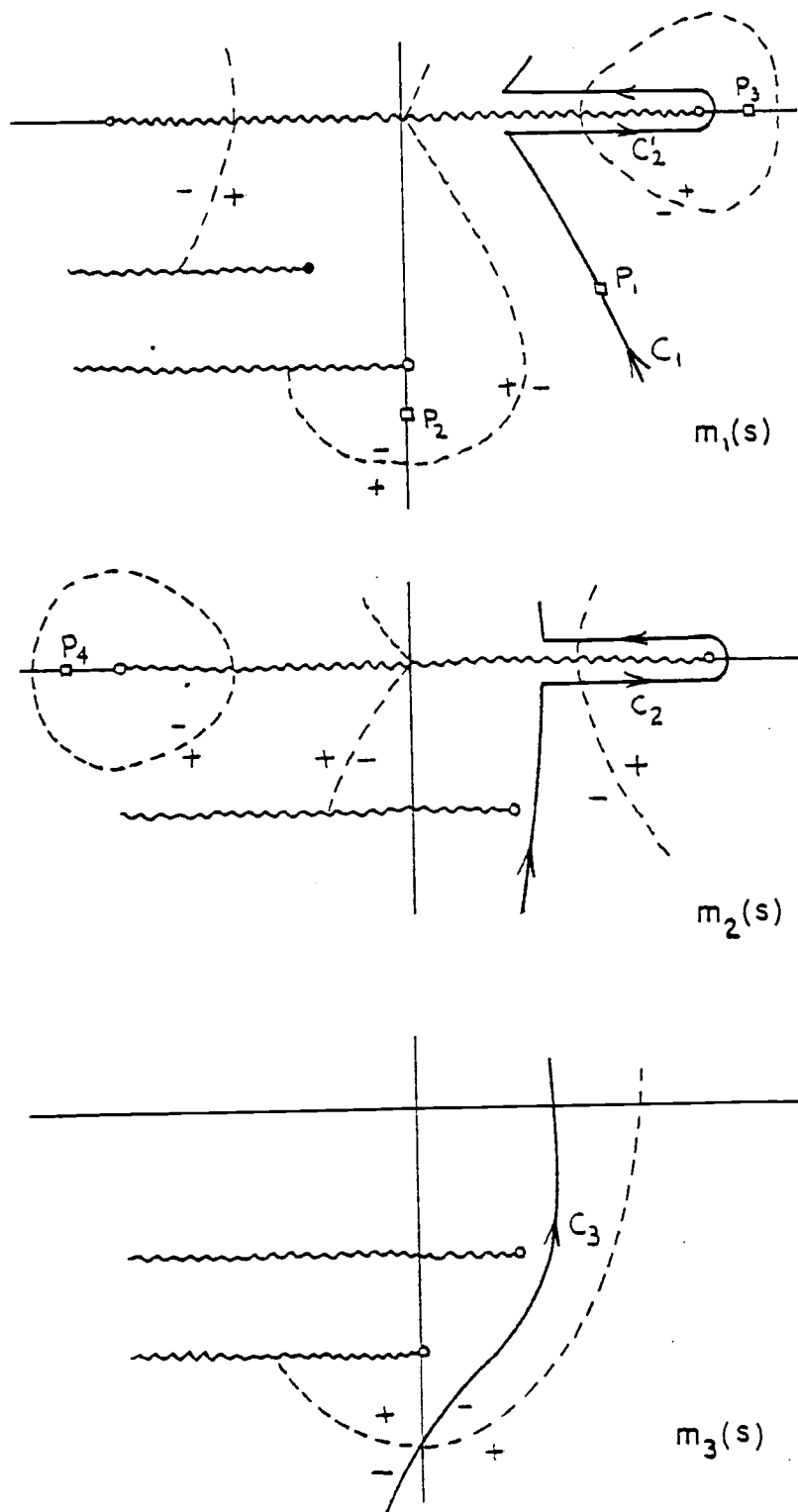


Figure 23. Typical contour for $x/t > 1.46$.

BIBLIOGRAPHY

- Abramowitz, M. and I. Stegun, eds, 1964: Handbook of Mathematical Functions. U. S. National Bur. of Standards, 55, Washington.
- Bernstein, R. L., and W. B. White, 1977: Zonal variability in the distribution of eddy energy in the mid-latitude North Pacific Ocean. J. Phys. Oceanogr., 7, 123-126.
- Buchwald, V. T., and J. K. Adams, 1968: The propagation of continental shelf waves. Proc. Roy. Soc. London, A305, 235-250.
- Feshchenko, S. F., N. I. Shkil' and L. D. Nikolenko, 1967: Asymptotic Methods in the Theory of Linear Differential Equations. American Elsevier, New York, 270 pp.
-
- Gadgil, S., 1976: Time-dependent topographic meandering of a baroclinic current. Dyn. Atmos. Oceans., 1, 127-161.
- Gaster, M., 1968: Growth of disturbances in both space and time. Phys. Fluids, 9, 723-727.
- Gaster, M., 1965: On the generation of spatially growing waves in a boundary layer. J. Fluid Mech., 22, 433-441.
- Heezen, B. C., M. Tharp and C. Bentley, 1972: Antarctic Map Folio Ser. 16. American Geogr. Soc., New York.
- Hogg, N. G., 1976: On spatially growing baroclinic waves in the ocean. J. Fluid Mech., 78, 217-235.
- Hogg, N. G., 1973: On the stratified Taylor column. J. Fluid Mech., 58, 517-537.
- Langer, R. E., 1959: The asymptotic solutions of a linear differential equation of the second order with two turning points. Trans. Am. Math. Soc., 90, 113-142.
- Lighthill, M. J., 1967: On waves generated in dispersive systems by travelling forcing effects, with application to the dynamics of rotating fluids. J. Fluid Mech., 27, 725-752.

- Longuet-Higgins, M. S., 1968a: Double Kelvin waves with continuous depth profiles. J. Fluid Mech., 34, 49-80
- Longuet-Higgins, M. S., 1968b: On the trapping of waves along a discontinuity of depth in a rotating ocean. J. Fluid Mech., 31, 417-434.
- McCartney, M. S., 1976: The interaction of zonal currents with topography with applications to the southern ocean. Deep-sea Res., 23, 413-427.
- McCartney, M. S., 1975: Inertial Taylor columns on a beta plane. J. Fluid Mech., 68, 71-95.
- McIntyre, M. E., 1968: On stationary topography-induced Rossby-wave patterns in a barotropic zonal current. Deut. Hydrogr. Z., 13, 132-141.
- Mofjeld, H., and M. Rattray, 1971: Free oscillations in a beta-plane ocean. J. Mar. Res., 29, 281-305.
- Mooers, C. N. K., 1976: Wind-Driven Currents on the Continental Margin. Chapter 4 in Marine Sediment Transport and Environmental Management, D. J. Stanley and D. J. P. Swift, eds. Wiley-Interscience, New York, 602 pp.
- Nayfeh, A. H., 1973: Perturbation Methods. Wiley, New York, 425 pp.
- Pedlosky, J., 1976: Finite-amplitude baroclinic disturbances in downstream varying currents. J. Phys. Oceanogr., 6, 335-344.
- Pedlosky, J., 1964a: An initial value problem in the theory of baroclinic instability. Tellus, 16, 12-17.
- Pedlosky, J., 1964b: The stability of currents in the atmosphere and the ocean, Part I. J. Atmos. Sci., 21, 201-219.
- Platzman, G. W., 1975: Normal modes of the Atlantic and Indian Oceans. J. Phys. Oceanogr., 5, 201-221.
- Rhines, P. B., 1977: The Dynamics of Unsteady Currents. Chapter 7 in The Sea, Vol. 6, Marine Modeling, E. D. Goldberg, I. N. McCave, J. J. O'Brien and J. H. Steele, eds. Wiley, New York.
- Rhines, P. B., 1969: Slow oscillations in an ocean of varying

- depth. (Parts 1 and 2). J. Fluid Mech., 37, 161-205.
- Rhines, P. B., 1970: Wave propagation in a periodic medium with application to the ocean. Rev. Geophys., 8, 303-319.
- Rhines, P. B., and F. Bretherton, 1973: Topographic Rossby waves in a rough-bottomed ocean. J. Fluid Mech., 61, 583-607.
- Roden, G. I., 1977: On long-wave disturbances of dynamic height in the North Pacific. J. Phys. Oceanogr., 7, 41-49.
- Smith, R., 1971: The ray paths of topographic Rossby waves. Deep-Sea Res., 18, 477-483.
- deSzoeko, R. A., 1972: Baroclinic flow over an obstacle in a rotating system. Woods Hole Ocean. Inst. G. F. D. Notes, Part 2, 1-10.
- Taylor, G. I., 1922: Tidal oscillations in gulfs and rectangular basins. Proc. London Math. Soc., 20, 148-181.
- Thacker, W. C., 1976: Spatial growth of Gulf Stream meanders. Geophys. Fluid Dyn., 7, 271-295.
- Veronis, G., 1966: Rossby waves with bottom topography. J. Mar. Res., 24, 338-349.
- Webb, D. J., 1976: A model of continental-shelf resonances. Deep-Sea Res., 23, 1-15.